Development of an Improved Round Window Stimulation Device to Treat Hearing Loss

Development of an improved round window stimulation device to treat hearing loss

A dissertation presented

by

Darcy Frear

to

The Division of Medical Sciences

in partial fulfillment of the requirements

for the degree of

Doctor of Philosophy

in the subject of

Speech and Hearing Bioscience and Technology

Harvard University

Cambridge, Massachusetts

March 2019

Dissertation Advisor: Hideko Heidi Nakajima Darcy Frear

Development of an improved round window stimulation device to treat hearing loss

Abstract

Hearing loss affects 14-15% of the US adult population, and can be caused by conductive, sensorineural or mixed pathologies; however, the contribution of these pathologies has not been quantified. Furthermore, recent studies show that conductive and mixed hearing loss can be treated by direct mechanical stimulation of the round window, though a reliably effective device is not available. To improve round window stimulation treatment, we performed several investigations.

The *first* was to quantify the types of hearing loss treated at the Massachusetts Eye and Ear hospitals. Hearing loss categories included: sensorineural, surgically-treatable conductive, acute otits media, earwax buildup, and unknown. Sixteen percent of cases were diagnosed with surgically-treatable conductive hearing loss. Conventional treatment for such cases includes hearing aids or middle ear surgery, which restores movement or continuity of the conductive pathway. However, in some cases, where conventional surgery is unsuitable or unsuccessful, round window (RW) stimulation has been used with some success.

The *second* studied the variability in efficacy of different middle ear treatments by quantifying the relevant mechanical and acoustical properties of human ears. We analyzed pressure and velocity measurements from 18 fresh cadaveric human specimens to create a computational impedance model to 1) quantitatively understand sound transmission through

the inner ear, and 2) to aid in the development of a RW stimulation device. This model has many applications in the future; like, understanding sound transmission mechanisms.

The *third* developed and tested several RW stimulation prototypes, where we demonstrated that our preliminary Interface Coupler (IC) prototype had improved performance compared to a commercial RW treatment device. The *fourth* described and tested an improved IC which better fits differences in the anatomy of the RW with an internalized actuator for surgical ease. The improved IC performed well across multiple anatomies, had a linear output with good dynamic range, and produced an equivalent hearing output of at least 90 dB SPL across a wide frequency range. The IC performance was consistent with our impedance model (produced by the second study), exemplifying the many useful applications of the impedance model.

Table of Contents

Acknowledgments

I first want to thank my PI, Heidi Nakajima, for accepting and mentoring me into the world of hearing mechanics. You are a very strong and dedicated person who I am glad to have in my life.

I would also like to thank John Rososwski for being my mentor and chairing both my Dissertation Advisory Committee and my Thesis Defense Committee. You are always willing to give advice and be helpful in any way you can. Thank you to Sunil Puria and Jennifer Lewis for lending their ears and wonderful insight on my Dissertation Advisory Committee.

Thank you Mike Ravicz for help with coding and debugging my experiments, you always have a way of making everything work. Ish Stefanov-Wagner, thank you for your help with creative building and lots of tiny tube cutting for my experiments. Thank you Melissa McKinnon for your help with navigating the administration hoops.

Thank you to my lab mates through the years. Stefan Raufer and Salwa Masud, thank you for being my office buddies, sounding boards, and anchors. Thanks Xiying Guan for all your help during experiments and coding – you were my favorite post-doc. Song Chen, thanks for always brightening up lab and your useful advice. Thank you Inge Knudson, Deepa Galaiya, and Aaron Remenschneider for all your help and advice.

Thank you to my fellow entering SHBT class of 2013 – Peter Bowers, Kevin Sitek, Claire Cordella, Claire Schenkel, and Sarah Gluck. My graduate school experience wouldn't have been the same without you and thanks for helping me get me through classes in one piece.

Thank you to all the friends I've made through SHBT, the Graduate Student Council, and the Harvard Dragon Boat club. A special thank you to Nicole Black, Kim Noij, Elaine Garcia, Elizabeth Jaensch, and John Gee.

Thank you to my parents for everything. You supported and encouraged me through my whole life and I will never be able to thank you enough. Love you both!

Thank you to my super significant other, Michael Kremer for supporting me through the toughest time in my life. I love you and can't wait to see what our future holds.

All those mentioned deserve pages of thanks and I wouldn't have made it this far without you.

Dedication

To Momo and Great Grandma:

Thank you for inspiring me.

List of tables and figures

Tables

Figures

CHAPTER 1.

Introduction

Hearing loss affects over 35 million people in the United States and is the third most common health problem (Pleis and Lethbridge-Cejku 2007). The most common form of hearing loss is sensorineural hearing loss and treatment for this type of loss tends to be through conventional hearing aids and cochlear implants with varying success rates. However, there is another group that has the potential for excellent prognosis with mechanical solutions, those with conductive and mixed hearing loss.

To better understand these types of hearing loss, we consider the anatomy of the ear and how sound travels through the auditory system (seen in Figure 1.1). Sound travels down the ear canal, moves the tympanic membrane, causing the middle ear bones to vibrate, thus vibrating the oval window of the cochlea. In the cochlea, the oval window vibrates the scala vestibuli fluid compartment which is divided from the scala tympani compartment by the cochlear partition (illustrated in Figure 1.2A). On the other side of the cochlear partition, in scala tympani, there is a flexible membrane, the round window. Because the round window is highly compliant and the rest of the fluid-filled spaces and cochlear partition have high impedance, the sound pressure produced by mechanical stimulation of the oval window (OW) in scala vestibuli is much higher than the sound pressure near the round window in scala tympani. This sound pressure difference across the partition at the base of the cochlea defines the input to the cochlea, and initiates the traveling wave along the cochlear partition that triggers sound transduction by the sensory cells residing on the partition that transduces mechanical to electrical signals. These sensory cells initiate the neural signals our brain interprets as sound.

If the first part of this pathway does not function (the ear canal, tympanic membrane, and/or middle ear ossicles do not operate normally), then the person has a conductive hearing loss (CHL). A person has sensorineural hearing loss (SNHL) if some part of the neuro-sensory mechanism of the cochlea or a pathway to the brain is not operational. Mixed hearing loss is a combination of both CHL and SNHL.

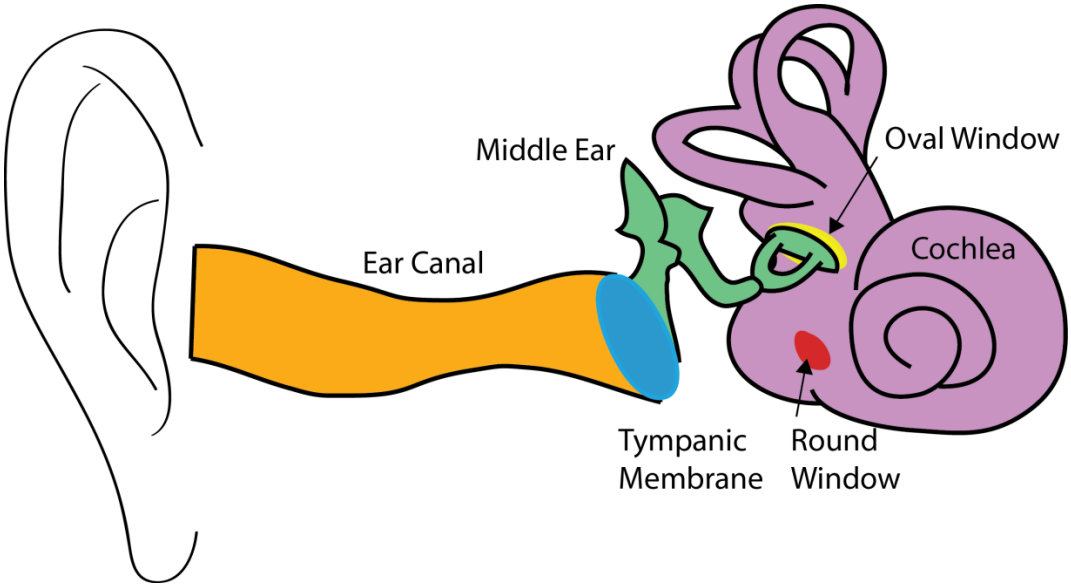

Figure 1.1: Anatomy of the Ear. Illustration of the ear from the ear canal to the cochlea including the oval window and round window membranes.

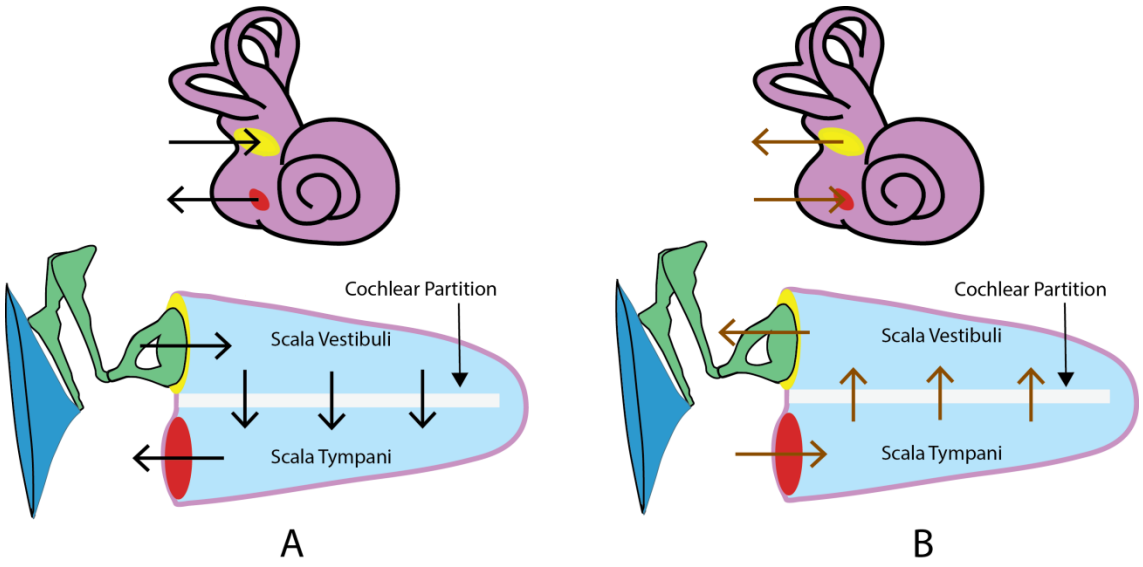

Figure 1.2: Illustrations of Air Conduction and Round Window Stimulation. The top images show the cochlea in 3D perspective drawings. The bottom images represent the cochlea unwound and sectioned to show the fluid compartments within a 2D representation. A) In air conduction, sound (volume velocity) enters the oval window, produces a sound pressure difference between scala vestibuli (SV) and scala tympani (ST), and exists through the RW. B) In round window stimulation, the RW is mechanically stimulated to produce a sound pressure difference between the ST and SV and exits through the oval window.

Sound flow (volume velocity) in the inner ear typically travels in the pathway pictured in Figure 1.2A during air conduction (AC) stimulation. However, by mechanically vibrating the round window membrane (RW), volume velocity can also enter the cochlea through the RW, pictured in Figure 1.2B (Maier et al. 2013; Schraven et al. 2011; Iwasaki et al. 2012; L. Colletti et al. 2011; Marco Mandalà, Liliana Colletti, and Vittorio Colletti 2011; Bernardeschi et al. 2011). The arrows at the OW, RW, and cochlear partition are simplified representations of the direction of volume velocity flow in the two cases.

The sound pressure-difference across the cochlear partition produced by mechanically stimulating the RW (without puncturing the RW membrane) elicits a traveling wave identical in

nature to the wave produced by OW stimulation (Wever and Lawrence 1950; Lupo et al. 2009; Stieger, Rosowski, and Nakajima 2013; Nakajima, Merchant, and Rosowski 2010; Voss, Rosowski, and Peake 1996). The benefit of RW stimulation is that it can bypass many conductive hearing problems to directly stimulate the cochlea. However, RW stimulation is relatively new and the currently implanted device has shortcomings that could be greatly improved upon (Rajan et al. 2011; Baumgartner et al. 2010; Martin et al. 2009; Beltrame et al. 2009). This thesis quantifies the mechanics of sound transmission through the middle and inner ear, and applies that knowledge to develop a new device specific to the needs of stimulating the RW.

To understand the mechanics of the ear and to test devices, we used fresh human cadaveric temporal bones. These specimens include the structures from the ear canal to the cochlea and are prepared (via surgical drilling) to access the middle ear ossicles and the OW and RW of the cochlea. The macro-mechanics of these fresh temporal bones are similar to the live ear (Chien et al. 2009; Nakajima, Ravicz, Merchant, et al. 2005; Nakajima, Ravicz, Rosowski, et al. 2005; Goode, Ball, and Nishihara 1993). Mechanical measurements include sound-induced vibrations of the tympanic membrane, middle ear ossicles, OW membrane, RW membrane (obtained by laser Doppler vibrometry), and the sound pressures within the cochlea. The latter are measured using micro fiberoptic pressure sensors (Olson 1998): one in the scala vestibuli near the OW and the second in scala tympani near the RW. The stapes velocity is required to determine the volume velocity at the OW.

Measurements of intracochlear sound pressure provide additional information to understand sound transmission (Stieger, Rosowski, and Nakajima 2013; Frear et al. 2018).

Differential pressure across the partition at the base of the cochlea is an estimate of the input to the cochlea, and can be used as a mechanical audiogram. Thus it allows one to study the effect of different pathologies and stimulation mechanisms, and their effects on the input to the cochlea (Nakajima et al. 2009; Pisano et al. 2012). Combining pressure and velocity measurements enables us to calculate impedances of the ear, as is extensively utilized to construct the model of the inner ear in Chapter 3.

Summary of Thesis:

In Chapter 2, we provide a quantitative overview of the types of hearing loss treated at Massachusetts Eye and Ear (MEE) hospitals. Although hearing loss is a common and devastating problem, we lack information regarding the incidence of different types of hearing loss. Such information is important to understand how to best allocate healthcare resources, and we sought to fill this gap using data about the diagnoses applied to patients seen at MEE hospitals. We define and sort patients with diagnosed hearing problems at the different MEE centers over 3.5 years. We quantify the relative incidence of various forms of hearing loss and determine the incidence of CHL conditions that are surgically treatable. This chapter provides much needed information to assess the impact of research focusing on specific types of hearing loss, especially CHL.

In Chapter 3, we use sound pressure and velocity measurements from fresh cadaveric temporal bones to calculate the acoustic impedances of the middle and inner ear. We create a database of "normal" ears (without history of ear disease and with normal middle and inner ear macro-mechanics) that can be used to compare past and future data. This data includes

measurements of intra-cochlear sound pressures and the velocity of the stapes when the inner ear is stimulated with AC sound or a mechanical RW driver. Using this data we calculate the impedances of the cochlear partition, RW, possible leakage paths from scala vestibuli and the middle ear driven from the stapes. We then develop a computational lumped-element model of the normal ear using the experimental data. This model provides an understanding of human sound transmission mechanisms for various sound stimulation methods such as AC, RW, and bone conduction, as well as sound transmission related to otoacoustic emissions.

In Chapter 4, we develop a prototype device for RW stimulation by focusing on efficient coupling between the device and RW membrane. From our impedance calculations in Chapter 3, we quantified the cochlea's scala vestibuli leak that can be advantageous during RW stimulation, because it enhances the sound pressure difference across the cochlear partition during RW stimulation. Currently clinical RW stimulation is accomplished using the floating mass transducer (FMT, Med-El), which has poor acoustic quality and unreliable device positioning. In this chapter we provide a proof of concept of an interface coupler (IC) prototype designed to address the problems encountered by the FMT. We compare the performance of the FMT and IC in one human temporal bone and find the IC produces an increase in sound transmission as well as larger bandwidth, superior linearity, and larger dynamic range compared to the FMT.

In Chapter 5, we improve upon the interfacing coupler design and test the new prototype in several temporal bones. We create a more compact device that could be used with various types of anatomy and focused primarily on safety for the patient and ease of surgical implantation for the surgeon. The new IC produces consistent results across varying

anatomies in multiple temporal bones with excellent linearity, dynamic range and frequency range. Using the computational model from Chapter 3, we estimate the equivalent AC ear-canal sound pressure associated with a similar cochlear input drive produced by RW stimulation in a normal ear. We find that the RW stimulation device can produce at least the equivalent of air-conducted 90dB SPL hearing with a 6 V_{peak} input to the IC actuator. Finally, we used the results of the IC with the impedance model produced in Chapter 3. The model enabled quantification of the leakage impedance at the RW during IC stimulation.

CHAPTER 2.

Overview of Hearing Loss at Massachusetts Eye and Ear Hospitals

Introduction

Hearing loss has been estimated to be prevalent in 14-15% of the US adult population (Pleis and Lethbridge-Cejku 2007; Hoffman et al. 2017) . Prevalence rates are frequently estimated by self-reported surveys with a minority of patients undergoing formal audiometry. Typically, hearing loss is defined as an average hearing threshold of 25dB above Normal Hearing Level (dB HL) or greater.

Hearing loss can be sensorineural (SNHL), conductive (CHL) or mixed. SNHL happens when hair cells within the cochlea are damaged and/or when the neurons connecting the hair cells to the brain are damaged. This loss is usually identified via a decrease in the sensitivity to bone conducted sounds (increased thresholds). CHL occurs due to problems conducting sound gathered by the external ear to the stapes footplate. Such a loss is usually identified by an air-conducted hearing loss that is accompanied by normal sensitivity to bone-conducted sound. Mixed hearing loss occurs as a consequence of pathology affecting both the conductive and sensorineural hearing pathways. Although much is known about the prevalence of hearing loss, there is surprisingly little data defining the relative prevalence of CHL or the pathologies that cause it. Such data are important for understanding the prevalence of various diseases such as superior canal dehiscence, otosclerosis and chronic otitis media. CHL is typically a mechanical problem with a mechanical solution, with solutions like stapedectomy, bone anchored hearing aids, tympanoplasty, etc. In general it is not possible to reverse SNHL and the most common solutions are hearing aids and cochlear implants. A contemporary study on the prevalence of different types of CHL is necessary to identify the needs of patients and assess if we need more solutions to meet those needs.

To better define prevalence rates of conductive hearing loss by type and by demographics, we undertook a review of patients presenting to a tertiary care center with hearing loss as a primary complaint. With this review, we aim to 1) understand the relative prevalence of various forms of hearing loss in all patients presenting to Massachusetts Eye and Ear (MEE) hospitals with hearing complaints over a recent 3.5 year period, and 2) segregate from its population those with CHL that is surgically treatable. Such an analysis will quantify the relative prevalence of surgical disease in the patient population at the MEE hospitals.

Methods

Data were gathered from patients visiting any of the 20 MEE hospitals for a clinical otolaryngology or audiology appointment over a three and a half year period from January 2015 to July 2018. The diagnostic code (ICD10) of each patient was reviewed. The ICD10 code is a code given to every patient seen at MEE by a physician or audiologist. Relevant diagnoses were separated into five categories – Surgical CHL, SNHL, Unknown, Earwax, and Acute Otitis Media (AOM). Appendix A2 describes how different diagnostic entities were broken down into the five categories noted above. Audiograms and doctor's notes were not consulted for this study. Of note, patients diagnosed with mixed loss were assigned to the sCHL category in our study, as these patients have the potential to improve with surgical intervention. Patients making multiple visits were generally only counted once and assigned the most significant diagnostic code; patients seen multiple times with multiple significant disorders were counted multiple times. Patients were excluded if they did not have a diagnosis of hearing loss. Our methods were reviewed and approved by the MEE IRB.

Surgical CHL (sCHL) included cases like rupture of the tympanic membrane, middle ear disorders, cholesteatomas, otosclerosis, superior semicircular canal dehiscence, and external-ear atresia. Note that sCHL includes chronic otitis media (COM), as the most common complication of COM is sCHL and there are many surgical interventions performed to treat the consequences of COM (Ballenger and Snow 2003).

The patient data was reduced to specific cases using the patient's medical records number (MRN) to find the most relevant diagnosis. Priority was given to SNHL and sCHL diagnoses over unknown and earwax cases. For example, if a patient was diagnosed with a rupture in their tympanic membrane in 2015 and diagnosed with excessive earwax in 2016, they would be counted as a case of sCHL not ear wax. However, if a patient was diagnosed with two very different types of sCHL or SNHL during the 3.5 years (like perforation of the tympanic membrane and otosclerosis), they were counted twice.

Demographic information was obtained if available in the medical record. The age of the patient was taken at the time of their diagnosis and was separated by decade, except under the age of ten where there are categories for under 5 and 5-9. The reason for this separation was because a majority of AOM cases are diagnosed to children under 5 years of age (Monasta et al. 2012). Race, ethnicity and veteran status was also reported, when available.

Results

Our patient population was composed of 174,948 unique individuals out of the 360,636 total patients who entered MEE between January 2015 and the end of June 2018. Thus 48.51% of the patients seen at our subspecialty institution were diagnosed with a hearing disorder. Demographics of the entire population are included in Table 2.1. Note that both Hispanic race and ethnicity were given as options to the patients so these responses are reflected in Table 2.1 and future tables.

able 2.1: Demographics of the Patient Population with a hearing disorder

	Patients	Female	Male	Veteran	Ethnicity	Race						
					Hispanic	White	Black	Native Am.	Asian	Hawaiian	Hispanic	Declined
n	174948	92472	82467	8839	7800	134960	6683	206	6626	118	1949	2983
%	48.51%	52.86%	47.14%	5.05%	4.46%	77.14%	3.82%	0.12%	3.79%	0.07%	1.11%	1.71%

Table 2.2: Demographic Characteristics of Study Sample Allocated by Hearing Loss Type. Percentages for the Patients column are the number in that category divided by the total number of patients. Percentages for all other columns are the number in that row divided by the total number of patients in that hearing loss category.

		Patients	Female	Male	Veteran	Ethnicity	Race						
						Hispanic	White	Black	Native Am.	Asian	Hawaiian	Hispanic	Declined
sCHL	n	28647	14922	13723	852	1240	21585	949	40	1209	20	297	456
	%	16.37%	52.09%	47.90%	2.97%	4.33%	75.35%	3.31%	0.14%	4.22%	0.07%	1.04%	1.59%
SNHL	n	46726	25192	21532	2986	1564	36886	1557	45	1790	39	413	802
	%	26.71%	53.91%	46.08%	6.39%	3.35%	78.94%	3.33%	0.10%	3.83%	0.08%	0.88%	1.72%
Unknown	n	23075	12622	10452	1433	1165	17727	1112	30	1059	19	345	391
	%	13.19%	54.70%	45.30%	6.21%	5.05%	76.82%	4.82%	0.13%	4.59%	0.08%	1.50%	1.69%
Wax	n	43812	23508	20301	3042	1227	34802	1591	44	1295	11	381	708
	%	25.04%	53.66%	46.34%	6.94%	2.80%	79.43%	3.63%	0.10%	2.96%	0.03%	0.87%	1.62%
AOM	n	32688	16228	16459	526	2604	23960	1474	47	1273	29	513	626
	%	18.68%	49.65%	50.35%	1.61%	7.97%	73.30%	4.51%	0.14%	3.89%	0.09%	1.57%	1.92%
Total	n	174948	92472	82467	8839	7800	134960	6683	206	6626	118	1949	2983
	%	100.00%	52.86%	47.14%	5.05%	4.46%	77.14%	3.82%	0.12%	3.79%	0.07%	1.11%	1.71%

The patients were separated into five categories (sCHL, SNHL, Unknown, Earwax, and AOM) as shown in Table 2.2. Table 2.2 also provides additional demographic information from this patient population. A visual representation of the percentage of each type of hearing loss is shown in Figure 2.1A. The largest cause of hearing loss is SNHL (27%), then earwax buildup/impaction (25%), AOM (19%), sCHL (16%) and unknown causes (13%).

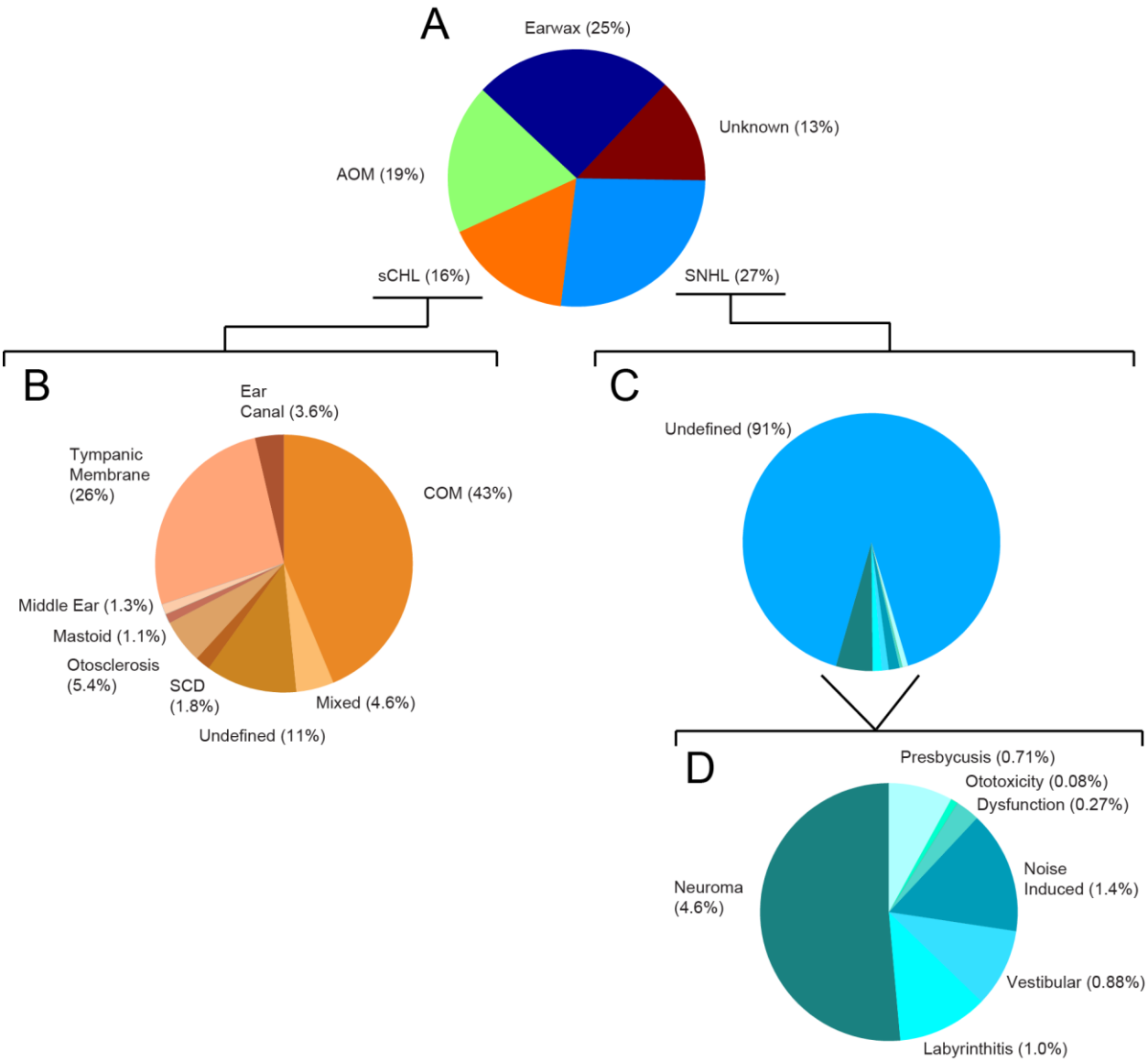

Figure 2.1: Percentages of the Hearing Loss: A) The five categories of hearing loss, B) surgical conductive hearing loss diagnoses, C) sensorineural hearing loss diagnoses, and D) specific SNHL diagnoses (no undefined).

Table 2.3: Demographic Characteristics of Surgical Conductive Hearing Loss

		Patients	Female	Male
COM	n	12373	5953	6419
	%	43.19%	48.11%	51.88%
Ear Canal	n	1013	598	415
	%	3.54%	59.03%	40.97%
Tympanic Membrane	n	7353	3871	3481
	%	25.67%	52.65%	47.34%
Middle Ear	n	383	169	214
	%	1.34%	44.13%	55.87%
Mastoid	n	250	123	127
	%	0.87%	49.20%	50.80%
Otosclerosis	n	1540	997	543
	%	5.38%	64.74%	35.26%
SCD/Fistula	n	526	315	211
	%	1.84%	59.89%	40.11%
Undefined	n	3092	1718	1374
	%	10.79%	55.56%	44.44%
Mixed	n	2117	1178	939
	%	7.39%	55.64%	44.36%

Table 2.4: Demographic Characteristics of Sensorineural Hearing Loss

		Patients	Female	Male
Neuroma	n	2155	1239	916
	%	4.61%	57.49%	42.51%
Labyrinthitis	n	531	337	194
	%	1.14%	63.47%	36.53%
Vestibular	n	412	262	150
	%	0.88%	63.59%	36.41%
Noise induced	n	640	183	457
	%	1.37%	28.59%	71.41%
Dysfunction	n	127	83	44
	%	0.27%	65.35%	34.65%
Ototoxicity	n	39	15	24
	%	0.08%	38.46%	61.54%
Presbycusis	n	332	167	165
	%	0.71%	50.30%	49.70%
Undefined	n	42490	22906	19582
	%	90.93%	53.91%	46.09%

Relative Incidence of Surgical CHL Types

A breakdown of sCHL cases into the structure affected is given in Table 2.3 and illustrated in a pie graph in Figure 2.1B. COM was the largest cause of sCHL (43%) and tympanic membrane pathology (26%) was the second most common case of sCHL.

Relative Incidence of SNHL Types

A breakdown of the SNHL cases into sub-diagnoses is included in Table 2.4 and Figure 2.1C. The SNHL with undefined cause was the large majority of SNHL cases at 91%. Figure 2.1D plots the breakdown of the seven other causes: acoustic neuroma (4.6%), noise induced (1.4%), labyrinthitis (1.0%), vestibular (0.88%), presbycusis (0.71%), dysfunction (0.27%), and ototoxicity (0.08%).

Age

Histograms of the age-distribution of the different hearing-loss types are illustrated in Figure 2.2, with the corresponding data in Table 2.5. The average age of this patient population was 49 with a median age of 57 where the age range was 0 to 105 years old.

AOM was the largest cause of a hearing related diagnosis for those 9 and under, while SNHL and earwax were the biggest problem for those 40 and above, where SNHL is the largest diagnosed hearing loss between ages 60-69. The group of 60-69 and under 5 years old were the groups most diagnosed for hearing problems at MEE hospitals. sCHL diagnoses were largest for the under 5 age group and second largest for the 50-69 age group.

The sCHL cases were further broken down by age in Figure 2.3. The largest age group affected by sCHL was largely due to COM for the under 5 age group (34%). COM was also most diagnosed for patients 5-9 and over 40 years old. A tympanic membrane issue was most diagnosed from ages 10-39. Otosclerosis and mixed hearing loss were most diagnosed from ages 40-79.

Table 2.5: Age Characteristics Allocated by Hearing Loss Type

		<5	5-9	10-19	20-29	30-39	40-49	50-59	60-69	70-79	>80
sCHL	n	5072	2007	2005	1871	2164	2846	4042	3943	2809	1888
	%	17.71%	7.01%	7.00%	6.53%	7.55%	9.93%	14.11%	13.76%	9.81%	6.59%
SNHL	n	488	393	1000	1591	2321	4174	8789	12045	9901	6023
	%	1.04%	0.84%	2.14%	3.40%	4.97%	8.93%	18.81%	25.78%	21.19%	12.89%
Unknown	n	1046	622	858	1225	1473	2174	3826	4827	4188	2836
	%	4.53%	2.70%	3.72%	5.31%	6.38%	9.42%	16.58%	20.92%	18.15%	12.29%
Wax	n	1776	1108	1993	2083	2059	2995	5465	8372	9009	8946
	%	4.05%	2.53%	4.55%	4.75%	4.70%	6.84%	12.47%	19.11%	20.56%	20.42%
AOM	n	12472	4187	2866	1752	1987	2207	2768	2385	1388	673
	%	38.15%	12.81%	8.77%	5.36%	6.08%	6.75%	8.47%	7.30%	4.25%	2.06%
Total	n	20854	8317	8722	8522	10004	14396	24890	31572	27295	20366
	%	11.92%	4.75%	4.99%	4.87%	5.72%	8.23%	14.23%	18.05%	15.60%	11.64%

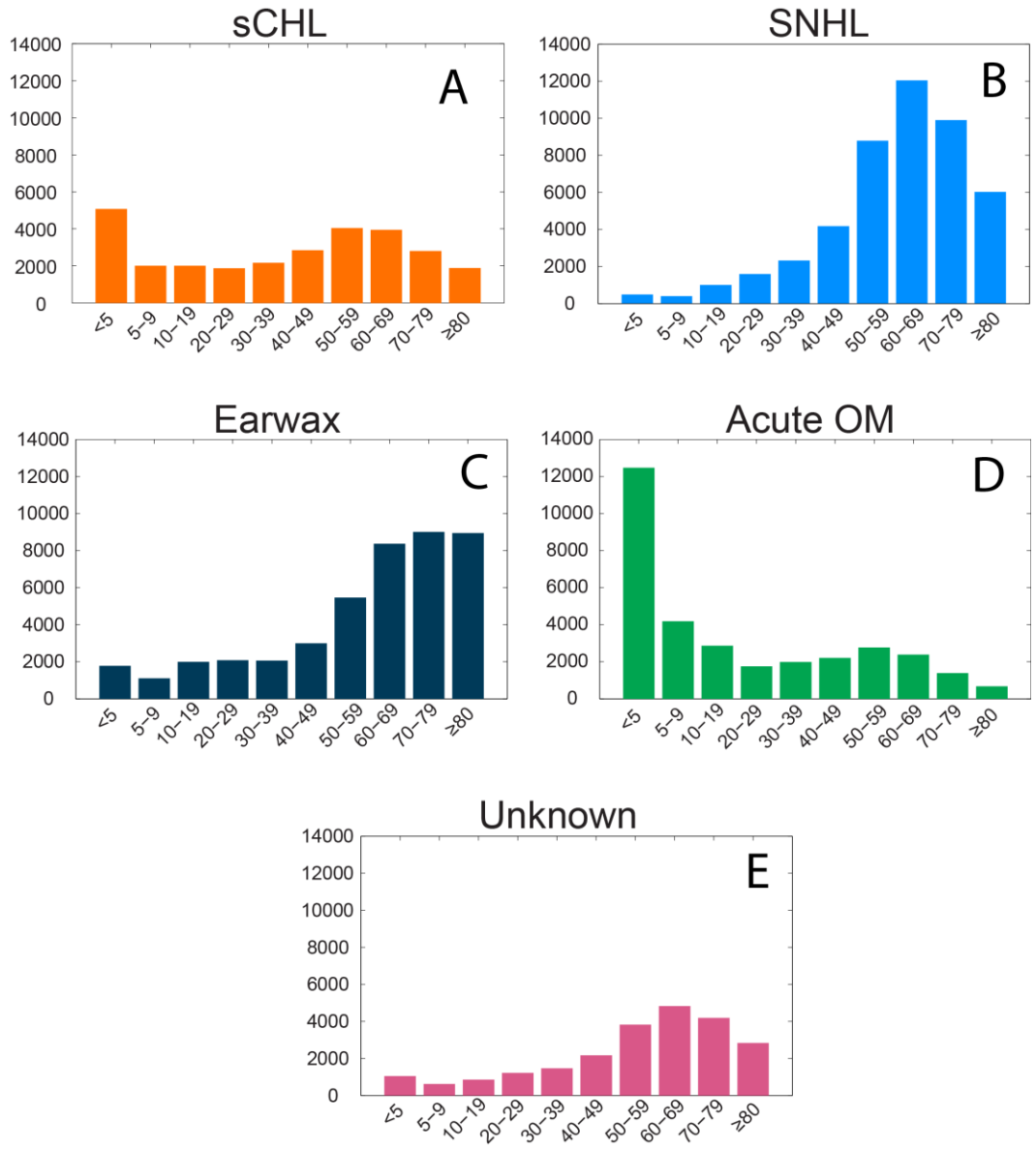

Figure 2.2: Hearing Loss Cases Separated by Age

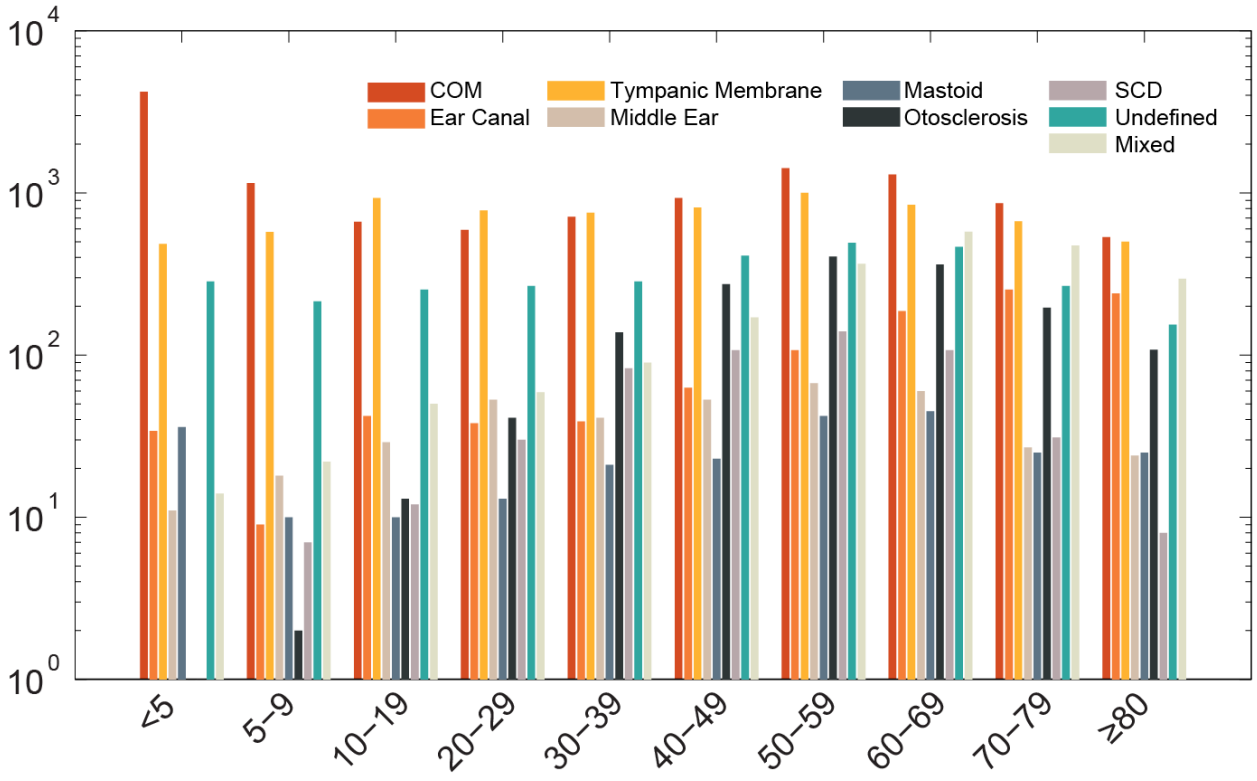

Figure 2.3: Surgical CHL Cases Separated by Age

Gender

There were more females than males in our population set (53% vs. 47%), where females were diagnosed more often than males in the sCHL, SNHL, Unknown, and Earwax cases. Specifically for SNHL cases, males were diagnosed more frequently than females in Noise Induced (71%, where the total number of patients was n=640) and Ototoxicity (62%, n=39) cases. For sCHL cases, males were more diagnosed for COM (52%, n=12373), Middle Ear (56%, n=383), and Mastoid problems (61%, n=250).

Ethnicity, Race, and Veteran Status

Those that reported veteran status, ethnicity, and race were reflected in Table 2.2 broken up by hearing loss type. Veterans represent 5.1% of this population where most were diagnosed with earwax, SNHL and unknown cases. Those that reported Hispanic ethnicity represented 4.5% of this data where the largest group was diagnosed with AOM. The largest racial group of this dataset was white at 77% where the most were diagnosed with ear wax buildup.

Discussion

Sensorineural Hearing Loss and Surgical Conductive Hearing Loss

For patients seeking care for hearing loss at Massachusetts Eye and Ear hospitals, 40% have treatable conditions – those with sCHL, AOM, and earwax buildup. This 40% could all be defined as CHL, but we narrow the sCHL definition to include only cases that usually lead to surgery to improve the conduction of sound to the inner ear. Even with our narrowed definition, sCHL prevalence in MEE patients was found to be 16%. Since sCHL can primarily be

solved via a mechanical solution, these patients have a chance to improve their quality of life, if surgical or implantable solutions to their problems exist or can be devised.

For instance, SCD is a relatively newly discovered disease (Lloyd B. Minor et al. 2001) that represents almost 2% of the sCHL population, which may be an underestimate of the incidence of this disorder (Agrawal, Ward, and Minor 2013). The literature suggests multiple surgical treatments for SCD (Crane et al. 2010; Crane, Minor, and Carey 2008; L. B. Minor et al. 1998) some of which produce less than satisfactory results. More research on these treatments 1) may provide improvements in treatment, and 2) raise the awareness of this disorder.

Furthermore, solutions that do not rely on the normal sound conduction pathway could benefit those that have resilient sCHL that persists despite conventional surgeries. Round window stimulation is one such solution that we delve into more detail in the upcoming chapters of this thesis.

Demographics

Sex

We observed that the percentages of females with hearing loss ICD10 diagnostic codes are larger than males for sCHL, SNHL, Unknown, and Earwax categories, but their statistical significance was not investigated. There are several diagnostic subcategories where males are the majority including AOM, COM, noise induced cases, ototoxicity, middle ear and mastoid problems. Females being diagnosed with hearing problems more often than males contradicts other studies that identify males as the more common sex with hearing related issues (Pleis and Lethbridge-Cejku 2007; Lin, Niparko, and Ferrucci 2011).

Age

As expected, AOM is most common in the 0-5 age group along with sCHL due to COM. sCHL is more common in 50-70 years old patients mostly due to COM, otosclerosis, mixed hearing loss, and tympanic membrane perforation. SNHL is most prevalent from 50-80 years of age where undefined SNHL is the most common diagnosis. Earwax affects more patients as they age up to 80, though some fraction of this increase may be related to the increase in hearing aid usage in this group (Browning 2008).

Ethnicity and Race

Given local demographics and referral patterns, our population was found to be overwhelmingly identifying as White at 77%. Patients identifying as Black or Asian both have their largest population in the unknown hearing loss type. Patients who identify as Hispanic ethnicity and/or race were most diagnosed with AOM.

Limitations

This study uses only ICD10 codes to distinguish types of hearing loss. Since audiograms were not consulted, there is no guarantee that every patient had hearing loss. Additionally, MEE is known to treat patients with rarer forms of hearing loss, so certain diagnoses are likely higher in this patient population than a general population. The diversity of this patient population is low with patients identifying as White being the largest percentage of race in this dataset. There is some missing demographic information for age, veteran status, ethnicity, race, and sex. Furthermore, there is no way to know if a patient went to another hospital network

where they were diagnosed with a specific hearing loss code. Finally, it is likely there are many more patients in the New England area that are not seeking care for their hearing loss.

Future Work

This study is a step toward an investigation of the incidence of different middle-ear disorders. Future work could include expansion of the data set to include multiple hospitals, and the analysis of procedure codes to identify patients that underwent surgery to correct their hearing loss. Furthermore, analyzing audiograms can help us confirm hearing loss in patients. Despite the limitations, the ICD10 diagnosis codes provide a look into the patient distribution for different types of hearing loss.

Conclusion

The general make up of patients diagnosed with hearing loss at MEE hospitals includes SNHL (27%), earwax buildup/impaction (25%), AOM (19%), sCHL (16%) and unknown cases (13%). SNHL is more prominent than sCHL, especially in adults 50 and older. The prevalence of sCHL was specifically defined to be surgically treatable cases.

CHAPTER 3.

Impedances of the inner and middle ear estimated from intracochlear sound pressures in normal human temporal bones

Published in Hearing Research, Volume 367, Pages 17-31
https://doi.org/10.1016/j.heares.2018.06.019

Authors:
Darcy L. Frear[1], Xiying Guan[2], Christof Stieger[2,3], John J. Rosowski[1,2], Hideko Heidi Nakajima[1,2]
[1]*Speech and Hearing Bioscience and Technology Program, Harvard University*
[2] *Department of Otolaryngology, Harvard Medical School, and Eaton-Peabody Laboratories, Massachusetts Eye and Ear, 243 Charles Street, Boston, MA 02114, USA*
[3]*University of Basel Hospital, Department of ENT, Hebelstr. 10, 4031 Basel, Switzerland*

Abstract

For almost a decade, we have measured intracochlear sound pressures evoked by air conducted (AC) sound presented to the ear canal in many fresh human cadaveric specimens. Similar measurements were also obtained during round window (RW) mechanical stimulation in multiple specimens. In the present study, we use our accumulated data of intracochlear pressures and simultaneous velocity measurements of the stapes or RW to determine acoustic impedances of the cochlear partition, RW, and the leakage paths from scala vestibuli and scala tympani, as well as the reverse middle ear impedance. With these impedances, we develop a computational lumped-element model of the normal ear that illuminates fundamental mechanisms of sound transmission.

To calculate the impedances for our model, we use data that passes strict inclusion criteria of: (a) normal middle-ear transfer function defined as the ratio of stapes velocity to ear-canal sound pressure, (b) no evidence of air within the inner ear, and (c) tight control of the pressure sensor sensitivity. After this strict screening, updated normal means, as well as individual representative data, of ossicular velocities and intracochlear pressures for AC and RW stimulation are used to calculate impedances. This work demonstrates the existence and the value of physiological acoustic leak impedances that can sometimes contribute significantly to

sound transmission for some stimulation modalities. This model allows understanding of human sound transmission mechanisms for various sound stimulation methods such as AC, RW, and bone conduction, as well as sound transmission related to otoacoustic emissions.

Abbreviations:

Note: italics represent a complex variable with magnitude and phase or real and imaginary parts.

AC = air conduction
RW = round window
OW = oval window
SV = scala vestibuli
ST = scala tympani
P_{EC} = sound pressure in the ear canal
P_{ST} = sound pressure in the scala tympani
P_{SV} = sound pressure in the scala vestibuli
V_{act} = velocity of the actuator on the RW
Z_{Diff} = differential impedance across the partition including the helicotrema
Z_{RW} = RW impedance
$Z_{ME'}$ = middle ear impedance from the cochlea looking out
Z_{lkSV} = leakage impedance of the SV and exterior of the otic capsule
Z_{lkSTRW} = leakage impedance of the ST and RW
U_{stap} = volume velocity of stapes during AC stimulation
U_{Diff} = volume velocity across the partition
U_{RW} = volume velocity of RW during AC stimulation
U'_{stap} = volume velocity of stapes during RW stimulation
U_{lkSV} and U'_{lkSV} = volume velocity through the SV leakage for AC and RW stimulation
U_{lkST} = volume velocity through the ST leakage for AC stimulation
U'_{lkSTRW} = volume velocity through the ST and RW leakage for RW stimulation
U_{act} = volume velocity entering the cochlea during RW stimulation with actuator

1. Introduction

Passive macro-mechanics in fresh cadaveric human temporal bones are similar to the living, as is evidenced by similarities in measurements of sound-induced stapes vibration in live ears and fresh cadaveric specimens (Chien et al. 2009). “Passive macro-mechanics” of the cochlea refers to the gross mechanical properties of the inner ear. These do not include the active mechanical processes within the cochlear partition of live ears. For example, the inner-ear sound pressures in scala vestibuli (P_{SV}) and scala tympani (P_{ST}) measured close to the surrounding bone (not the partition near the traveling wave), quantifies the human *cochlear input pressure drive* (P_{SV} - P_{ST}), the complex differential pressure across the cochlea partition at the cochlear base that is dominated by fast wave sound pressure and starts the traveling wave along the cochlear partition (Olson 1998). The cochlear input pressure drive has been shown to have the same frequency response as sensory potentials (cochlear microphonic) measured at the same location in animals (Dancer and Franke 1980; Lynch, Nedzelnitsky, and Peake 1982). Furthermore, the effects of middle and inner ear lesions (e.g. ossicular discontinuity and superior canal dehiscence) on the cochlear input drive in temporal bones are similar to clinical findings for hearing in live humans (Nakajima et al. 2009; Niesten et al. 2015; Pisano et al. 2012).

Measurements of intracochlear sound pressures and ossicular motions quantify important mechano-acoustic properties of the ear. Knowledge of the impedances of the middle and inner ear are necessary to understand the intricacies of sound transmission through the inner ear (Elliott, Ni, and Verschuur 2016; Nakajima et al. 2009; Stieger, Rosowski, and Nakajima 2013). Our pressure measurement techniques combined with velocity measurements

of the stapes and round window are valuable in determining the sound transmission mechanisms that dominate during various forms of inner-ear stimulation (e.g. air conduction (AC), bone conduction (BC), round window (RW) stimulation, soft tissue stimulation, etc.).

Previously, we showed that the paths of sound-related volume velocity through the inner ear differ between ear-canal AC and actuator-driven RW stimulation (Stieger, Rosowski, and Nakajima 2013). For AC stimulation, evidence supports the two-window hypothesis: the input to the inner ear – the volume velocity produced by stapes motion (U_{stap}) at the oval window (OW) – and the output of volume velocity from the inner ear via the compliant RW (U_{RW}) are approximately equal (Kringlebotn 1995; Stenfelt, Hato, and Goode 2004a). Therefore, in AC, other potential sound paths, such as vestibular and cochlear aqueducts, contribute little to sound transmission and have insignificant volume velocity sound flow.

Different from AC, RW stimulation results in inner-ear volume velocities that do not well conform to the two-window hypothesis (Stenfelt, Hato, and Goode 2004a; Stieger, Rosowski, and Nakajima 2013), where the volume velocity elicited by the RW actuator flowing into scala vestibuli does not all flow through the oval window, but splits, such that a significant fraction flows through a leakage path on the vestibular side of the cochlear partition (likely the vestibular aqueduct and/or neurovascular channels) (Dancer and Franke 1980; Stieger, Rosowski, and Nakajima 2013; Tonndorf 1972). A physical factor that contributes to this leak with RW stimulation is that the volume velocity elicited by stimulation faces an impedance at the OW (the reverse middle-ear impedance) that is similar in magnitude to the high impedance of the scala vestibuli leakage path (Stieger, Rosowski, and Nakajima 2013).

The major goal of the present study is to determine the values of the impedances that influence sound transmission within the inner ear. As a prerequisite for this task, we determine a "standard" set of sound-pressure transfer functions for "normal" human temporal bones – those without history of ear disease and with normal middle and inner ear macro-mechanics. From our accumulated measurements of intracochlear sound pressures and ossicular velocities during normal air conduction (AC) and round window (RW) stimulation, we implement strict inclusion criteria to describe the intracochlear sound pressure characteristics in normal ears. This set of standards, expressed as transfer functions, is useful for a) comparisons to past and future experiments, b) validation of computational models of the ear, and c) improving our understanding of the mechanism of sound transmission within the inner ear.

Using this data, we focus on the impedances that most influence the transmission of sound: the differential impedance across the partition measured at the base of the cochlea (Z_{Diff}, which includes the influence of the helicotrema), the RW impedance (Z_{RW}), the reverse middle-ear impedance from the cochlea looking out towards the middle ear ($Z_{ME'}$), the leakage impedance of the SV to the exterior of the otic capsule (Z_{lkSV}), and the leakage impedance of the ST and RW (Z_{lkSTRW}) to the exterior of the otic capsule. We use a combination of AC and RW stimulation results to determine these impedances. Based on these results we develop a lumped-element model that can help us understand more complex sound transmission mechanisms, such as bone- or soft-tissue-conducted sounds (Stenfelt and Goode 2005; Stenfelt 2016; Perez, Adelman, and Sohmer 2016). This model can also impact our understanding of inner-ear sound transmission in pathological and perturbed states, where the flow of volume

velocity through the inner ear is altered by changes in the relevant impedances or by the introduction of new volume velocity paths (e.g. superior canal dehiscence).

2. Methods

A total of 37 fresh human cadaveric temporal bones provide normative data. Pressure data from 22 specimens were already published including AC stimulation data from Nakajima et al. 2009, Stieger et al. 2013, Pisano et al. 2012, and Niesten et al. 2015. The RW stimulation data came from Stieger et al. 2013. In the aforementioned studies, except for Nakajima et al 2009, there was a computational error such that the reported intracochlear pressures were 7 dB lower than the actual level; this error is now corrected. The methods for the present study were detailed in previous publications (Nakajima et al. 2009, 2010; Stieger, Rosowski, and Nakajima 2013). Therefore, only brief descriptions are given here.

2.1 Temporal Bone Preparation

The temporal bones were harvested within 24 hours of death with surrounding dura kept intact, and used either fresh or after freezing and thawing. Inspection of the ear with a surgical microscope was normal with no noticeable pathology. The major difference between fresh and previously frozen is that fresh bones rarely showed evidence of air in the inner ear, while several of the thawed bones did (Ravicz, Merchant, and Rosowski 2000). Prior to specimen preparation, the fresh and thawed specimens were stored at 4^{o}C in 0.9% normal saline. A mastoidectomy was performed to widely open the facial recess, and the stapedial tendon was usually removed to allow access to the area surrounding the oval window. In the

RW stimulated ears, the bony overhang around the perimeter of the RW was reduced to facilitate the coupling of the actuator to the RW membrane.

2.2 AC and RW Stimulation

For AC stimulation, a loudspeaker (either Radio Shack 40-1377 or Beyer Dynamic DT48) was coupled to the bony ear canal. Pure tones of 77 ms length at 74 logarithmically-spaced frequencies between 0.1 and 10 kHz were presented and responses averaged 25 or 50 times. The sound pressure within the ear canal (P_{EC}) was recorded with a probe microphone (ER-7C, Etymotic) with the tip located 1-2 mm from the umbo. The stimulus sound pressures were generally between 50 and 120 dB SPL.

For RW stimulation we used a piezoelectric actuator firmly coupled to a transparent-glass rod (1 mm diameter). In 5 specimens the tip of the rod was coupled to the RW membrane directly or with an interfacing disk (1.5 mm diameter) punched out of a soft contact lens. The glass rod was brought into contact with the RW membrane and pushed towards the inner ear in small increments until the stapes velocity and intracochlear pressure measurements stopped increasing in magnitude (Schraven et al. 2012; Maier et al. 2013). The RW stimulator was driven at the same frequencies as for AC stimulation. The magnitude of the stimulus displacement was generally between 55 nm and 85 nm.

2.3 Pressure and Velocity Measurements

Intracochlear sound pressure measurements were performed with micro fiber-optic pressure sensors (Olson 1998). Cochleostomies slightly larger than the sensor diameter (167-

200 um) were drilled by hand while the cochlea was immersed in saline to prevent air from entering the cochlea. The sensors were inserted into scala vestibuli near the OW and scala tympani near the RW. The depth of insertion was approximately 100-200 μm from the otic bone-fluid interface. While maintaining saline around the sensors, the gaps between the sensors and the bone were sealed with dental impression material (Jeltrate, L.D. Caulk Co.). In later experiments, a layer of dental cement (Durelon, 3M Corp) was overlaid on the dried Jeltrate and surrounding bone to firmly fix the sensor to the promontory.

We measured intracochlear sound pressures close to the otic bone to maximize measurement of the fast-wave component of intracochlear sound pressure (distant from the cochlear partition), and minimize the "physiologically vulnerable" slow-wave components produced by the motion of the cochlear partition. Therefore, the pressures we measured are not vulnerable to the physiological condition of the sensory mechanism in the living ear, but are related to the mechanisms of gross macro-mechanical sound transmission, which is similar in living and fresh cadaveric specimens.

Simultaneous with the pressure measurements in the cochlea and ear canal, velocities of the stapes (posterior crus), round-window membrane, actuator or cochlear promontory were measured with a laser Doppler vibrometer (Polytec CLV), using reflective tape (0.1-0.2 mm^2) on the vibrating surface. To measure the velocity of the stapes (V_{stap}), the laser was aligned along the plane defined by the anterior and posterior crus and as close to orthogonal to the stapes footplate as possible to maximize sensitivity to the piston-like motion of the stapes and to minimize sensitivity to rocking motions. To measure the velocity of the RW (V_{RW}), the laser beam was positioned orthogonal to the plane of the RW membrane and at its center. The

velocity of the promontory was measured during AC and RW stimulation to determine the level of artifact motion of the entire temporal bone. Actuator velocity (V_{act}) was measured at the side of the glass rod with an angle of 20 to 30 degrees relative to the direction of the actuator motion.

Data were analyzed using software coded in Matlab. All pressure and velocity measurements with a signal-to-noise ratio (SNR) below 10 dB were excluded. Geometric averages and standard deviations (computed in the log domain) were used to describe the mean data and variation.

2.4 Criteria Set for Normal Ears and Accuracy of Measurements

Experimental data were only included in this study if three criteria were fulfilled for each specimen: 1) normal stapes velocity to ear-canal sound pressure transfer function; 2) no evidence of inner-ear air or fluid leak; 3) consistency (within 2 dB) of the pressure-sensor sensitivity throughout the experiment.

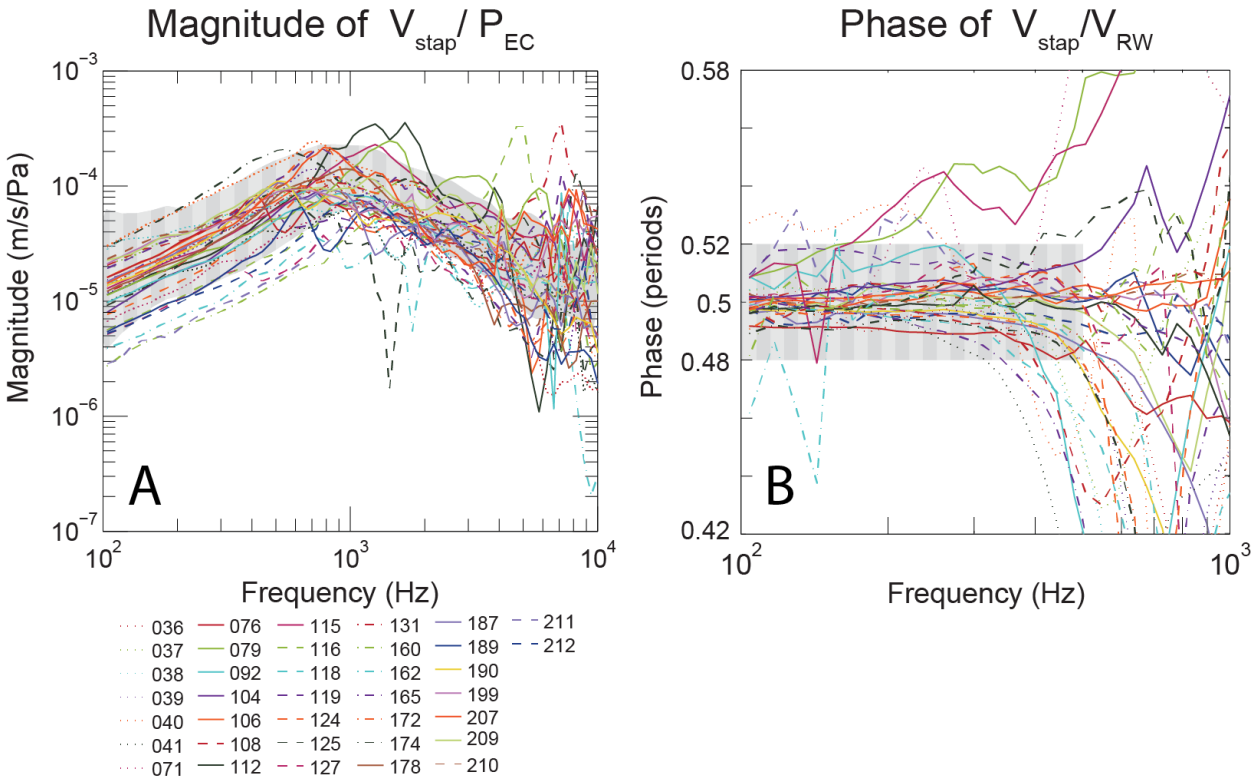

Figure 3.1: Inclusion criteria (striped gray area) compared to measurements in 37 temporal bones. A) Comparison of air-conducted middle ear transfer function (magnitude of V_{Stap}/P_{EC}) against the range (gray area) set by Rosowski et al. (2007). B) The difference in phase between the velocity of the stapes and RW (phase of V_{Stap}/V_{RW}) is plotted against frequency. Only experiments with data that fell within the striped gray areas at frequencies <2000 Hz in A and <500 Hz in B were used in this study.

2.4.1 Stapes Velocity to Ear-Canal Sound Pressure Transfer Function

The velocity of the stapes normalized to the sound pressure in the ear canal (V_{stap}/P_{EC}), was used as a measure of the normality of the ears' responses to sound and compared to the normal magnitude range reported by (J.J. Rosowski et al. 2007) (Figure 3.1A). Experiments that fell outside the normal range (gray shaded area) below 2 kHz were excluded. The 2 kHz limit was chosen because the motion of the stapes becomes complex (not a simple piston-like motion) above this range (Chien et al. 2006; Hato, Stenfelt, and Goode 2003; Heiland et al.

1999; Sim et al. 2010), and the one-dimensional laser measurement can vary greatly depending on the three-dimensional direction of the motion.

2.4.2 Tests for air within the cochlea

We tested for the presence of air in the cochlea using two tests. First, we used the observation that during AC stimulation, the motion of the incompressible fluid within the inner ear produces a half-cycle phase difference between the velocities of the stapes and RW (V_{stap}/V_{RW}) at frequencies below 500 Hz (Kringlebotn 1995; Stenfelt, Hato, and Goode 2004a, 2004b) (above 500 Hz, the mode of RW velocities can become complex). If air enters the inner ear, the inner-ear contents become compressible and the low-frequency phase difference varies from 0.5 cycles. This half cycle relationship was checked before and after the sensors were inserted and sealed in place. Second, we made certain that the phases of V_{stap} and V_{RW} relative to the stimulus sound pressure were unchanged (within 0.02 cycles) before and after pressure sensor insertions. Figure 3.1B plots the phase of V_{stap}/V_{RW} with the sensors in place for all 37 temporal bones. Only experiments that exhibited phase differences between -0.48 and 0.52 cycles (corresponding to ± 7.2°) at frequencies less than 500 Hz were included in this study.

2.4.3 Consistency of sensor sensitivity

To ensure accuracy of our inner-ear pressure measurements, we checked the sensitivity of our pressure sensors to determine if their calibrations remained within 2 dB of the initial measurement during the experiment. In earlier studies, we did this by comparing the calibrations of the sensors before inner-ear insertions, and after removal of the sensors at the

end of the entire experiment. In later studies, we adopted a different method described as follows:

At the beginning of the experiment we calibrated the sensors outside the ear with a fluid-filled shaker in the manner described previously (Nakajima et al. 2009; Stieger, Rosowski, and Nakajima 2013), and then measured the AC stimulus-generated sound pressures within the inner ear after sealing the sensors with Jeltrate® – a flexible quick-setting gel used for dental impressions. The sensors were then removed and recalibrated outside the ear. If the new calibrations were within 2 dB of the originals, these initial measurements in scala vestibuli and scala tympani were considered reliable and accurate and used as comparators for subsequent measurements. The sensors were reinserted and secured using much firmer dental cement that prevented the removal of the intact sensor and did away with the possibility of retesting sensor sensitivity. Repeated new measurements of AC induced sound pressures were compared to the initial measurements to test for consistency of sensor sensitivity and specimen preparation throughout the experiment. Frequency-independent changes in the magnitude (and stable phase) of the AC pressure response that remained relatively stable were considered to indicate slow changes in sensor sensitivity and were used to correct later measurements. Changes from the initial measurements that were complex (frequency dependent magnitude or phase changes) were considered indicators of sensor failure or uncontrolled changes in the preparation.

2.4.4 Summary of inclusion for this study

A summary of the experiments using the inclusion criteria is shown in Table 3.1. Eighteen out of the 37 experiments passed our strict criteria. Also noted in Table 3.1 are reasons for the exclusion, which included the failure to perform one or more of the inclusion tests, abnormal stapes-velocity transfer function, abnormal ear structure, air in the inner ear or fluid leak (failed half-cycle phase test), and unstable sensor sensitivity.

Table 3.1: Summary of experiments. (Experiments that were halted early due to different issues are not listed here).

Experiment Number	**Status**
39, 104, 116, 119, 124, 131, 165, 172, 178, 187, 189, 190, 199, 207, 209, 210, 212	Included for impedance calculation
106	AC stimulation included for impedance calculation. RW stimulation excluded due to inefficient coupling
36, 37, 71, 76, 79, 92	Excluded. Cannot ensure proper seal of pressure sensors
38, 41, 112, 125, 127, 160, 162, 174, 211	Excluded. Abnormal middle ear transfer function or anatomy
40, 41, 115, 162, 211	Excluded. Air in inner ear or fluid leak (failure of half-cycle test)
108, 118	Sensor calibration varied by more than 2 dB

2.5 Impedance Modeling

Based on the functional anatomy, the structures, impedances and volume velocity paths relevant to inner-ear sound transmission are presented in block diagrams in Figure 3.2. AC stimulation is presented in Figure 3.2A and RW stimulation in Figure 3.2B. The acoustic impedances are calculated based on experimental results.

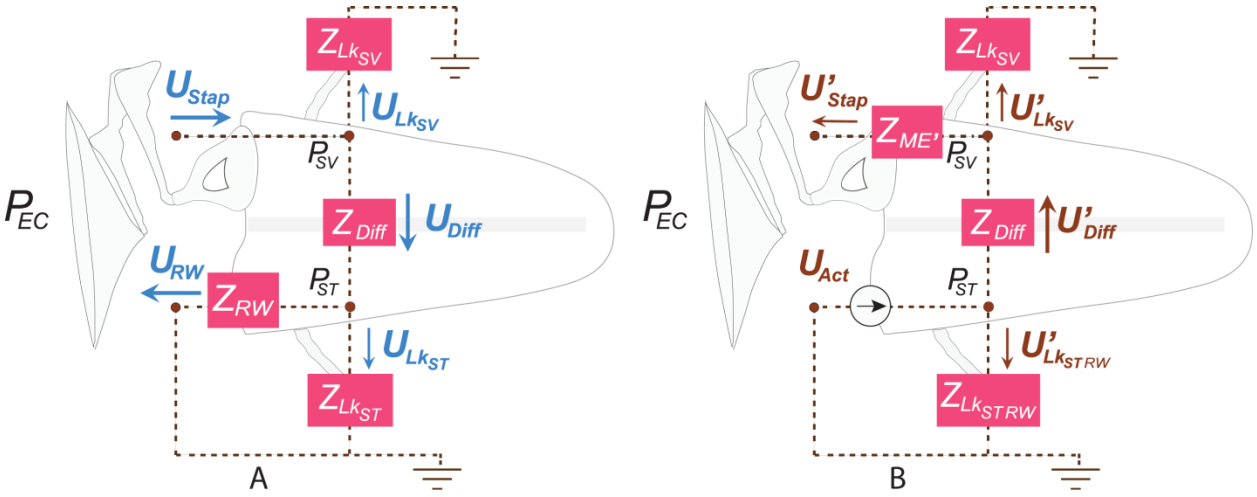

Figure 3.2 A) AC and B) RW stimulation impedance models. The path of the volume velocity changes based on the stimulation type. The impedances of our models do not change their values from AC to RW stimulation. A) For AC, the volume velocity enters through the stapes, across the cochlear partition (including the helicotrema) and out the RW. The AC model assumes the two-window hypothesis, and assumes the volume velocities through the leakage paths are negligible. B) For BC, the volume velocity enters through the RW via a mechanical stimulus and passes through the cochlear partition or a leakage area in the ST. If it passes through Z_{Diff} the volume velocity splits out into the leakage in the SV or middle ear. The leakage in the ST, Z_{lkST}, is not determined in this paper, but a combination of ST leakage and the leakage at the RW-actuator interface during RW stimulation, Z_{lkSTRW}, is estimated.

The blocks include: Z_{lksv} which accounts for any leakage or compressibility on the vestibular side of the cochlear partition, Z_{Diff} which accounts for both the cochlear partition and the helicotrema (Dallos 1970; Lynch, Nedzelnitsky, and Peake 1982; Dancer and Franke 1980) (the pressure across this block is the differential pressure across the cochlear partition), Z_{lkst}

which accounts for any leakage or compressibility on the scala tympani side of the cochlear partition, Z_{RW} is the impedance of the RW, $Z_{ME'}$ is the impedance of the middle ear looking out from the cochlea via RW stimulation, and Z_{lkstRW} which accounts for Z_{lkst} as well as leakage near the RW-actuator interface during RW stimulation. Associated with these impedances are P_{SV} which is the sound pressure in the scala vestibuli near the stapes, and P_{ST} which is the sound pressure in the scala tympani near the round window. There are also volume velocities that flow through each impedance block. In AC stimulation (3.2A) the stimulus volume velocity U_{stap} is estimated as the product of the measured stapes velocity and the area of the stapes footplate. In RW stimulation (3.2B) the stimulus volume velocity U_{act} is estimated as the product of the stimulator actuator velocity and the area in contact with the round window. $Z_{ME'}$ is not required to specify AC stimulation, and Z_{RW} is not required to specify RW stimulation. Detailed calculation of the five impedances from the measured sound pressures and stimulus velocities are explained in the results.

The choice of element values to model the impedances was performed using a least squares fit to both the magnitude and phase of the experimentally-derived impedance calculations. The equations used to calculate the Total Error and obtain a good fit of the data to the model are further explained in Appendix A3.

3. Results

3.1 Air Conduction Stimulation

The intracochlear sound pressures (P_{SV} and P_{ST}) were measured simultaneously with sound pressures in the ear canal (P_{EC}) and stapes velocity (V_{stap}). As shown in Figure 3.3, P_{SV} is higher than P_{ST} in magnitude for AC stimulation regardless of its reference (referenced to P_{EC} or V_{stap}) for a wide frequency range, except for the lowest and highest frequencies. P_{ST} is generally lower in magnitude due to its proximity to the high compliance (low impedance) RW membrane (Nedzelnitsky 1980; Lynch, Nedzelnitsky, and Peake 1982; Nakajima et al. 2009). As shown in Figure 3.3A, P_{SV}/P_{EC} peaks in magnitude around 700 Hz on average, but the frequency and the prominence of the peak varies among individuals. The phase is between 0 and 0.25 periods at low frequencies and decreases with increased frequency at a steady rate as it crosses zero near 700 Hz (the same location as the peak in the magnitude). Figure 3.3B shows that P_{ST}/P_{EC} dips in magnitude at about 600 Hz on average, but this dip ranges from 400-1000 Hz for the individual experiments. The phase starts at 0 periods, increases slightly from about 400-1000 Hz, and then decreases steadily as frequency increases.

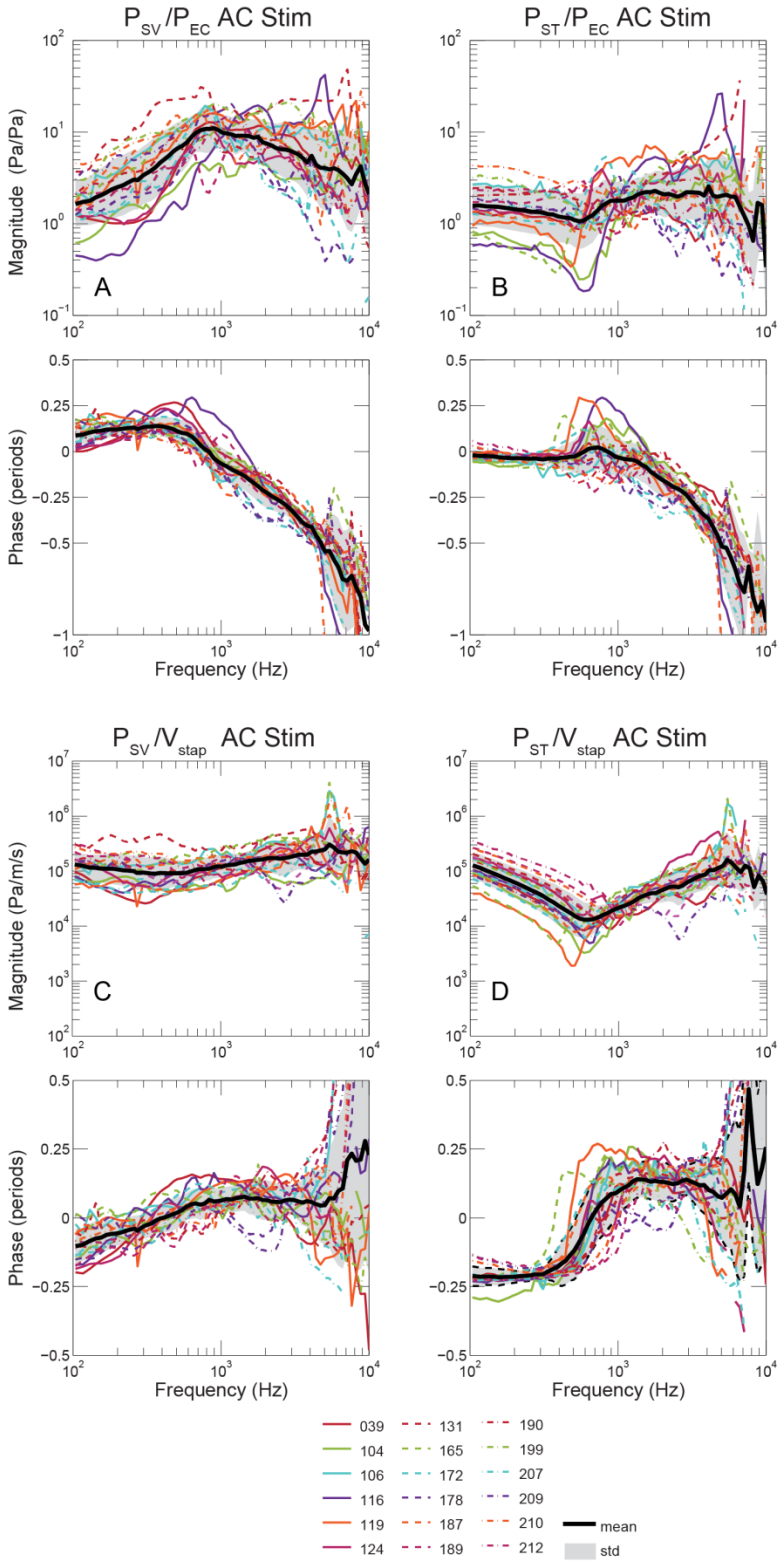

Figure 3.3: The magnitude and phase frequency responses of the intracochlear sound pressures referenced to P_{EC} (A, B) or V_{stap} (C, D), measured in 18 normal ears (colored lines). The mean is plotted as a thick black line and the standard deviation as the gray fill.

Because referencing the intracochlear pressure measurements to P_{EC} includes the effect of the middle-ear impedance, we plot intracochlear pressures referenced to V_{stap} to obtain transfer functions related to the input at the cochlea. P_{SV}/V_{stap}, plotted in Figure 3.3C has a magnitude that is generally flat over the measured frequency range with a shallow dip at lower frequencies (200-400 Hz) that is more notable in individual experiments. The phase at the lowest frequency is negative but steadily increases and plateaus slightly above 0 periods between 1000 and 4000 Hz. P_{ST}/V_{stap} (Figure 3.3D) dips in magnitude between 400-1000 Hz. The average smooths the sharp valleys of the individual magnitude measurements (which occur at different frequencies). The phase transitions from around -0.25 periods to almost 0.25 periods over the 100 – 6000 Hz range. This transition is steep in the individual experiments and occurs at frequencies from 400-1000 Hz, also varying across ears similarly to the magnitude valleys. The low-frequency magnitudes (below the valley) vary considerably, but maintain a -20 dB per decade slope across ears, while the phases are generally consistent at these low frequencies. This pattern is consistent with the dominance of a RW compliance at low frequencies but with the value of the RW compliance varying across ears.

3.2 Round Window Stimulation

During RW stimulation, the intracochlear sound pressures (P_{SV} and P_{ST}) were measured simultaneously with the actuator velocity (V_{act}). These data are seen in Figure 3.4. P_{SV}/V_{act} and P_{ST}/V_{act} are approximately equal during RW stimulation in both magnitude and phase. The magnitudes are high at low frequencies, decrease steadily up to 1-2 kHz, then level off. The phase of both P_{SV}/V_{act} and P_{ST}/V_{act} starts at about -0.25 periods at 100 Hz, increases to 0 periods

around 1000 to 2000 Hz, and increase further at higher frequencies. The individual pressures in RW stimulation are less smooth compared to the AC stimulation case.

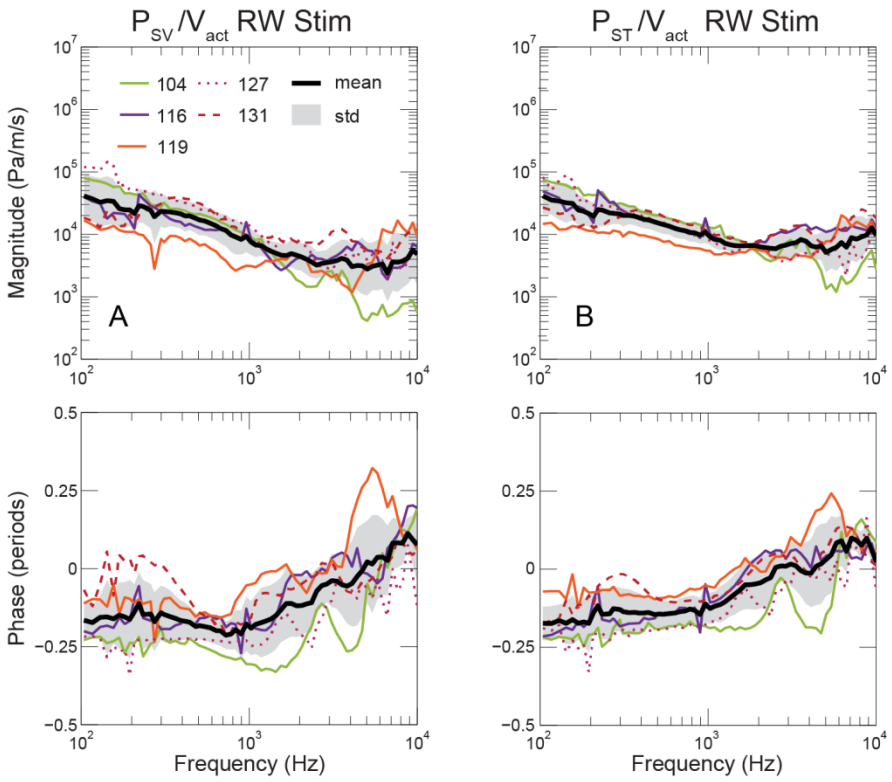

Figure 3.4: The intracochlear sound pressures measured in five ears with RW stimulation (colored lines). The pressures are referenced to the velocity of the actuator V_{act}. The mean is plotted as a thick black line and the standard deviation as the gray fill.

3.3 Impedance Calculations

In both AC and RW stimulation, volume velocity at the oval window was calculated as $U_{stap} = V_{stap} * A_{stap}$ where $A_{stap} = 3.22\ mm^2$ is the nominal area of the stapes footplate, consistent with the estimates of von Békésy et al. and Aibara et al. (Aibara et al., 2001; Georg von Békésy and Ernest Glen Wever, 1960) . In order to compute Z_{Diff} and Z_{RW}, we use AC stimulation measurements of U_{stap}, P_{SV}, and P_{ST} along with the assumption that $U_{stap} \approx U_{Diff} \approx U_{RW}$, as would be the case if $Z_{lksv} >> (Z_{Diff} + Z_{RW})$ and $Z_{lkst} >> Z_{RW}$ in Figure 3.2A. We also assume that the

cochlear walls are rigid and the cochlear fluid is incompressible (Kringlebotn 1995; Sim et al. 2012; Stenfelt, Hato, and Goode 2004a). With these assumptions:

$$Z_{Diff} = \frac{P_{SV} - P_{ST}}{U_{Diff}} \approx \frac{P_{SV} - P_{ST}}{U_{stap}}, \text{ and} \qquad \text{Eqn 3.1}$$

$$Z_{RW} = \frac{P_{ST}}{U_{RW}} \approx \frac{P_{ST}}{U_{stap}} \qquad \text{Eqn 3.2}$$

As shown in Figure 3.5A, Z_{Diff} magnitude and phase is fairly flat across frequency, but the phase at low frequencies is consistently above zero periods for all experiments. In Figure 3.5B, the magnitude of Z_{RW} at low frequencies (below 400-700 Hz) starts high and decreases at around 24dB/decade, with a corresponding phase of around -0.25 periods. At frequencies between 700 and 7000 Hz, Z_{RW} increases in magnitude by around 22dB/decade and with a constant mean phase of about 0.15 periods.

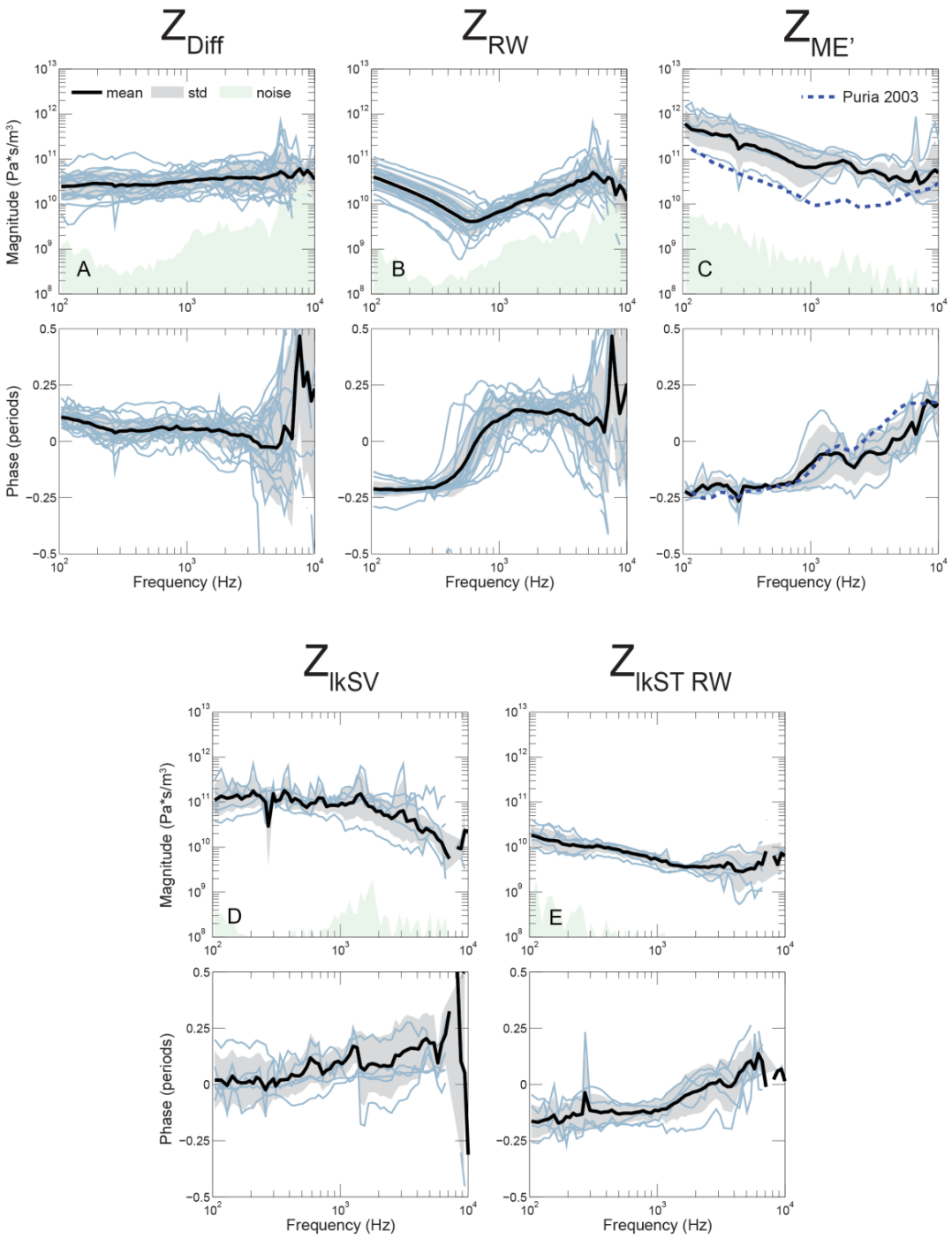

Figure 3.5: Impedance Magnitude and Phase Frequency Response Plots. The acoustic impedances were calculated for the A) differential across the partition (at the base which includes the influence of the helicotrema) Z_{Diff}, B) round window Z_{RW}, C) reverse middle ear $Z_{ME'}$, D) leakage in the scala vestibuli Z_{lkSV}, and E) leakage in the scala tympani and RW Z_{lkSTRW}. Individual experiments are plotted in light blue lines, the geometric mean in black lines, & the standard deviation in a gray fill and a noise floor estimate in light green fill. Results from Puria 2003 are also plotted in C. Only data with SNR of at least 10dB are plotted.

Measuring intracochlear sound pressures and stapes volume velocity during RW stimulation (U'_{stap} in Figure 3.2B) allows the determination of the impedance of the middle ear driven in reverse ($Z_{ME'}$ in Figure 3.2B, which includes the effects of the stapes, other ossicles, middle-ear ligaments, TM and ear canal). The reverse middle ear impedance is simply related to P_{SV} and U'_{stap} measured during RW stimulation:

$$Z_{ME'} = \frac{P_{SV}}{U'_{stap}} \qquad \text{Eqn 3.3}$$

To compute Z_{lkSV} we assume Z_{Diff} has the same value for AC and RW stimulation. Then we calculate the volume velocity U'_{Diff} (across Z_{Diff}) during RW stimulation using the measured intracochlear sound pressures:

$$U'_{Diff} = \frac{P_{ST} - P_{SV}}{Z_{Diff}} \qquad \text{Eqn 3.4}$$

The model of Figure 3.2B then specifies the leakage volume velocity during RW stimulation U'_{lkSV} to equal the difference between U'_{Diff} and U'_{stap}:

$$U'_{lkSV} = U'_{Diff} - U'_{stap} \qquad \text{Eqn 3.5}$$

and the impedance Z_{lkSV} is:

$$Z_{lkSV} = \frac{P_{SV}}{U'_{lkSV}} \qquad \text{Eqn 3.6}$$

Computations of the volume velocity and impedance of the ST leakage path were complicated by possible differences between the volume velocity produced by the round window stimulation and U_{RW}. Such a difference could result from the difference in area between the smaller RW actuator and the RW itself. This area difference would allow some of the actuator volume velocity to leak around the actuator and out the uncoupled RW area. Because of this uncertainty we use the RW stimulation methods to estimate the impedance of a *combination* of the ST and RW leakage path (Z_{lkSTRW}). The volume velocity of the actuator (U_{act}) is calculated by multiplying the velocity of the actuator times the diameter of the rod (1 mm) touching the RW membrane. We first compute the leakage volume velocity and then solve for the impedance:

$$U'_{lkSTRW} = U_{act} - U'_{Diff} \qquad \text{Eqn 3.7}$$

$$Z_{lkSTRW} = \frac{P_{ST}}{U'_{lkSTRW}} \qquad \text{Eqn 3.8}$$

The three impedances calculations using the RW stimulation data are also illustrated in Figure 3.5 (C, D, E). $Z_{ME'}$, the impedance looking out of the cochlea through the middle ear (Figure 3.5C) has a high impedance magnitude and phase of -0.25 periods at low frequencies. At higher frequencies, the $Z_{ME'}$ magnitude starts to flatten out with frequency and the phase approaches 0.25 periods. Also plotted in Figure 3.5C is the $Z_{ME'}$ estimated by Puria et al., 2003 (Puria 2003). The Puria estimate is about 7 dB lower in magnitude than our mean results with RW stimulation.

The SV leakage impedance Z_{lkSV} from Eqn. 3.6 (Figure 3.5D) is similar or even slightly lower in magnitude to $Z_{ME'}$ with a less intense decline across frequency. The phase is 0 periods at low frequencies and slowly increases to almost 0.25 periods.

The combination of leakage at the ST and around the RW actuator during RW stimulation, Z_{lkSTRW}, (Figure 3.5E) is nearly an order of magnitude lower than Z_{lkSV} across all frequencies. The phase starts at -0.25 periods and increases steadily to 0 periods at high frequencies.

3.4 Computational Modeling of Impedances

We modeled the five computed impedances with basic circuit components (i.e. resistance, conductance, and inductance) using simple component combinations based on anatomical considerations with element values fitted to the experimental data using least squares techniques (Figure 3.6). At frequencies above a few kHz, mean magnitude and phase are influenced by large variations in the individual measurements. Furthermore, the stapes motion at frequencies above 2 kHz becomes less piston-like and incorporates a rocking motion that is not measured well by our one point LDV measurement (Hato, Stenfelt, and Goode 2003; Heiland et al. 1999; Sim et al. 2010). Therefore we focused our analysis and modeling to the frequency range between 100 - 2000 Hz. Separate sets of element values (Table 3.2) were fit to the average data and to two individual experiments for each impedance that were selected because their magnitudes fell just outside the standard deviations in Figure 3.5. The two individual experiments for each impedance are described in Table 3.2 as “Experiment Hi” and “Experiment Lo” in order to model the extremes of the impedance magnitude range across

ears; the individual experiment numbers are listed in brackets on each figure legend. Table 3.3 lists the root mean square error of the difference between the model and fitted data at frequencies below 2 kHz. This Total Error is the combined error of the model and measured magnitudes and phases (described in Appendix A3).

Table 3.2: Circuit values for the acoustic impedance models. R = resistor, C = capacitor, L = inductor. In the average Z_{RW}, RW parameters R and L are iterated for N = 6. Experiment Hi and Lo represent the range of impedance variability across ears. For the individual Z_{RW}, RLC are in series. For experiment 116: R = $2.04\text{x}10^{9}$, L = $1.77\text{x}10^{6}$, and C = $4.13\text{x}10^{-14}$. For experiment 189: R = $4.19\text{x}10^{9}$, L = $1.36\text{x}10^{6}$, and C = $1.80\text{x}10^{-14}$.

Impedance	Orientation	Parameter	SI Units	Average	Experiment Hi	Experiment Lo
					Exp 199	Exp 172
Z_{Diff}	Parallel	R_{Diff}	N s m^{-5}	$3.04\text{x}10^{10}$	$5.18\text{x}10^{11}$	$1.58\text{x}10^{10}$
		L_{Diff}	N s^2 m^{-5}	$6.46\text{x}10^{7}$	$1.66\text{x}10^{8}$	$1.34\text{x}10^{7}$
					Exp 212	Exp 119
Z_{RW}	Foster Network / Series	R_{RW}	N s m^{-5}	$5.00\text{x}10^{7}$	$6.33\text{x}10^{9}$	$6.32\text{x}10^{8}$
		L_{RW}	N s^2 m^{-5}	$7.30\text{x}10^{5}$	$1.24\text{x}10^{6}$	$1.47\text{x}10^{6}$
		C_{RW}	N^{-1} m^5	$3.59\text{x}10^{-14}$	$1.38\text{x}10^{-14}$	$7.62\text{x}10^{-14}$
					Exp 127	Exp 119
$Z_{ME'}$	Series	$R_{ME'}$	N s m^{-5}	$4.76\text{x}10^{10}$	$8.40\text{x}10^{10}$	$2.74\text{x}10^{10}$
		$L_{ME'}$	N s^2 m^{-5}	$7.78\text{x}10^{5}$	$8.60\text{x}10^{5}$	$8.68\text{x}10^{5}$
		$C_{ME'}$	N^{-1} m^5	$2.56\text{x}10^{-15}$	$1.01\text{x}10^{-15}$	$1.13\text{x}10^{-14}$
					Exp 127	Exp 104
Z_{lkSV}	Series	R_{lkSV}	N s m^{-5}	$9.80\text{x}10^{10}$	$4.30\text{x}10^{10}$	$1.18\text{x}10^{10}$
		L_{lkSV}	N s^2 m^{-5}	$5.00\text{x}10^{6}$	$4.70\text{x}10^{6}$	$2.00\text{x}10^{6}$
					Exp 127	Exp 119
Z_{lkSTRW}	Series	R_{lkSTRW}	N s m^{-5}	$4.10\text{x}10^{9}$	$2.71\text{x}10^{9}$	$4.19\text{x}10^{9}$
		C_{lkSTRW}	N^{-1} m^5	$7.49\text{x}10^{-14}$	$5.00\text{x}10^{-14}$	$3.04\text{x}10^{-13}$

Table 3.3: Root mean square total error between model and experimental data including log magnitude and phase error up to 2kHz. The smaller the number, the better the model fits to the experimental data.

	Z_{Diff}	Z_{RW}	$Z_{ME'}$	Z_{lkSV}	Z_{lkSTRW}
Average	0.094	0.052	0.114	0.182	0.149
Experiment Hi	0.176	0.164	0.086	0.128	0.148
Experiment Lo	0.186	0.159	0.300	0.430	0.217
[116]		0.118			
[189]		0.070			

Figure 3.6: Impedance plots and models. For experimentally obtained impedances, the average is in thick black lines. The “Experimental Hi” and “Experimental Lo” are representative magnitude extremes of the total range of each impedance measured (Note, each “Experimental Hi” and “Experimental Lo” differ in experiment number, as listed in brackets); they are plotted in thin solid lines. Our model was fit to the three experimental curves up to 2 kHz, plotted with dotted and dashed thick lines. The gray high-frequency (>2 kHz) area indicates the region where the data is not used for model fitting. A) Z_{Diff} B) The average Z_{RW} data is best fit with the black circuit. The individual data are best fit with the red circuit. Because of the large variability in experiments, two additional experiments are modeled. C) $Z_{ME'}$ D) Z_{lkSV} E) Z_{lkSTRW}. Only data with SNR of at least 10dB are plotted.

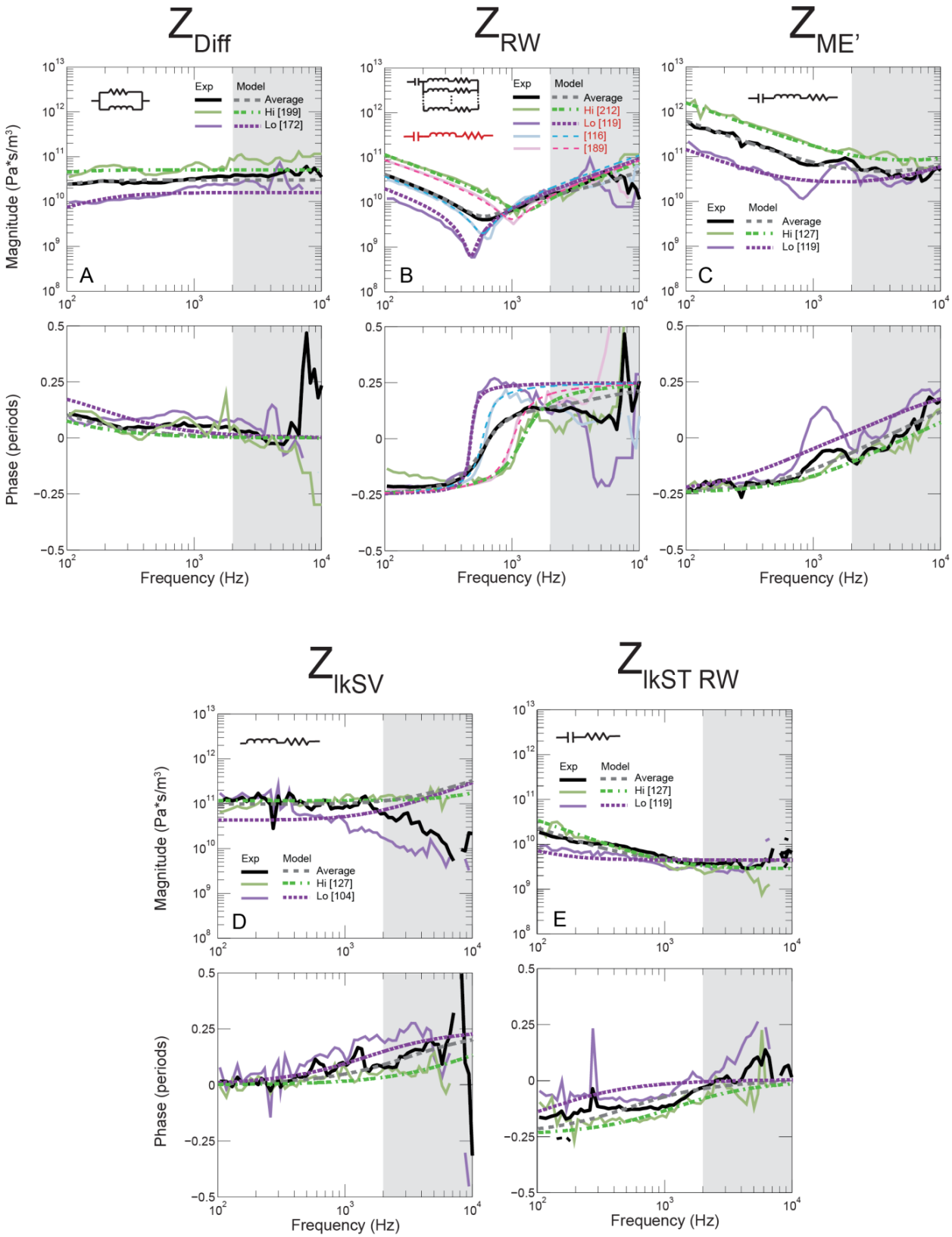
Z_{Diff}
Z_{RW}
$Z_{ME'}$
Z_{lkSV}
$Z_{lkST\ RW}$
Magnitude (Pa*s/m³)
Phase (periods)
Frequency (Hz)
Exp
Model
Average
Hi [199]
Lo [172]
Hi [212]
Lo [119]
[116]
[189]
Hi [127]
Lo [119]
Hi [127]
Lo [104]
A
B
C
D
E

3.4.1 Differential Impedance (Z_{Diff})

The magnitude of Z_{Diff} (Figure 3.6A) is relatively independent of frequency with a phase near zero, as is consistent with a simple resistance. However, the phase at low frequencies is consistently (for all experiments, Figure 3.5A) greater than zero, which can be modeled with the addition of a parallel inductor that can be attributed to the helicotrema, where the resistor represents the wave impedance of the cochlear partition and surrounding fluid (Lynch, Nedzelnitsky, and Peake 1982). The influence of the inductor (and helicotrema) is to shunt volume velocity around the partition resistance at low frequencies. The combined total error for the fit of the Z_{Diff} model to the average data was lower (0.094) than the fits to the individual data, and was the second lowest error for all the model fits. The individual data has approximately double the total error as compared to the average.

3.4.2 Round Window Impedance (Z_{RW})

The magnitude and phase of Z_{RW} (Figure 3.6B) at frequencies below 400-700 Hz is well modeled with a capacitor, analogous to the acoustical compliance of the RW membrane. The magnitude of Z_{RW} at frequencies of 700 Hz to 2 kHz is well modeled by the addition of a series inductor and resistor – an acoustic mass and resistance. Due to large difference between individual experiments, two additional representative experiments are modeled ([116] and [189] in Figure 3.6B). The model fits the experimental data very well up to 1 kHz, and reasonably well up to 2 kHz (the total error is lower than 0.17). However, a simple series combination of the three elements does not match the average Z_{RW} phase, which is lower than 0.25 periods phase above 1 kHz. To account for this lower phase, a model in which the mass

and resistance change with frequency is necessary. We chose an iterated Foster network of resistors and inductors (N=6 branches), as described in Nakajima et al. (2009), to better fit the average phase data. Using a Foster network model for the individual data did not improve the fit to the data; therefore the simpler RLC circuit was used for the individual plots.

3.4.3 Reverse Middle Ear Impedance ($Z_{ME'}$)

$Z_{ME'}$ (Figure 3.6C) at low frequencies has an impedance magnitude that decreases with increasing frequency and a phase of -0.25 periods, suggesting a compliance related to the acoustic compliance of the annular ligament surrounding the oval window as well as compliant characteristics of the middle-ear chain including the tympanic membrane. At higher frequencies the magnitude becomes more constant with frequency and the phase approaches 0.25 periods – evidence of a series inductor and resistor. From the perspective of the vestibule the inductance is probably related to the mass of the middle-ear ossicles and tympanic membrane. The resistor may reflect losses in the middle ear. The circuit models the experimental data well at low frequencies. Notice that the value of $C_{ME'}$ is an order of a magnitude smaller than that of C_{RW} for the three models in Table 3.2, such that the magnitude of the middle ear impedance at low frequencies is an order of magnitude greater than the magnitude of the RW impedance. The average and Experiment Hi have errors of 0.114 and 0.086 respectively. Experiment Lo has a higher total error (0.300) due to additional frequency dependences in the magnitude and phase data between 500 and 2000 Hz.

3.4.4 Scala Vestibuli Leakage Impedance (Z_{lkSV})

The SV leakage impedance (Figure 3.6D) has a magnitude that is generally flat but sometimes decreases above a kHz, and a phase that increases from 0 to 0.25 periods as frequency increases. Assuming the leak was similar to an open tube, we chose to fit this with the series combination of a resistor and inductor. The best-fit model is Experiment Hi with a total error of 0.128. Experiment Lo has the highest total error of all impedance fits (0.430) because the magnitude decreases at high frequencies while the phase increases, behavior that is inconsistent with a series combination of a resistor and inductor. For similar reasons, the fit to the mean data produce a relatively high error of 0.182.

3.4.5 Scala Tympani and Round Window Leakage Impedance (Z_{lkSTRW})

The ST and RW leakage impedance (Figure 3.6E) has a low-frequency magnitude that decreases with frequency and flattens out above 1 kHz; the phase increases with frequency from -0.25 to 0 periods. We modeled this impedance with a resistor and capacitor in series, where the capacitor may represent some of the leakage around the round window stimulator and the resistance models the impedance of a narrow tube. Experiment Hi is fit with the lowest error of the three models at 0.148. The fit to the average and Experiment Lo yields total errors of 0.149 and 0.217 respectively.

4. Discussion

In this paper we present the data and best-fit models that describe the mechano-acoustic measurements of human temporal bone specimens without noticeable mechano-

acoustic pathologies. To obtain our most reliable estimates of the normal case, we improved our experimental techniques and implemented strict inclusion criteria to represent healthy specimens and accurate intracochlear pressure measurements. The criteria include normal anatomy, normal ossicular velocity with respect to AC input sound pressure (similar to Rosowski et al. 2007), no evidence of air in the inner ear (checked by measurements described above), and high repeatability of our pressure sensor sensitivity. Implementing these criteria decreased the measurement variability within our population. We then used selected results to compute and model the impedances of structures within and surrounding the inner ear. These analyses quantify how sound is transmitted within the normal inner ear during AC and other forms of cochlear stimulation. The description of middle-ear function based on our selected measurements is valuable for our computational models as well as other analyses (e.g. Puria et. al. 2003, Elliott et. al. 2016, Stenfelt 2015) requiring accurate estimates of sound transmission in the human ear.

Our population of 'normal' measurements included velocity and pressure data that were similar but not identical across ears. This variability may be related to differences in anatomy and mechanical properties of middle-ear and inner-ear structures. While the average of the experiments provides a simple way to compare our data to pre-existing and future data, averaging inevitably smooths the frequency responses, and thus does not represent the frequency variations seen in the responses of individual ears. For some data types, there are considerable variations in the frequency-dependence seen across ears, resulting in an average that is not representative of individual ears. Therefore, we also model the results from individual ears (Figure 3.6).

4.1 Impedance Calculations and Modeling

Z_{Diff} represents the differential impedance of the cochlear partition and scala fluids including the helicotrema measured at the base of the cochlea (Figures 3.2 & 3.5A). The magnitude of Z_{Diff} is generally independent of frequency, and has a relatively small standard deviation across ears of about ±5 dB (a logarithmic standard deviation of a factor of 1.6). The phase is slightly above 0 (0.1±0.05 periods) at low frequencies. The components used to model Z_{Diff} (Figure 3.6A) are the same as Elliott et al. 2016 and has a parallel orientation as similar to the model of Lynch et al. 1982. The model resistance accounts for the distributed partition and scala impedance (Zwislocki 1963), while the parallel inductor can be attributed to the helicotrema (Dallos 1970). (Note, Z_{Diff} differs from previous reports of Z_C, the "cochlear impedance," in that $Z_C = Z_{Diff} + Z_{RW}$.) Despite limiting our model fit to data from 100 to 2000 Hz, the model matches the data well up to 7000 Hz.

Z_{RW} represents the impedance of the round window and the contributions of the fluids entrained by its motion (Figures 3.2 & 3.5B). During AC stimulation, we assume any volume velocity leakage out of ST (though Z_{lkST}) is insignificant because Z_{lkST} is greater in magnitude than the combination of $Z_{RW} + Z_{Diff}$ (consistent with the two-window hypothesis). Z_{RW} has a similar frequency response shape across ears, but at low frequencies the magnitude varies moderately across ears (a standard deviation of 6 to 7 dB), and all experimental data demonstrate the characteristics of a capacitor below 400Hz (with a phase angle of -0.25 to -0.18 in Figure 3.5B). We attribute this compliant behavior to the RW membrane's flexibility, where the variations may be related to variations in the membrane's thickness, size and shape across ears, consistent with our observation of significant variety in the RW anatomy across ears. At

frequencies above 1000 Hz the magnitude of Z_{RW} is less variable (a logarithmic standard deviation of a factor of 1.5 equivalent to 3-4 dB), which suggests the mass term (which we associate with the effective mass of fluid entrained with the RW membrane at high frequencies) is more similar across ears.

In this study we fit our models to the data at frequencies of 2 kHz and below (resulting in deviation between model and data for high frequencies). The models chosen to describe the average and individual Z_{RW} data do reasonably well up to 2 kHz, but at higher frequencies, the phase data is generally limited below 0.13 periods while the model goes to 0.25 periods. This difference could be due to the complex motion of the stapes above 2 kHz – the addition of complex modes produces less smooth data and could produce some downward shift in the phase data. The four individual data are modeled in a similar manner (RLC) as in Elliott et al. 2016. Above 1 kHz, the model phase does not perfectly fit the data in both Elliott et al. 2016 and this present study.

Our Z_{RW} element model for the average data is similar to the model used by Nakajima et al. 2009 (Figure 3.6B). The Foster form iterated network of the resistor and inductor leads to frequency dependence in the network resistance and inductance, and represents a distributed system. Thus, similar to the data, the phase above 1 kHz in the model is flat at about 0.13 periods instead of the 0.25 periods (as in a simple RLC); this high frequency phase was closely modeled in (Nakajima et al. 2009). However, the average data is not a good representation for any individual experiment as the sharp magnitude valleys and steep phase transitions are lost in averaging the data. While capturing the average well, the Foster network was not able to fit the magnitude peaking and steep phase change relative to frequency of the individual data.

$Z_{ME'}$ is the reverse impedance load of the middle ear (the load affected by the oval window annular ligament, ossicles, middle-ear cavity, tympanic membrane, and ear canal) measured during sound transmission from the inner ear to the ear canal that results from RW stimulation (Figure 3.5C). Variations in reverse middle ear impedance $Z_{ME'}$ magnitudes are largest at frequencies less than 800 Hz (standard deviations of ±10 dB). However, the phase is consistent across experiments with a value of -0.25 periods at the lowest frequencies, implying compliant behavior due to the flexible components of the middle ear (e.g. OW, ossicles, tympanic membrane, etc.), moving towards 0 as frequency increases. At mid-to-high frequencies, the variation in magnitude is smaller, but the variation in phase is increased. Puria 2003 also estimated $Z_{ME'}$ by stimulating the scala tympani with a hydrophone (Puria 2003). His $Z_{ME'}$ estimated is about 7 dB lower in magnitude than our results. The cause of this discrepancy could be due to different measurement techniques. Puria 2003 used a hydrophone to drive the middle ear in reverse, while we used stimulation of the round window. Puria 2003 also found that comparison of no occlusion and different volumes of air with occlusion did not change the reverse middle-ear impedance $Z_{ME'}$. In our setup we had a large volume of air between speaker and ear canal. We found, similar to Puria 2003, that $Z_{ME'}$ remained stable whether the speaker was connected or removed (open system) during RW stimulation. We modeled $Z_{ME'}$ with a compliance, mass, and resistance in series (Figure 3.6C). Elliott et al. 2016 also estimated the impedances described above using a combination of data (our early Nakajima et al. 2009 data and Puria et al. 2003 data) with a similar lumped-element model. Despite limiting our model from 100 Hz to 2 kHz, the model fits well up to 10 kHz for the average and Hi Experiment.

Z_{lkSV} represents the combination of sound leakage paths between the scala vestibuli and the exterior of the otic capsule in our temporal bone preparation (Figure 3.5D). These could include the vestibular aqueduct, and any vascular and neural channels that penetrate the bone around the vestibule and scala vestibuli (Georg von Békésy and Ernest Glen Wever 1960; Otto F. Ranke 1953). The standard deviation within our estimates of Z_{lkSV} is about ±6-7 dB. To fit the phase response, we model the SV leakage impedance with a resistor and inductor (Figure 3.6D), similar to the model of Elliott, Ni, and Verschuur 2016. As seen in Figure 3.6D, there is a reasonable match between a simple RL circuit model and both the averaged data and experiment Hi data below 2 kHz. Many of the discrepancies happen above 2 kHz (though with experiment Lo discrepancies happen below 2 kHz) where the single-point laser measurements made are less reliable due to the addition of complex motion of the stapes. It is also possible that calculation of the leakage impedance for that ear was unusually affected by compounding of errors from the pressure sensor sensitivity calibrations. The variability of Z_{lkSV} across experiments suggests significant anatomical differences across ears (e.g. in the dimensions of the vestibular aqueduct (Elliott, Ni, and Verschuur 2016; Saliba et al. 2012)), but may also reflect its computational dependence on a difference between two volume velocities of similar magnitude (Eqn. 3.5).

Z_{lkSTRW} (Figure 3.5E) is the leakage path of the scala tympani and round window during RW stimulation. The dominant leakage path from the ST is likely due to the incomplete coupling between the interface of the actuator and the RW membrane (e.g. volume velocity leakage where the actuator does not directly touch the RW membrane) and the cochlear aqueduct. We model the ST and RW leakage impedance with a resistor and capacitor (Figure 3.6E). This is

different than other models that represent just Z_{lkST} (RLC circuit from Stenfelt et al. 2016 or RL circuit in Elliot et al. 2016). The capacitor element is used to model the low frequency phase, and may be needed to explain any volume velocity leaks in the areas of the RW that surround the areas directly coupled to the actuator. To separate the contribution of imperfect actuator coupling, we need to better define the actual volume velocity of the RW that is induced by mechanical RW stimulation. An alternative method is to determine Z_{lkST} by measuring stapes velocity and intracochlear pressures in the normal condition and then with the immobilization of the RW membrane during AC stimulation. To specifically determine the impedance of the cochlear aqueduct, one could also experimentally block the cochlear aqueduct. Anatomical measurements of the vestibular and cochlear aqueducts could also provide estimates of their impedances, as we performed for cat in John J. Rosowski, Bowers, and Nakajima 2017.

Our measurements and models demonstrate that some of the acoustical properties of inner-ear and middle-ear structures (embodied in the acoustic-impedance elements of our model) can be very similar across ears, while other structures vary across individuals. The model and defined parameters are powerful tools to understand complex sound transmission mechanisms, the effects of pathologies that change inner-ear impedances such as superior canal dehiscence, and consequences of implants that changes impedances surrounding the inner ear such as cochlear and vestibular implants. Various computational models from simple lumped-element model as used here to more complex 3-D models, such as finite element models, can also benefit from our measurements and models which describe the impedances and other transfer functions important in characterizing sound transmission in the human ear.

4.2 Errors and Variability in Estimating SV Leakage Impedance

To compute Z_{lkSV}, assumptions are made and multiple equations are used. Every pressure calculation (particularly difference calculations) has some error associated with the solution; and the need for multiple calculations can compound any error made in the pressure measurements. Although the error in the intracochlear sound pressure measurement was kept to a minimum (e.g. less than 2 dB shift from the start to the end of the experiment), accumulation of those small errors in the calculations can make significant errors in the final result. Small errors in the measured volume velocity of the stapes and volume-velocity calculated from differential pressure could in particular contribute to errors in the leakage impedance estimates (Eqn 3.4 & 3.5). Figure 3.7 illustrates the ratio of U_{stap} and U_{Diff} during RW stimulation. If we have accurately defined the leak in the SV, the differential volume velocity U_{Diff} should be larger than the stapes volume velocity U_{stap} (a ratio of less than 1 in Figure 3.7), and this is generally the case; most experiments remain below 1 (dashed line) for frequencies up to 2 kHz, as seen by the thick black line representing the average. The model chosen for Z_{lkSV} fits reasonably well up to 2 kHz (Figure 3.6D), but could use improvement. Future experiments will focus on improvements in the quantification of round-window volume velocity, which will decrease the dependence on assumptions of equal volume velocity during air conduction stimulation.

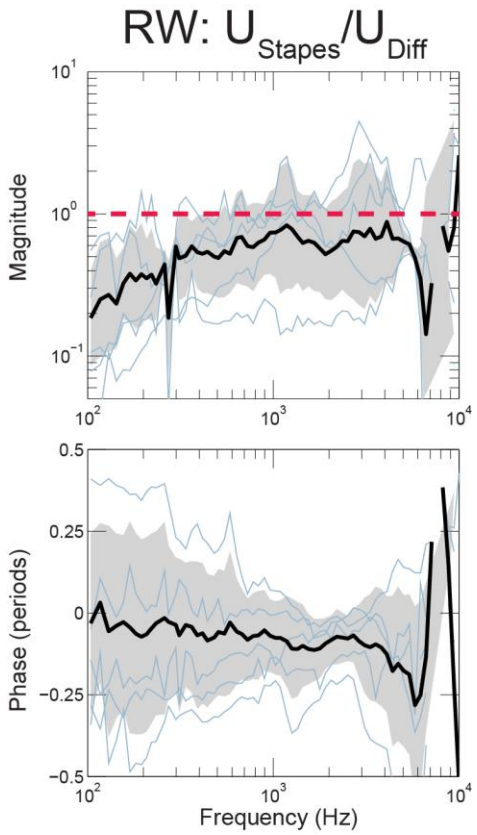

Figure 3.7: Ratio of volume velocities through the stapes oval window to the differential volume velocity (velocity across the cochlear partition and helicotrema), computed during round window stimulation. The ratio should have a magnitude lower than 1 (dashed line); almost all are below this level for frequencies up to 1kHz. Data are only plotted if the SNR of the U_{stap} measurement is at least 10dB.

4.3 Two-window Hypothesis

In this study, a major assumption made for AC stimulation is the two-window hypothesis, where significant volume velocity flows only through the round and oval windows. In order to determine if this approximation is appropriate, we compare the averaged calculated impedances and standard deviation of Z_{lkSV} and Z_{Diff} in Figure 3.8. If the two-window hypothesis holds during AC stimulation, differential pressure impedance, Z_{Diff}, should be considerably lower in magnitude than the leakage impedance, Z_{lkSV}. If the impedance of Z_{lkSV} is lower than or approximates Z_{Diff} at any frequency, then there is likely some significant volume velocity flow

exiting through the Z_{lkSV} during AC stimulation. Up to 500 Hz the average Z_{lkSV} is at least four times (average ten times) the magnitude of Z_{Diff} but this difference falls to a factor less than two by 2kHz.

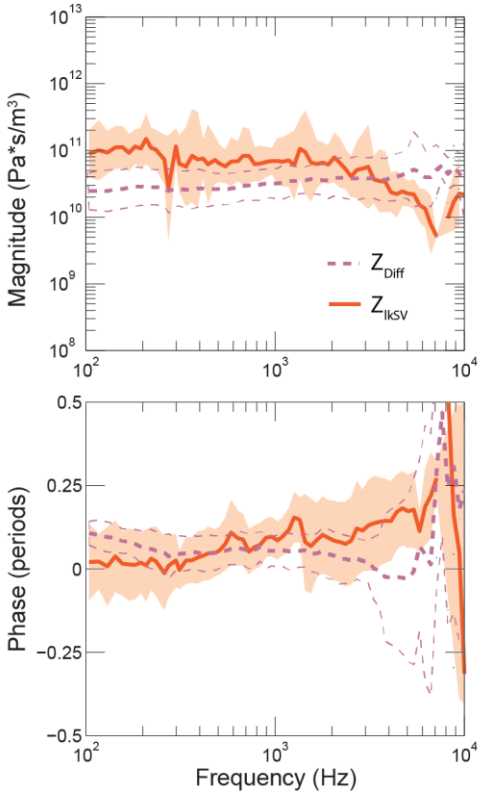

Figure 3.8: Average and standard deviations of the differential and SV leakage impedances. The leakage impedance, Z_{lkSV}, is on average greater in magnitude than Z_{Diff} up to about 2 kHz, where they start becoming comparable. The standard deviations are indicated by dashed lines for Z_{Diff} and shading for Z_{lkSV}.

The above finding is not contradictory to the work of Stenfelt et al. (2004a). The general conclusion of that past work is that the two-window hypothesis holds during AC from experiments showing similar volume velocities for OW and RW (Figure 3.5 of Stenfelt et al. 2004a). However, close inspection of this data also shows frequency-dependent deviation between oval and RW volume velocities (Figure 3.6 of Stenfelt et al. 2004a). At higher frequencies the deviation between individual experiments is greater (4 dB, factor of 1.6) than

that at low frequencies (<2dB, factor of 1.3) and there are more instances of the ratio growing and shrinking across higher frequencies. Furthermore, the individual ratio of the RW to OW volume velocity for each experiment are between 0 to -4dB below 500Hz indicating the RW volume velocity is less than the OW volume velocity. Therefore, there is variability across ears and in some ears there is a visible volume velocity loss between the OW to the RW, as shown in Stenfelt et al. 2004a, consistent with what we show in our present study. However, given that the volume velocity losses are small, the two-window hypothesis generally holds well for AC stimulation, especially at low frequencies.

5. Conclusions

In this study of fresh cadaveric normal ears we provide a carefully selected set of simultaneous measurements of intracochlear pressures in SV and ST, near the otic capsule at the base of the cochlea. These pressures are normalized with stapes velocity during AC and RW stimulation and ear canal pressure during AC stimulation.

From these measurements, component acoustical impedances are calculated and fit to simple lumped element models: The differential impedance, Z_{Diff}, is represented by a resistance due to distributed partition and scala impedance and a parallel fluid mass, due to the helicotrema. The impedance through the RW, Z_{RW}, has compliant behavior due to the flexibility of the RW membrane. A mass and resistor in series can generally simulate the individual data well for frequencies below 2 kHz. However, in the average data the iterated network of a mass and resistance leads to a frequency dependent network to represent a distributed system, consistent with less than ¼ cycle phase at higher frequencies. The reverse middle ear

impedance, $Z_{ME'}$, contains a mass to account for the OW, annular ligament, ossicles, TM, and middle ear cavity. Its compliance is likely dominated by the flexibility of OW owing to the annular ligament, and the entire middle-ear chain. The leakage in the SV, Z_{lkSV}, is represented by a resistor and inductor and is a combination of leakage between SV and exterior of the otic capsule. It is likely the vestibular aqueduct or small channels that innervate the SV. The leakage in the ST and RW, Z_{lkSTRW}, is represented by a resistor and capacitor and is perhaps the cochlear aqueduct. The compliance is likely due to volume velocity leaks at the RW surrounding the actuator-RW interface.

The simple lumped-element models help us understand complex sound transmission mechanisms, effects of pathologies that change inner-ear impedances, and the consequences of implants that change impedances surrounding the inner ear. Finally, we showed that individual measurements can be fitted to this model, which allows us to study the large variations in different specimens.

CHAPTER 4.

Improving round window stimulation with an interface coupler

Submitted to Otology and Neurotoloty in January 2019

Darcy L. Frear[1,2], Hideko Heidi Nakajima[1,2,3]
[1]*Speech and Hearing Bioscience and Technology Program, Harvard University, Boston, MA, USA*
[2] *Eaton-Peabody Laboratories, Massachusetts Eye and Ear, Boston, MA, USA*
[3] *Department of Otolaryngology, Harvard Medical School, MA, USA*

Abstract:

Hypothesis:

To mechanically stimulate the round window (RW) membrane, an actuator with a novel interfacing coupler (IC) greatly improves sound transmission to the cochlea as compared to RW-stimulation devices implanted today or other designs.

Background:

A variety of hearing pathologies resulting in mixed and conductive hearing loss can be addressed by mechanically stimulating the RW to transmit sound to the cochlea. This RW stimulation is accomplished clinically using the floating mass transducer (FMT, Med-El), which has poor acoustic quality and unreliable device positioning. Here we show proof of concept of an IC prototype designed to address some of the shortcomings of other RW stimulation methods.

Methods:

Comparison was made between RW stimulation using the IC with an actuator and an FMT in a fresh human temporal bone. Velocities of stapes, FMT, and IC actuator were measured with laser Doppler vibrometry to determine bandwidth, linearity, and dynamic range of the devices and cochlear sound transmission.

Results:

Stimulation with the proposed IC provided a linear output for larger dynamic range and wider frequency range as compared to the FMT. The IC also produced an increase in sound transmission ratio as compared to the FMT.

Conclusions:

We showed proof-of-concept that our prototype IC stimulates the RW membrane with improved acoustic performance as compared to the FMT. This paves the way for the development of a safe, effective and mechanically RW stimulator.

Introduction

Conductive hearing loss (CHL), a reduction in sound transmission from the external environment to the inner ear, accounts for a significant portion of the hearing loss experienced by patients. There are a variety of pathologies causing this reduction, such as an abnormal or absent outer or middle ear, and Eustachian tube dysfunction leading to non-aerated middle-ear cavity. Although there are treatments to correct some forms of CHL, for a variety of chronic CHL pathologies, treatment can be challenging and can fall short of acceptable hearing. For example, prosthetic replacement surgery to reconstruct a large segment of the middle-ear apparatus is difficult and has a high failure rate, and even when successful often falls short of attaining near-normal function (Lee and Schuknecht 1971; Brackmann, Sheehy, and Luxford 1984; Merchant et al. 2003).

For patients with a functioning inner ear (or slight sensorineural hearing loss) with a pathological sound-transmission mechanism, bone conduction hearing aids are a potential

solution. However, some patients, especially with those with significant hearing loss, experience poor hearing with bone conduction hearing aids, and others cannot use bone-conduction devices. Bone conduction hearing aids can be non-linear (cause distortion) and are limited in their dynamic and frequency ranges. Additionally, infection at the site of the bone-anchored screw can be problematic.

Instead of relying on transduction of sound via the normal air-conduction path (through the path of the ossicular chain via reconstruction) or accepting the limitations of bone-conduction hearing aids, an alternative method known as round window (RW) stimulation has shown some success (Maier et al. 2013; Schraven et al. 2011; Iwasaki et al. 2012; L. Colletti et al. 2011; Marco Mandalà, Liliana Colletti, and Vittorio Colletti 2011; Bernardeschi et al. 2011). Previous studies in animals and human temporal bone specimens have shown that both RW stimulation and oval window stimulation produce the sound-pressure difference across the cochlear partition necessary to elicit a hearing response (Wever and Lawrence 1950; Lupo et al. 2009; Stieger, Rosowski, and Nakajima 2013; Nakajima, Merchant, and Rosowski 2010). This has been confirmed in patients who were helped by a RW stimulator device when conventional treatments have failed (V. Colletti et al. 2005; L. Colletti et al. 2011; Kiefer, Arnold, and Staudenmaier 2006; Henning Frenzel et al. 2008). Although RW stimulation has improved hearing loss in some patients, available devices have considerable limitations, such as poor acoustic fidelity, consistency, and migration of the device (Rajan et al. 2011; Baumgartner et al. 2010; Martin et al. 2009; Beltrame et al. 2009). A major determining factor for the success of RW stimulation is the effectiveness of coupling the vibrating actuator to the RW membrane (Stieger, Rosowski, and Nakajima 2013).

The devices used today for RW stimulation were not designed and optimized for stimulating the RW, but rather to mechanically stimulate the middle-ear ossicles. Thus, surgically "fitting" these ossicular devices for RW stimulation is suboptimal, and yields poor and inconsistent results. Some types of devices modified for RW stimulation can risk traumatizing the cochlear sensorineural mechanism. Although many patients could potentially benefit from RW stimulation, most otologic centers throughout the world do not perform surgeries for RW stimulation because of the lack of an optimal RW stimulation device.

Anatomy

To better understand how a device can couple to and stimulate the RW, we study the anatomy of the RW area in intact temporal bone specimens. Histological sections provide detailed information regarding the proximity of the RW membrane to the cochlear partition and the complex architecture of the RW niche area. Study of the anatomy helps determine design criteria for a device to safely couple motion to the RW membrane in a stable and consistent manner. Figure 4.1A is a histologic cross section of the RW niche area through the middle region of the RW membrane (similar to Figure 3B in Li et al. 2007). The RW membrane is close to the cochlear partition at the middle of the RW membrane, especially at the superior/medial edge of the RW membrane (< 300µm, as shown in Fig. 3A in Li et al. 2007). Figure 4.1B is a simplified illustration depicting a similar cross section as 4.1A, and used in subsequent figures.

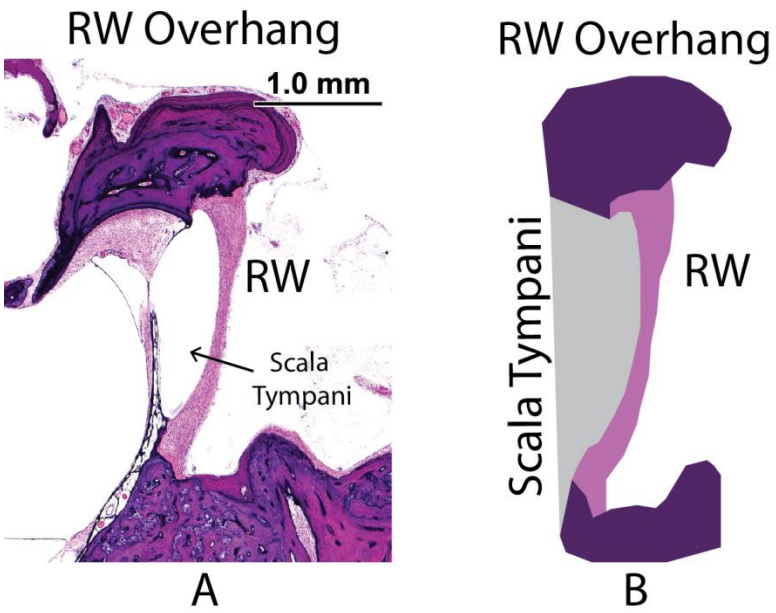

Figure 4.1: Round window (RW) niche.
A) histological section through the center of the RW-membrane area. B) A schematic illustration of the histological section in (A).

Current Devices

Floating Mass Transducer (FMT)

The active middle-ear prosthetic device most implanted for RW stimulation, and which has yielded positive results, is the floating mass transducer (FMT) (Vibrant Soundbridge, MED-EL) (V. Colletti et al. 2005; Baumgartner et al. 2010; Vittorio Colletti et al. 2006). It is an electromagnetic actuator shaped as a small cylinder, with a small metal arm to crimp on to a middle-ear ossicle. To vibrate the middle-ear ossicle to which the FMT is attached, the entire FMT has to freely vibrate without touching other surrounding structures.

For RW stimulation, the FMT's crimping arm piece for the ossicle is removed, and one end of the flat circular face of the FMT is then placed adjacent to the RW membrane to vibrate it. However, the diameter of the FMT is larger than the diameter of the RW membrane's

surrounding bone (RW overhang) and there is considerable air volume within the RW niche; thus the FMT cannot interface the RW membrane directly and is impeded in its motion by the bony overhang. Consequently, the bony overhang is drilled almost flush to the RW membrane. To fill residual air volume and to cushion between the remaining surrounding bone and FMT face, fascia is used between the FMT and the RW membrane to improve the transmission of vibration. The placement of the FMT at the RW niche is illustrated in Figure 4.2A, with the RW overhang drilled down close to the level of the RW membrane surface, and fascia sandwiched between the FMT and the RW membrane as well as the surrounding bone to improve sound transmission to the cochlea. The FMT is then secured in place by wrapping fascia around the whole device. The intent is to prevent the FMT from displacing away from the RW membrane, but at the same time, to allow for free motion of the entire FMT, which is necessary for its function.

Because the entire FMT device needs the freedom to vibrate (it cannot be held stationary at any point), the FMT is loosely held in place by wrapping the FMT with fascia and/or wedging soft-tissue between the FMT and surrounding bone inferiorly (Beltrame et al. 2009; Nakajima et al. 2010). This positioning method can be unstable and inconsistent across varying anatomy. Poor transmission of sound to the cochlea has been reported immediately or delayed after surgery due to poor FMT coupling to the RW and displacement of the FMT (Bernardeschi et al. 2011; Rajan et al. 2011; Marino et al. 2013). Even with optimal positioning, RW stimulation with the FMT is limited to a narrow frequency band and dynamic range (Nakajima et al. 2010).

Actuator and Tip

Another method to vibrate the RW, used experimentally and proposed for clinical use, incorporates an actuator (piezoelectric or electromagnetic) that vibrates an attached rigid tip (e.g. cylindrical or ball tip) that is considerably smaller in diameter than the RW membrane diameter for direct vibration (Maier et al. 2013; Schraven et al. 2011; Lupo et al. 2009; Stieger, Rosowski, and Nakajima 2013; Schraven et al. 2012). Sometimes tissue (e.g. fascia, cartilage, etc.) or a contact lens is sandwiched between the actuator tip and RW membrane (Figure 4.2B). To improve sound transmission to the cochlea, the tip pushes the RW membrane into the cochlea (approximately 20-50 μm from just touching the RW membrane towards the scala tympani (Stieger, Rosowski, and Nakajima 2013)) with static force of as much as 3.9 mN (Maier et al. 2013) to put tension on the RW membrane. This method has been shown in temporal bones to attain sound transmission reproducibly across specimens (Maier et al. 2013; Stieger, Rosowski, and Nakajima 2013; Schraven et al. 2012). However, it imposes a risk of puncturing the RW and damaging the cochlear partition close to the RW membrane as discussed above (Figure 4.1A and in Lee et al. 2007 Fig. 3)(Maier et al. 2013; Schraven et al. 2011; Li et al. 2007). Furthermore, some ears have a thin plate of bone at the level of or just behind or in front of the RW membrane as shown in Figure 4.3; this bony plate can take up to more than half the area of the normal round-window membrane area. If the tip of the actuator tries to push and vibrate this thin plate of bone, then vibration of the RW membrane would be impeded. Moreover, damage to the cochlea, such as the partition, can occur if the tip is pushed in and breaks this thin plate of bone.

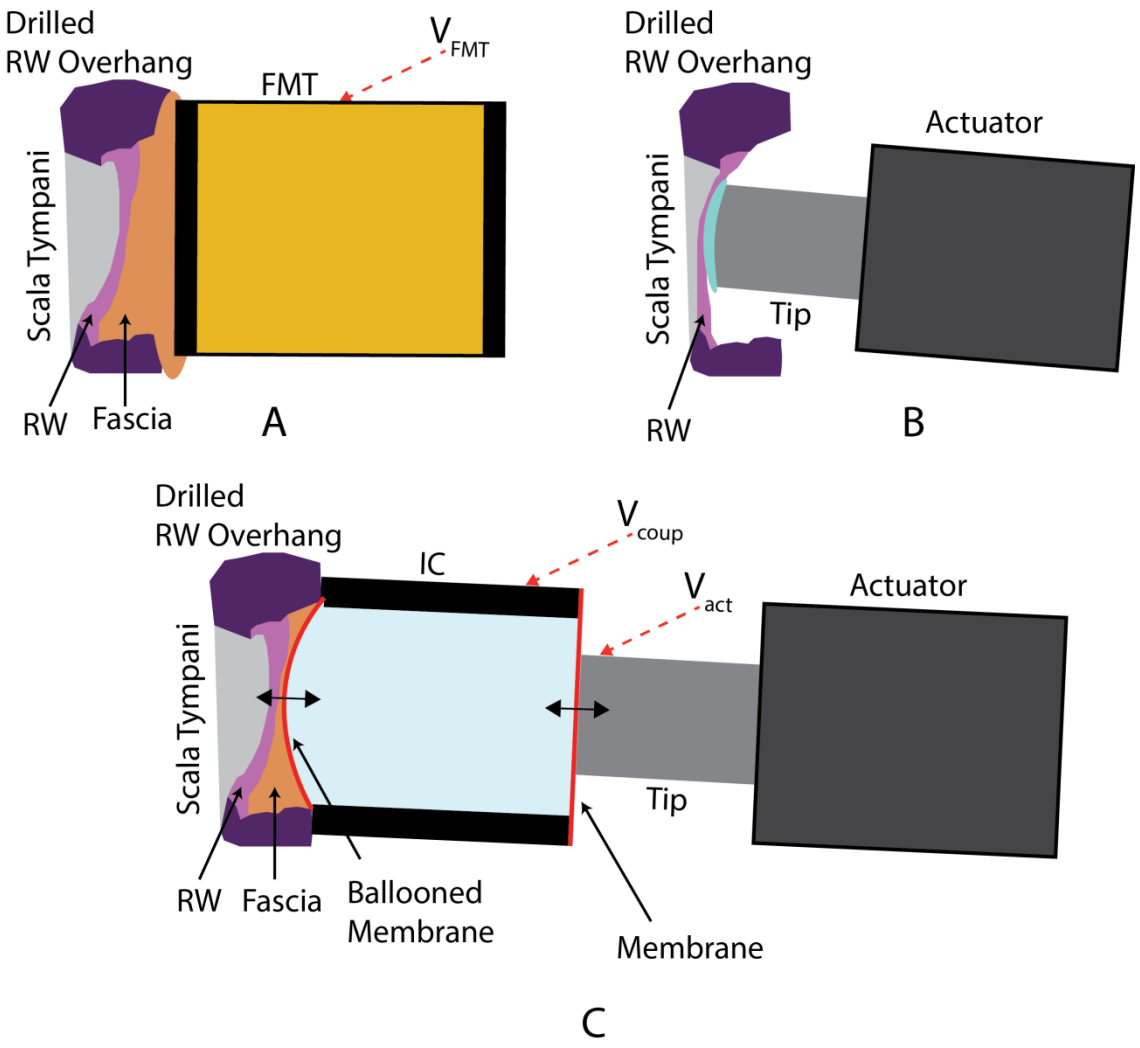

Figure 4.2: Illustrations of three methods to stimulate the RW.
A) FMT. The RW overhang has been drilled away to allow close proximity of the FMT to the RW membrane. Fascia (orange) is inserted between the device and the RW membrane to increase sound transmission. (The fascia wrapped around the entire FMT for stabilization is not depicted.) B) Actuator and tip. The actuator tip (light gray) is smaller in diameter than the RW membrane for direct RW interface. It needs to be pushed towards the cochlea providing tension on the RW membrane to improve sound transmission. A disc of plastic contact lens (blue) or tissue can be placed between the tip and RW to protect the RW membrane. C) The interface coupler (IC) and actuator. Fascia fills the volume between the 'ballooned' membrane of the interface coupler and the RW membrane to increase sound transmission. At the opposite end of the coupler, an actuator tip vibrates the coupler's flat membrane. Direction of Laser Doppler vibrometry measurements are shown with red dashed lines with arrow heads.

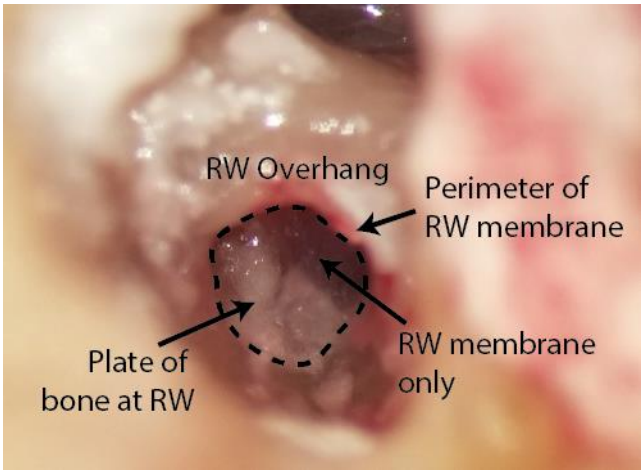

Figure 4.3: Temporal bone with large area of bone growth (thin plate of bone) at the surface of the RW membrane. The bone is identified as being lighter and whiter in color than the darker region of just the RW membrane.

Given the major shortcomings of current RW stimulator devices, a device and method for RW stimulation that improves sound transmission and functions more consistently across ears is necessary. We hypothesize that an actuator equipped with an *interface coupler* (IC) for RW stimulation will improve transmission of sound to the cochlea in a manner that will be safe and more consist across varying RW anatomy. The main goals of this study are to demonstrate proof of concept of our novel IC and to compare performance of an actuator with IC to the FMT (the most popular device and method used). This test, carried out in one specimen, is sufficient to demonstrate the efficacy of the proposed approach, and will serve as the basis for its future refinement.

Methods

Interface Coupler (IC) Development

Our IC prototype was composed of a brass tube of approximately 2mm in length and 2.5mm in diameter (2.05mm inner diameter) filled with degassed water encased by two membranes at both circular openings, as shown in Figure 4.2C. The thin (~0.05mm) flexible membranes that seal the two tube circular openings were made with ultra-violet cured photopolymer (Northland Optical Adhesive 68, Norland Products, Inc.). The membrane that interfaces the RW has a ballooned out shape towards the RW membrane to better mold to its surroundings within the RW niche. The metal tube's circular perimeter with the ballooned membrane was larger than the circumference of the RW membrane, thus rested against the bone surrounding the RW membrane (preventing possible harm to the RW membrane itself). A small amount of fascia was required between the RW membrane and balloon membrane of the IC to improve mechanical contact and prevent air pockets between the IC balloon membrane and the RW membrane. At the opposite end of the IC tube, a flat compliant membrane was coupled to a solid cylindrical tip (about 2mm in diameter), which is in turn glued to a stack piezo-electric actuator.

Temporal Bone Experiment

A fresh human cadaveric temporal bone specimen donated with permission for research was extracted within 24 hours post mortem, then refrigerated for use within two days (Nadol and McKenna 2005). Such specimens have similar anatomy and passive macro-mechanical properties to living ears (Chien et al. 2009; Nakajima, Ravicz, Merchant, et al. 2005; Nakajima,

Ravicz, Rosowski, et al. 2005), and the specimen used was prepared in a manner described in previous publications (Nakajima, Merchant, and Rosowski 2010; Nakajima et al. 2010; Stieger, Rosowski, and Nakajima 2013). A posterior tympanotomy with a widely opened facial recess provided access to the stapes and RW area. Sound was presented to the ear canal via air conduction (AC) with a Beyer Dynamic speaker (DT48) while velocities of the stapes and RW (V_{Stap} and V_{RW}) were measured with laser Doppler vibrometry (LDV, Polytec CLV 1000). To ensure that air did not enter the inner ear and that there was no cochlear fluid leak, the relative phase between V_{Stap} and V_{RW} was checked (±0.5 period phase relationship below 500 Hz indicates no air or leak) (Stieger, Rosowski, and Nakajima 2013; Merchant et al. 2003) before and after RW stimulation.

For FMT implantation, we optimized for "best" coupling and stability procedures performed in a similar manner as Nakajima et al. 2010 (Nakajima, Merchant, and Rosowski 2010); an 'idealized' configuration that is stable and difficult to achieve intra-operatively. This included drilling away the bony overhang surrounding the RW membrane until surrounding bone was almost flush to the RW membrane. Fascia was placed between the RW and the FMT. The FMT was stably held in place by two methods, 1) by wrapping with fascia as is performed in surgery, or 2) using a soft dental impression material (Jeltrate) as used in Nakajima 2010 (Nakajima, Merchant, and Rosowski 2010) placed between the FMT and surrounding bone inferiorly. While the fascia or Jeltrate surrounding the FMT kept the FMT in position in front of the RW, the FMT still had the freedom to vibrate.

For RW stimulation with the IC, fascia was placed in front of the RW membrane and the ballooned membrane of the IC was brought into contact with the fascia. On the opposing

surface of the IC cylinder with the flat membrane, the tip of the actuator was brought into contact (Figure 2C). In this paper, we present data from one human cadaveric temporal bone to demonstrate proof of concept of the IC prototype, and to compare the performance of the actuator with IC to that with the FMT.

Velocity measurements of the stapes (V_{stap}), promontory (V_{prom}), coupler cylinder (V_{coup}), and FMT or IC-actuator (V_{FMT} or V_{act}) were made with LDV. The laser was aligned to be 30-40 degrees to the stapes footplate for V_{stap} and almost 20-30 degrees with respect to the motion of V_{FMT}, V_{coup} and V_{act} (Figures 4.2 A&C). All these velocity measurements were >10 dB above the cochlear promontory velocity.

Results

Velocities

We compared RW-stimulated sound transmission to the cochlea between the actuator with IC and the FMT in the same specimen. The output and input velocities were plotted in Figure 4 for actuator and IC (A) and FMT (B), stimulated by constant voltage of 140 mV_{peak} for the IC actuator and 56 mV_{peak} for the FMT to produce comparable V_{stap} output magnitudes.

For the IC-actuator, the output V_{stap} and input V_{act} frequency responses are demonstrated in Figure 4.4A; both increased proportionally with frequency (~20 dB/decade). We also measured the velocity of the IC's rigid cylinder coupler motion V_{coup}, which was considerably lower than V_{stap} and V_{act}, and similar to the velocity of the bony promontory V_{prom}. Thus, stimulus vibrations from the actuator were not transmitted to the otic capsule or the IC

cylinder; therefore there was no evidence of bone conduction and the IC cylinder was stationary as compared to the stimulus vibrations.

In comparison, during constant voltage drive of the FMT (Figure 4.4B), the V_{stap} and V_{FMT} were low at low frequencies, increasing with frequency (~40 dB/decade), peaking at 1.2 kHz, and then decreasing with further increase in frequency. These frequency responses are similar to that reported in the past (Nakajima et al. 2010). Generally, for the IC, the magnitudes of V_{stap} were a factor of 2 lower than V_{act}, while for the FMT, V_{stap} was a factor of 10 lower than V_{FMT}. For both the IC and FMT, the phases of V_{stap} and V_{act} generally differed by a half cycle, though the phase difference increased at high frequencies (with 0.70 periods difference at 10 kHz) likely due to the complex three-dimensional stapes motions above approximately 2 kHz (Chien et al. 2006; Hato, Stenfelt, and Goode 2003; Heiland et al. 1999; Sim et al. 2010).

Our previous work showed that V_{stap} is not usually an accurate measure of cochlear input during RW stimulation because volume velocity does not just flow out the oval window, but also via leak impedances through scala vestibuli (possibly from the vestibular aqueduct and/or scala-vestibuli neural and vascular connections) that are of similar magnitude to the reverse middle-ear impedance through the oval window (Stieger, Rosowski, and Nakajima 2013; Frear et al. 2018). There are also variations across ears and frequency dependencies in the magnitudes of these leak impedances (Stieger, Rosowski, and Nakajima 2013; Frear et al. 2018). However, because we made comparisons between our IC-actuator prototype and the FMT in the same ear (with the same leak impedances through scala vestibuli), relative comparison of the two device types can be made based on the basis of V_{stap} measurements.

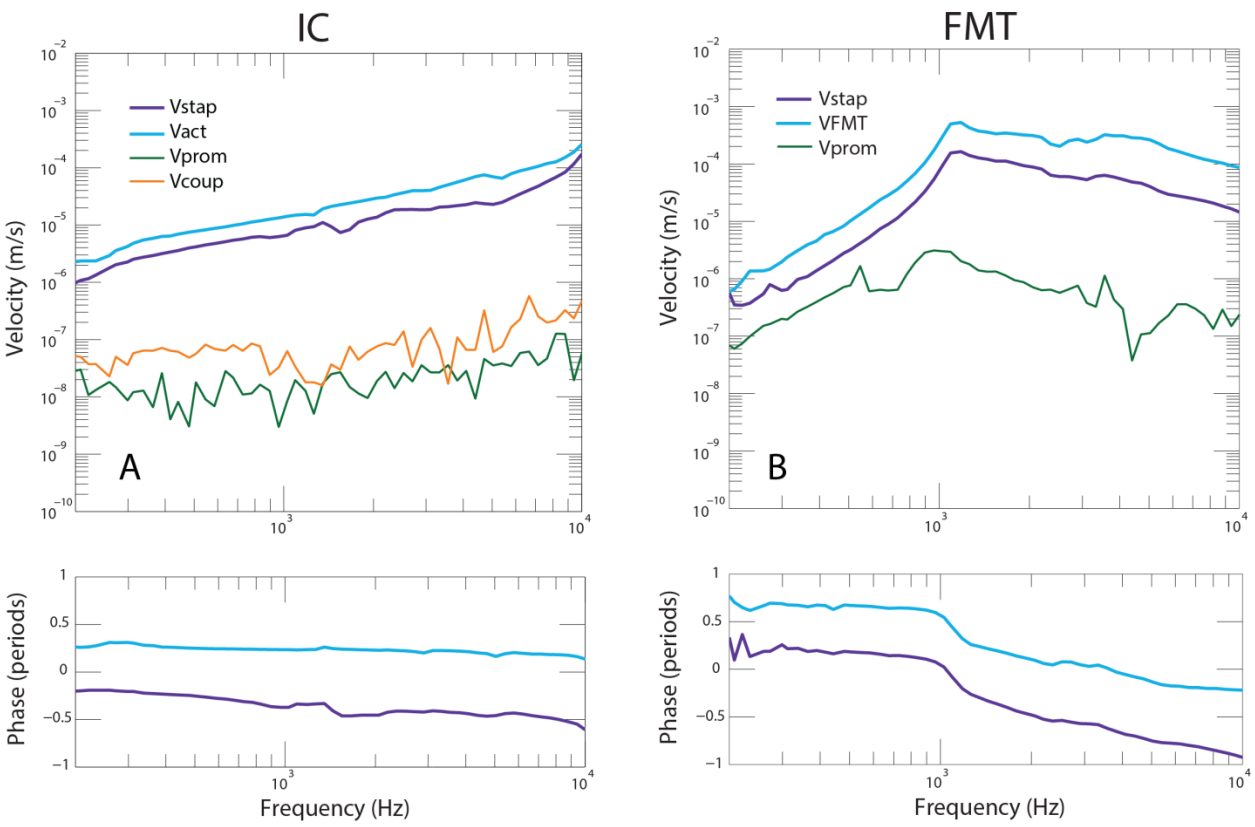

Figure 4.4: Velocity Responses of the (A) IC and (B) FMT. IC actuator, FMT and stapes velocities (V_{act}, V_{FMT}, V_{stap}) have magnitudes over 20 dB above the velocities of the cochlear promontory (V_{prom}). The IC actuator is driven with 140 mV_{peak}, while the FMT is driven with 56 mV_{peak}. The FMT was stabilized with Jeltrate in this case.

Volume Velocities

As shown in Figure 4.5, we compared sound transmission performance between the devices via the volume velocity output/input ratios. IC volume velocity ratio was the stapes and IC actuator tip ratio (U_{stap} /U_{act}), and the FMT volume velocity ratio was the stapes and FMT ratio (U_{stap} /U_{FMT}). The volume velocities were calculated by multiplying the velocity and the surface area (e.g. $U_{stap} = V_{stap}*A_{stap}$, where the area of the stapes footplate (A_{stap}) was 3.2mm^2). The area of the IC actuator tip (A_{act}) was 1.8mm^2, while the area of the FMT (A_{FMT}) was 2.5mm^2. The volume velocity ratio is 0 dB if the output (U_{stap}) is equivalent to the input (U_{act} or U_{FMT}).

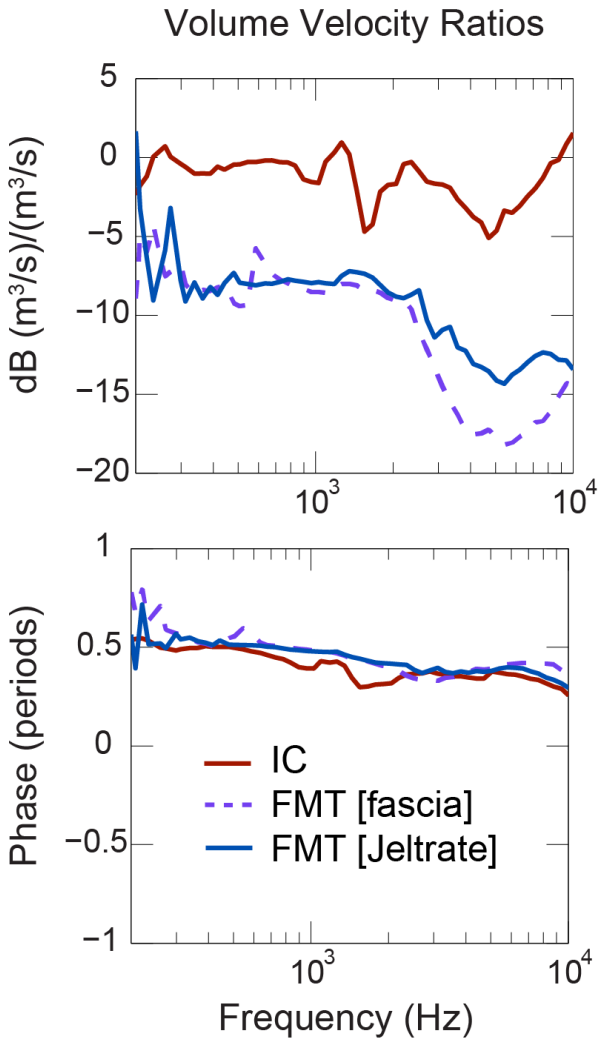

Figure 4.5: Volume Velocity Ratio of the Stapes to the Actuator
Sound transmission performance is compared with volume velocity ratios between IC and FMT. Two methods of stabilizing the FMT are included – with the FMT wrapped by fascia and braced by Jeltrate, respectively.

As shown in Figure 4.5, comparison of RW stimulation sound transmissions showed that the IC volume velocity ratio was about 3-8 dB higher than the FMT volume velocity ratio up to 3kHz, and more than 8dB higher above 3kHz. Figure 4.5 also shows that the bandwidth of sound transmission for the IC was wide, but the transmission capability of the FMT fell above 3 kHz. The FMT was stabilized using two different methods to prevent displacement: 1) wrapping

fascia around the device as is performed in surgery and 2) stabilizing the FMT with Jeltrate towards the inferior bony wall of the middle-ear cavity (as in Nakajima et al. 2010). Comparison showed that Jeltrate stabilization improved the FMT's ability to transmit sound more effectively at frequencies above 3kHz than fascia (Figure 4.5). For both the IC and FMT, the phase ratios were near 0.5 period below 1 kHz, as would be expected from an inward RW motion producing an outward stapes motion. At higher frequencies there was an additional delay in the stapes response.

Linearity

Linearity and dynamic range of the two RW stimulation systems were compared. Deviation from linearity relates to distortion of sound transmission. Input-output linearity relationships for the actuators – IC actuator and FMT velocity outputs with respect to the input voltages – are plotted for a range of frequencies in Figures 4.6A and B, where a linear relationship would be parallel to the gray dashed lines (decade/20 dB). Linearity relationships of the cochlear sound transmissions were also assessed using stapes velocity outputs V_{stap} with respect to the input voltages for both the IC and FMT, plotted across frequency in Figures 4.6C and D. For RW stimulation using the IC-actuator, the actuator velocity V_{act} was linear, and the sound transmission V_{stap} was generally linear for a wide frequency range and large dynamic range. The FMT performed linearly in terms of actuator velocity V_{FMT} at higher frequencies, but deviated from linearity at low frequencies and between 500-1000Hz where the voltage-to-velocity gain of the FMT almost peaks (Figure 4.4, Figure 4.6B, 1 kHz line). This characteristic

tends to limit the useful frequency bandwidth and dynamic range of the FMT. In Figure 4.6D, the FMT's sound transmission V_{stap} was shown to be nonlinear at most frequencies.

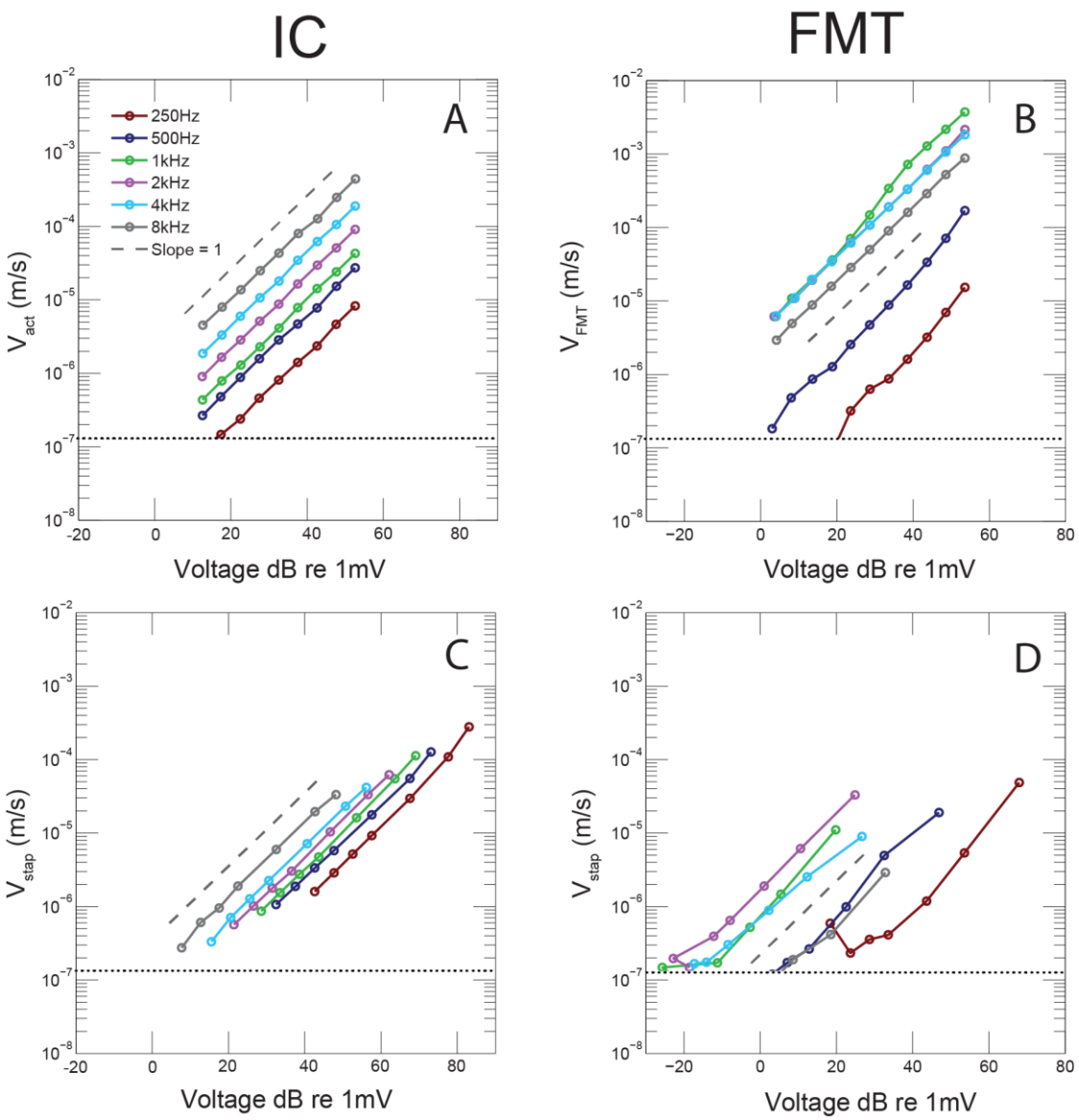

Figure 4.6: Assessment of linearity between IC and FMT.
Input-output curves of the actuators: A) V_{act} for IC-actuator and B) V_{FMT}, versus input voltage driving the actuator (IC or FMT) for various frequencies (represented by different colors). Input-output curves of the cochlear sound transmission measured by output V_{stap} for the C) IC-actuator and D) FMT, plotted against the input voltage. Dashed gray lines show the slope representing linearity.

Discussion

This report presents proof of concept of using an actuator with interfacing coupler IC to stimulate the RW. The design improves upon and solves some of the shortcomings of other methods to mechanically vibrate the RW for cochlear transmission, including sound transmission performance, stability and safety.

Development of the Prototype Interfacing Coupler (IC)

We considered several factors in designing and developing an early prototype system for improved RW stimulation. Our anatomical study revealed that the RW area is complex and variable across ears, posing challenges to the design of such a system. We thus designed a coupler for RW stimulation that can conform to a wide range of anatomical shapes with safety as the highest priority. Our IC prototype has a flexible ballooned membrane to interface closely with the RW membrane yet its rigid rim is larger than the circumference of the RW (thus the bone surrounding the RW prevents the rigid rim of the IC from touching the RW membrane). Our IC can be adapted to use various existing middle-ear actuators for RW stimulation. The IC was designed to improve transmission of volume velocity between the actuator and RW membrane to provide improved fidelity of sound transmission to the cochlea, with large dynamic and frequency ranges and high linearity.

RW stimulation with FMT

As described in the introduction, the FMT (the device used most for RW stimulation) was not designed for RW stimulation. Because the entire FMT needs to freely vibrate, it is

loosely stabilized with fascia during surgery, resulting in incidences of displacement (Nakajima, Merchant, and Rosowski 2010; Arnold, Stieger, et al. 2010; Pennings et al. 2010; Arnold, Kompis, et al. 2010). Even under ideal positioning for RW stimulation, the FMT is not able to produce adequate vibrational displacements below 1 kHz (Figure 4.4 and also shown in Nakajima et al. 2010). While the FMT does show nonlinearities, those occur at displacements that are larger than those of the IC.

Comparing the IC to the FMT

Compared to the FMT, the actuator and prototype IC has better fidelity during RW stimulation, and is designed for stability and versatility across the wide range of anatomical shapes of the RW area. The IC can be held firmly in place, as only the IC flexible membranes need to vibrate, reducing the chance of device displacement. Various existing FDA approved middle ear actuators can be used with the IC. The performance of the IC shows excellent linearity, large dynamic range and wide bandwidth to potentially aid conductive and mixed hearing loss due to a variety of etiologies (Figure 4.6A and C). Finally, the IC can transmit the volume velocity of the actuator to the cochlea with minimal loss, demonstrated by a high output/input volume velocity ratio (3-8 dB better than the FMT for all frequencies measured, Figure 4.5). Because the IC has excellent vibrational coupling to the RW membrane, volume velocity output is close to the actuator input, demonstrating high efficiency of sound transmission to the cochlea.

Future Work

This study demonstrated proof of concept of an early IC prototype and compared the performance of a system incorporating the IC to that with the FMT on the same specimen. Now that we have quantitatively demonstrated the potential benefits of the IC for RW stimulation, we plan further developments to optimize it. Here, we drilled the bone surrounding the RW membrane to optimize for FMT performance, and used the same preparation for the IC. However, drilling the RW overhang has potential to cause physical and acoustic trauma. We plan to optimize the ballooned flexible membrane of the IC to conform to the RW niche and enable transmission of sound without or with minimal drilling of the RW overhang. We will also study anatomical variation across ears to optimize the IC to even better conform to wide anatomical variations of the RW niche and overhang. Additionally, we need to investigate and optimize attachment methods of various actuators to the coupler. With the variations in anatomy in mind, the shape of the entire device will be optimized for easy surgical implantation and mechanical stabilization. After these future developments for an improved IC prototype, performance will be tested on different ears with varying anatomy with no or minimum drilling of the bony RW overhang. After such performance analyses, consideration of materials for biocompatibility and tests for biocompatibility and long-term durability with animal testing will be performed.

Conclusion

Preliminary measurements show proof of concept with an early prototype of an interface coupler for RW stimulation. The results indicate the IC prototype allows for efficient transmission of sound by an actuator to the cochlea with excellent linearity, dynamic range and wide frequency bandwidth, exceeding the performance of the FMT for RW stimulation.

CHAPTER 5.

Improvements to the Interface Coupler for Round Window Stimulation

Introduction

Conductive hearing loss (CHL) and mixed hearing loss are often treated by surgery and/or hearing aids. The study in Chapter 1 of this thesis showed that about 16% of patients seen at all Massachusetts Eye and Ear hospitals for hearing problems are due to either CHL or mixed hearing loss. Conventional solutions for common forms of pathology include surgery to repair the tympanic membrane and/or the ossicular chain. Conventional hearing aids as well as bone conduction hearing aids are also used. However, there remains an unmet need for patients that fail multiple middle-ear reconstruction surgeries and hearing aids do not restore their hearing to a level for normal auditory communication (Lee and Schuknecht 1971; Brackmann, Sheehy, and Luxford 1984; Merchant et al. 2003).

Round window (RW) stimulation is a potential solution for these difficult cases and has been shown to be a good alternative (Stieger, Rosowski, and Nakajima 2013; Spindel, Lambert, and Ruth 1995; Nakajima, Merchant, and Rosowski 2010; Voss, Rosowski, and Peake 1996; Nakajima et al. 2010). Clinically, patients who have either failed multiple middle-ear reconstruction surgeries, or have a previously obliterated middle-ear cavity, aural atresia, and stapes fixation have been shown to be helped by RW stimulation (Vittorio Colletti et al. 2006; Kiefer, Arnold, and Staudenmaier 2006; Beltrame et al. 2009; Martin et al. 2009; Baumgartner et al. 2010) . The RW stimulator most often used is the floating mass transducer (FMT), but it has multiple limitations (Rajan et al. 2011; Baumgartner et al. 2010; Martin et al. 2009).

One major limitation is that the FMT is generally larger in diameter than the diameter of the RW membrane (Su et al. measured over 550 temporal bones and found that the average RW membrane diameter is 1.65 mm while the FMT diameter is 1.8mm) (Su et al. 1982). This

results in the FMT vibrating against the bone surrounding the RW instead of moving the RW membrane (Nakajima, Merchant, and Rosowski 2010). Therefore, drilling away the bone surrounding the RW is often required and fascia or other soft tissue is often placed in the RW niche and between the surrounding bone and the FMT (Skarzynski et al. 2014; Cuda, Murri, and Tinelli 2009; Tringali et al. 2010).

Drilling close to the RW risks physical trauma to the RW membrane as well as the acoustic trauma to the cochlea (Kylén and Arlinger 1976; Pau et al. 2007; Zou et al. 2005; Holmquist, Oleander, and Hallén 1979). Microscopic inspection of histologically prepared human ears and fresh temporal bone specimens reveals that the RW's outer mucosal lining and the fibrous layers within the membrane can be continuous with the tissues overlaying the bone near the RW perimeter. The continuous tissues include the outer mucosal membrane but also the other two layers of the RW membrane (Goycoolea and Lundman 1997), though this anatomical relationship varies considerably across ears. Therefore, drilling bone near the RW can result in the detachment of the membrane from its bony rim. This can cause trauma to the nearby cochlear partition with its sensorineural structures close by, as well as introduce air into the cochlea (which happened in two of our aborted experimental preparations after RW stimulation).

Previously, we created an early prototype RW interface coupler – a cylindrical fluid-filled tube with each end terminated by a flexible membrane: one membrane was designed to contact the RW and its surrounding bone, the other was stimulated by a rod attached to an actuator (details found in Chapter 4 of this thesis). This prototype exhibited improved performance compared to the FMT. The flexible design of the membrane contacting the RW

made it more adaptable to varying RW anatomy, though in that study we still drilled the bone surrounding the RW to directly compare to the FMT. A complication was that adequate vibration of the fluid within the interface coupler required a range of specific orientations of the vibrating actuator and its coupled rod. Proper surgical placement of the actuator, its stabilizing rod and the interface coupler tube could be challenging.

In this chapter we describe an improved prototype RW interface coupler (IC) that reduces the need for drilling near the RW, and incorporates the actuator within the IC. We test this new device in human cadaveric temporal bones to 1) see if it performs consistently across ears with various anatomy, 2) measure linearity, dynamic range, bandwidth, and 3) estimate the equivalent ear-canal sound pressure.

Methods

Development of the Round Window Interface Coupler

The IC was constructed from a stainless steel tube of approximately 3mm in length and 2.41 mm in outer diameter (2.15mm inner diameter). At one end of the IC tube opening, an actuator (Figure 5.1 A) was fit partially inside the IC tubing and glued in place (Figure 5.1 B). This "bellows actuator" (Figure 5.1A) was cylindrical in shape, 3mm in length and 1.8mm in diameter. The actuator was developed by our collaborators in Dr. Jin-ho Cho's research group in Korea. Earlier, they developed an electromagnetic bellows actuator (Shin et al. 2016) similar in size and shape to the actuator used in the present study. The new bellows actuator used in this study incorporates a piezoelectric drive for compatibility with magnetic resonance imaging. The actuator was fixed inside the stainless steel tube by a continuous ring of cyanoacrylate around

the actuator's non-mobile base. The remaining space between the actuator and the inside of the tube was filled with de-gassed water. This fluid filled IC tube was then sealed by a thin flexible membrane (~0.05mm in thickness) made from ultra-violet cured photopolymer (Northland Optical Adhesive 68, Norland Products, Inc.). This polymer was floated on the water's convex meniscus (ballooning out) and then cured to better couple with the RW niche space. The IC with internalized actuator is illustrated in Figure 5.1B.

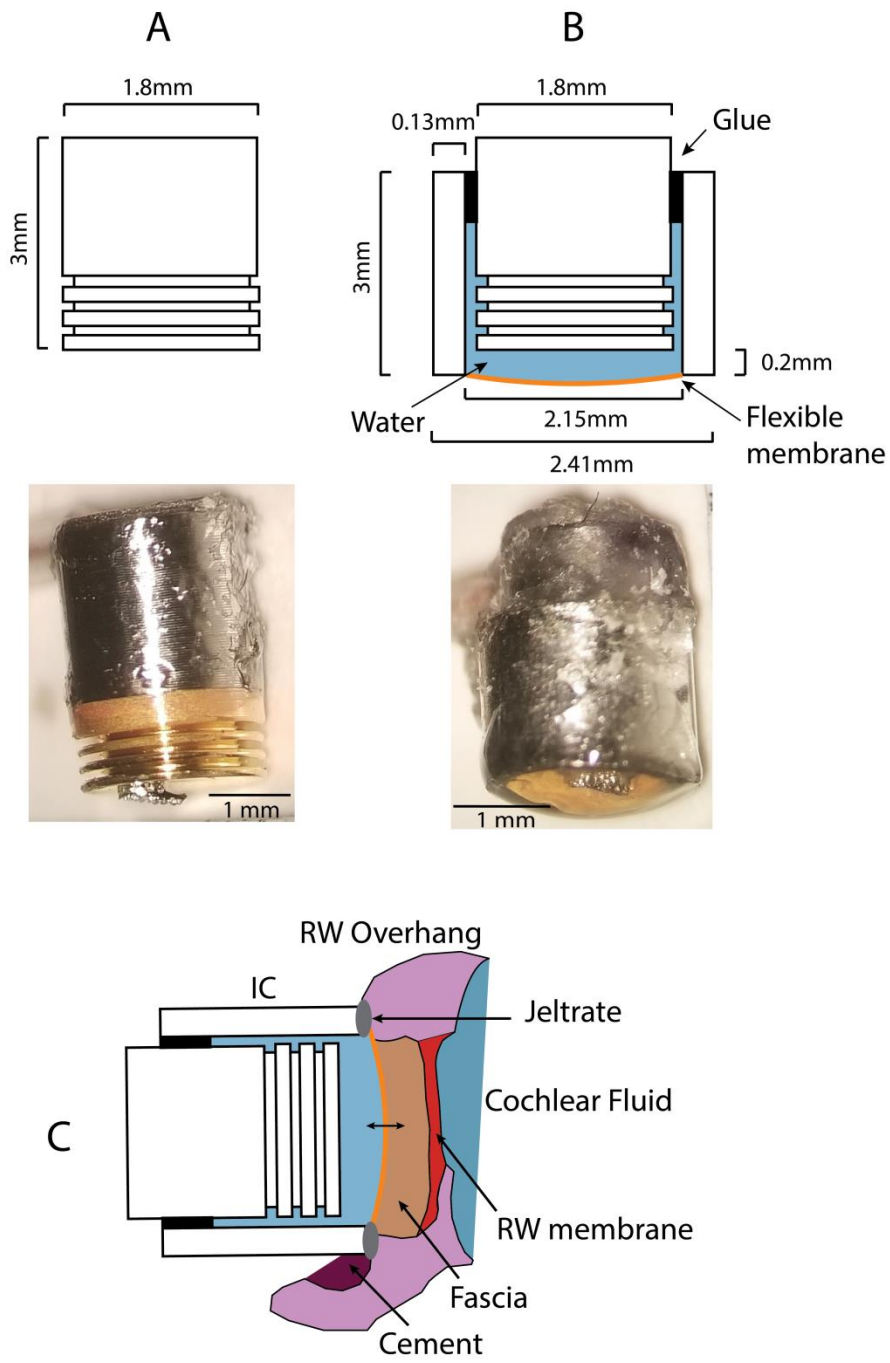

Figure 5.1: Schematics and photographs of the interface coupler (IC). A) Bellows actuator illustration and photograph, B) IC illustration and photograph, and C) illustrated IC interfacing the RW niche. Facia was used to fill the RW niche, Jeltrate to cushion and seal the interface between the IC ring and bone, and cement to fill crevasses. A and B photographs show a reflector on the face of the bellows actuator that was used to measure the velocity response with laser Doppler vibrometry.

Temporal Bone Experiments

The IC was tested in five fresh de-identified human cadaveric temporal bone specimens donated specifically for research purposes. The bones were extracted within 24 hours post mortem and immediately frozen until thawed just prior to the experiment (Nadol and McKenna 2005).

Such post-mortem specimens have similar anatomy and passive macro-mechanical properties to living ears (Chien et al. 2009; Nakajima, Ravicz, Merchant, et al. 2005; Nakajima, Ravicz, Rosowski, et al. 2005). The specimens were prepared as described in previous publications (Nakajima, Merchant, and Rosowski 2010; Nakajima et al. 2010; Stieger, Rosowski, and Nakajima 2013).

Briefly, the facial recess was opened via a posterior tympanotomy to provide access to the stapes and RW area. Sound stimulation via air conduction was presented to the ear canal using a Beyer Dynamic speaker (DT48) while velocity measurements were made of the stapes and RW (V_{stap} and V_{RW}) using laser Doppler vibrometry (LDV, Polytec CLV 1000). We ensured the inner ear was intact (no air, no fluid leak, etc.) by verifying that the phase between the air-conduction driven V_{stap} and V_{RW} was half a cycle at frequencies below 500 Hz before and after every experiment (Stieger, Rosowski, and Nakajima 2013; Merchant et al. 2003).

Generally, the otic capsule did not require drilling, but in three cases with a large boney protrusion surrounding the RW niche (that produced a highly uneven coupling surface for the IC device) minimal drilling was performed. A mild uneven surface was not an issue because we used a soft rubbery material (Jeltrate – alginate, a soft dental impression) to seal between the IC ring and the surrounding bone.

Figure 5.1C illustrates the interface between the IC and the RW. The IC (at the static end of the bellows actuator) was held with a rod and positioned by a micromanipulator. To improve coupling (reduce volume velocity leaks) between the device and the RW membrane, we used dental cement to fill large bony crevices surrounding the RW niche, while carefully avoiding the RW membrane protected by thin fascia. After the cement dried, the niche was filled with more fascia to eliminate any air between the membrane and the IC. A thin ring of Jeltrate was used to seal the IC to the bone around the RW niche. The flexible membrane side of the IC was then brought into contact with the fascia-filled RW niche, where the tube rim of the IC rested on the rubbery Jeltrate around the edge of the niche opening. We found that best results were obtained if the IC gently rested on the surface of the Jeltrate.

LDV measurements were made of the unloaded bellows actuator velocity ($V_{bellows}$) before it was glued to the IC tubing. (Loaded bellows actuator measurements were not possible because the laser was not accessible to the moving diaphragm of the actuator when coupled to the RW.) Once the IC was assembled with the bellows glued internally, LDV measurements were made of the IC driven velocities of the stapes (V_{stap}) and cochlear promontory (V_{prom}). To measure V_{stap}, the laser was aligned to within 30-40 degrees of a direction orthogonal to the stapes footplate. All the velocity measurements were greater than 10 dB above V_{prom}. The input stimuli were 74 logarithmically-distributed sinusoidal waves with a frequency range of 100 Hz to 20 kHz with a voltage input from 0.1 V_{peak} to 9 V_{peak} (responses were averaged ten times). A voltage input of 6 V_{peak} to the unloaded bellows actuator produced a linear volume velocity of the bellows ($U_{bellows}$) from 1.3e-5m^{-10}/s to 2.3e-2m^{-8}/s in magnitude across frequency.

Results

Anatomy

The anatomy of each temporal bone greatly varied; variations were seen in the depth of the RW niche and bony overhang, and number and size of crevasses in the bone within the bony outline of the RW niche. As depicted in Figure 5.2, the overhang of each temporal bone can be nearly nonexistent (bone df11, Figure 5.2A) or significant (bone df16, Figure 5.2B).

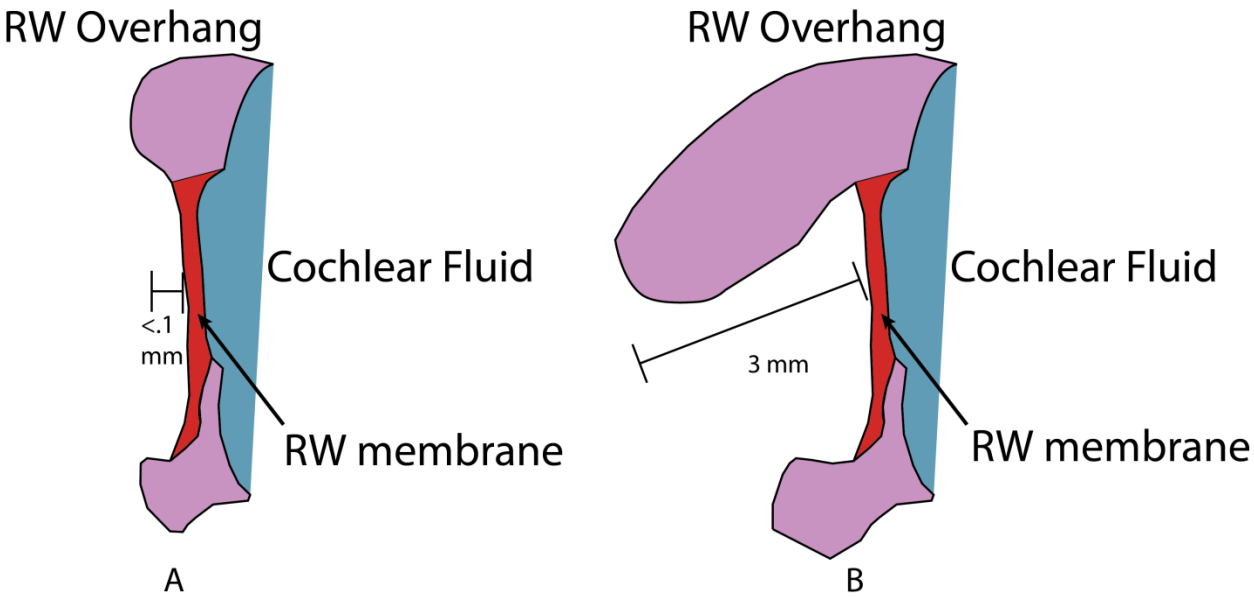

Figure 5.2: Example of the differing anatomy of the RW overhang measured as shown. The RW overhang varied from A) under 0.1 mm to B) 3 mm in length across the five temporal bones tested.

Velocity Measurements

Measurements of the magnitude and phase of V_{stap} normalized by the voltage drive to the IC in specimens df11 and df13 (5.4 V_{peak} input), and in df14, df15, df16 (6.0 V_{peak} input) are shown in Figure 5.3. The phase was consistently 0.25 periods for all five experiments up to 2kHz

before decreasing slightly at higher frequencies. The magnitude of the normalized velocity generally increased proportionally with stimulus frequency (the dashed line in Figure 5.3 indicates direct proportionality). Three experiments slightly deviated from direct proportionality above 4kHz (df13, 14,16).

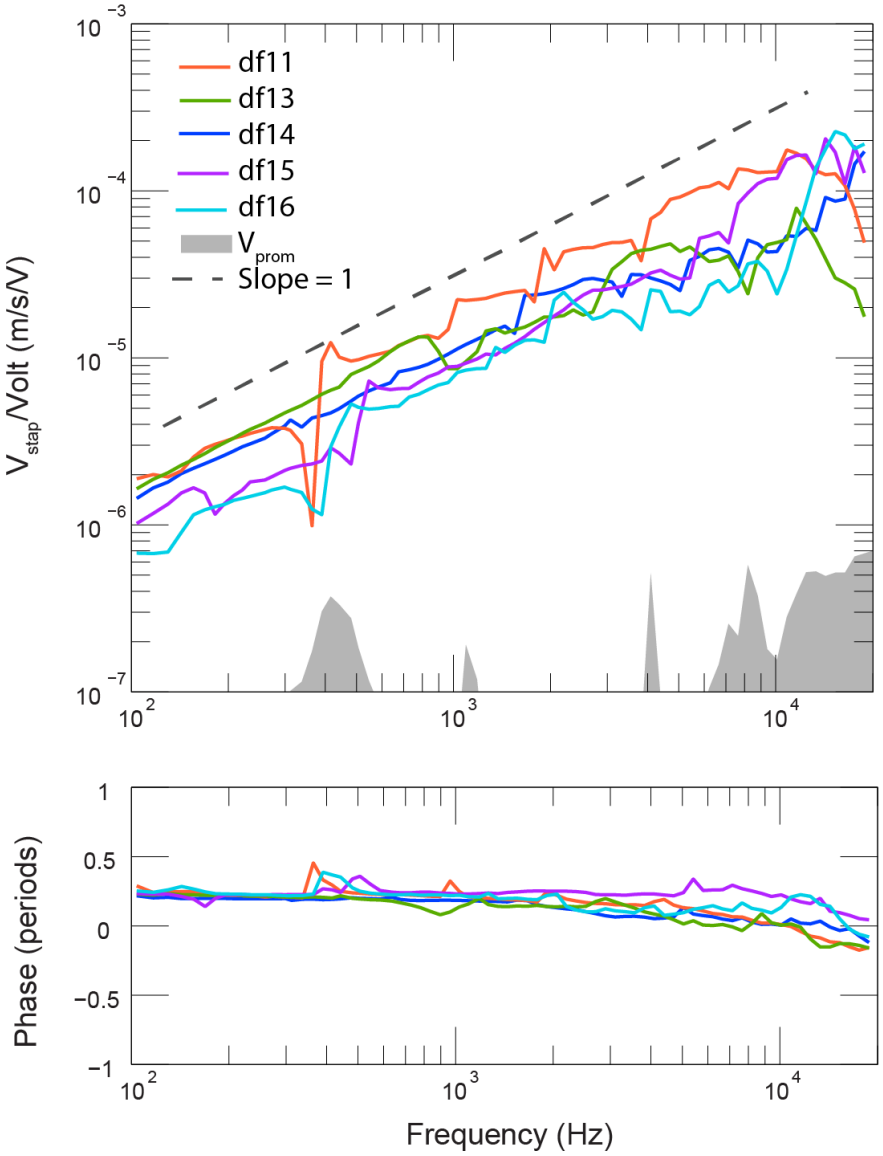

Figure 5.3: Stapes velocity response normalized by the input voltage to the IC. The normalized stapes velocity generally increased proportionally with frequency while the phase was t +0.25 periods for low and mid frequencies. The bellows actuator was driven with 5.4-6 V_{peak}. Dashed line shows proportional relationship. The gray area represents the noise.

Linearity

Linearity of cochlear sound transmission was tested by determining the relationship of the output V_{stap} with respect to the input voltage to the IC stimulating the RW. Figure 5.4 shows an example of the frequency response of the gain (V_{stap}/Voltage). A perfectly linear system would produce equivalent gain for various input voltages. Generally, stapes velocity grew approximately linear with input voltage over the frequency bandwidth of the measurements. Input-output plots detail the linear relationship, as shown in Figure 5.5. On this log/dB scale, a linear relationship would produce an order of magnitude increase in output for a 20 dB increase in drive, as shown in the dashed line of Figure 5.5. Though the data in Figure 5.4 and 5.5 describe a somewhat expansive non-linearity at lower voltages (relatively larger motions at higher stimulus levels up to about 3 V_{peak}), these deviations from perfectly linear behavior are small (< 3 dB over a 35 dB input range). This is possibly due to weaker coupling of the IC to the RW at low voltages (low stroke of the IC motion); the coupling then became stronger with higher voltages (higher stroke). Overall, sound transmission through the cochlea due to RW stimulation with the IC showed near linearity over a wide dynamic range and wide frequency bandwidth.

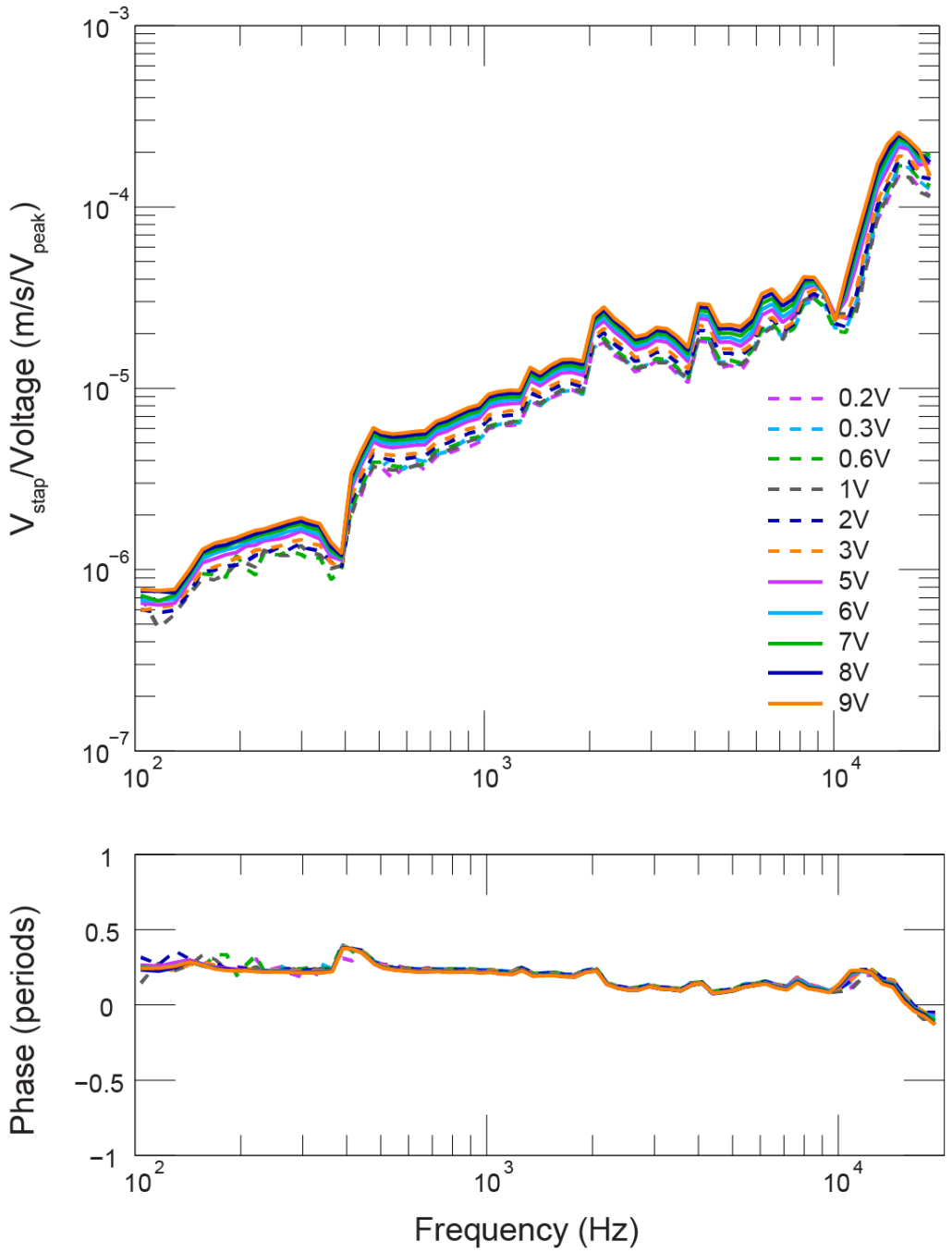

Figure 5.4: Gain frequency response of sound transmission through the inner ear for varying input voltages to the IC device to vibrate the RW (df16). Because the gain (V_{stap}/Volt) is generally the same for all voltage inputs across all frequencies, it demonstrates good linearity of sound transmission to the cochlea for a wide dynamic range and wide frequency bandwidth. All data are 10 dB above noise.

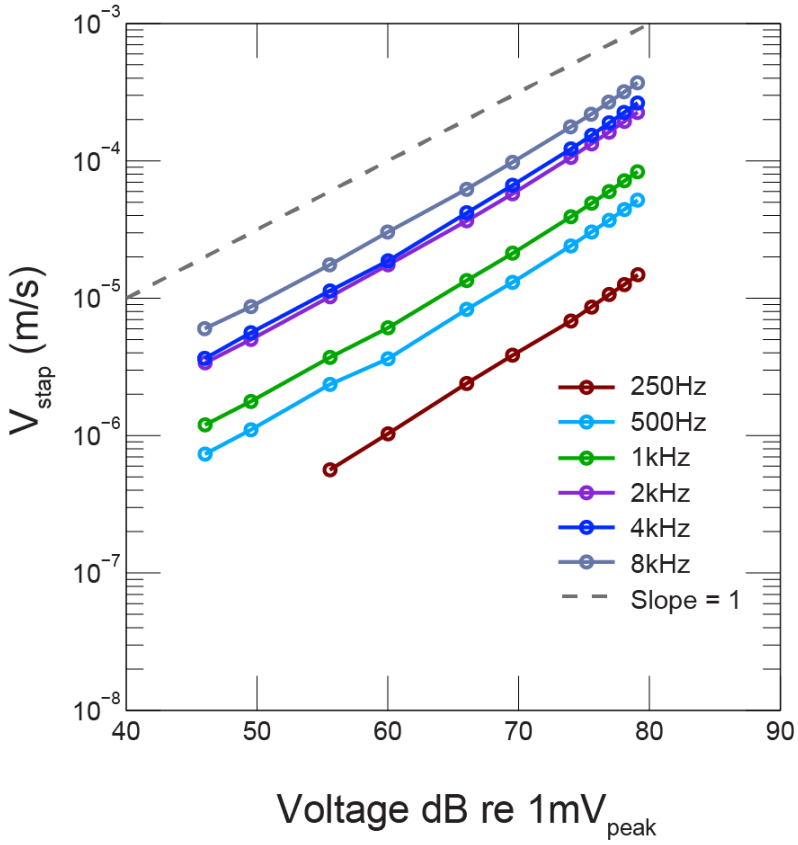

Figure 5.5: Input-output relationship of sound transmission through the cochlea from the IC input drive (df16). Generally, V_{stap} output versus voltage input to the IC device vibrating the RW exhibits linear relationships for various frequencies. For reference, the gray dashed line shows perfect linear relationship. All data plotted are 10 dB above the noise.

Equivalent Level of Hearing During Air Conducted Sound

To determine the level of hearing achieved by IC stimulation of the RW, we estimate the equivalent level of input sound pressure at the ear canal during air-conducted sound required for the same cochlear input drive as achieved with RW stimulation. To do so we use information gained from our previous study in Chapter 3 (Frear et al. 2018).

The input to the cochlea, the cochlea drive, is the magnitude of the vector difference in sound pressure between scala vestibuli (P_{SV}) and scala tympani (P_{ST}) at the base of the cochlea. We assume that the differential pressure across the basal cochlear partition (P_{SV} - P_{ST}) is the

cochlear input drive to start the traveling wave for both AC and RW stimulation (Dancer and Franke 1980; Lynch, Nedzelnitsky, and Peake 1982). We use the relationship during RW stimulation between the output stapes velocity $\left(V_{stap_{RW}}\right)$ and cochlear drive $\left(P_{SV_{RW}} - P_{ST_{RW}}\right)$ magnitudes, as well as the relationship during AC stimulation between cochlear drive $\left(P_{SV_{AC}} - P_{ST_{AC}}\right)$ and input ear canal pressure (P_{ec}). These relationships during RW stimulation and AC stimulation were obtained by directly measuring P_{SV}, P_{ST}, V_{stap}, and P_{EC} experimentally in fresh temporal bones. It is important to note that during AC stimulation, the path of volume velocity starts at the driven oval window, produces pressure difference across the cochlear partition and exits the low-impedance round window (thus a two-window system). However, during RW stimulation, we found that because the reverse middle-ear impedance is high, the volume velocity driven by RW vibration producing pressure difference across the cochlear partition divides between a leakage path in scala vestibuli (likely the vestibular aqueduct) and the oval window. This finding was detailed previously (Stieger et al., 2013 and Frear et al. 2018). Thus, to accurately predict the relationship between stapes velocity output due to cochlear pressure drive during RW stimulation, it is important to have experimentally derived relationships measured during RW stimulation.

The two components are illustrated in Figure 5.6.

From the multiple studies summarized by Frear et al. (2018) we plot the average and standard deviation of five measurements of the differential pressure divided by the stapes velocity during RW stimulation, $\left(P_{SV_{RW}} - P_{ST_{RW}}\right)/V_{stap_{RW}}$, and the average and standard deviation of 18 measurements of the ear canal pressure divided by the differential pressure during ear canal sound stimulation, $P_{ec_{AC}}/\left(P_{SV_{AC}} - P_{ST_{AC}}\right)$ (plotted in Figure 5.6A and B

respectively). In order to calculate the equivalent ear canal pressure using the IC to stimulate the RW, we multiply the above ratios with the stapes velocity using the IC at the RW ($V_{stap_{IC}}$):

$$P_{ec_{equivalent}} = \left(V_{stap_{IC}}\right) * \left(\frac{P_{SV_{RW}} - P_{ST_{RW}}}{V_{stap_{RW}}}\right) * \frac{P_{ec_{AC}}}{P_{SV_{AC}} - P_{ST_{AC}}} \qquad \text{Eqn 5.1}$$

The equivalent ear canal pressures, $P_{ec_{equivalent}}$, for all experiments are plotted in Figure 5.7 for voltage inputs of 5.4 - 6 V_{peak} to the IC for RW stimulation. For low frequencies up to 1 kHz, 5.4 - 6 V_{peak} drive to the IC resulted in $P_{ec_{equivalent}}$ output of 80 - 100dB SPL. For higher frequencies above 1 kHz, $P_{ec_{equivalent}}$ increased steadily up to 140dB SPL (30-40 dB/decade). The phase starts at -.25 periods and increases with increasing frequency where it is about 0 near 1 kHz, and up to 0.5 periods at 10kHz.

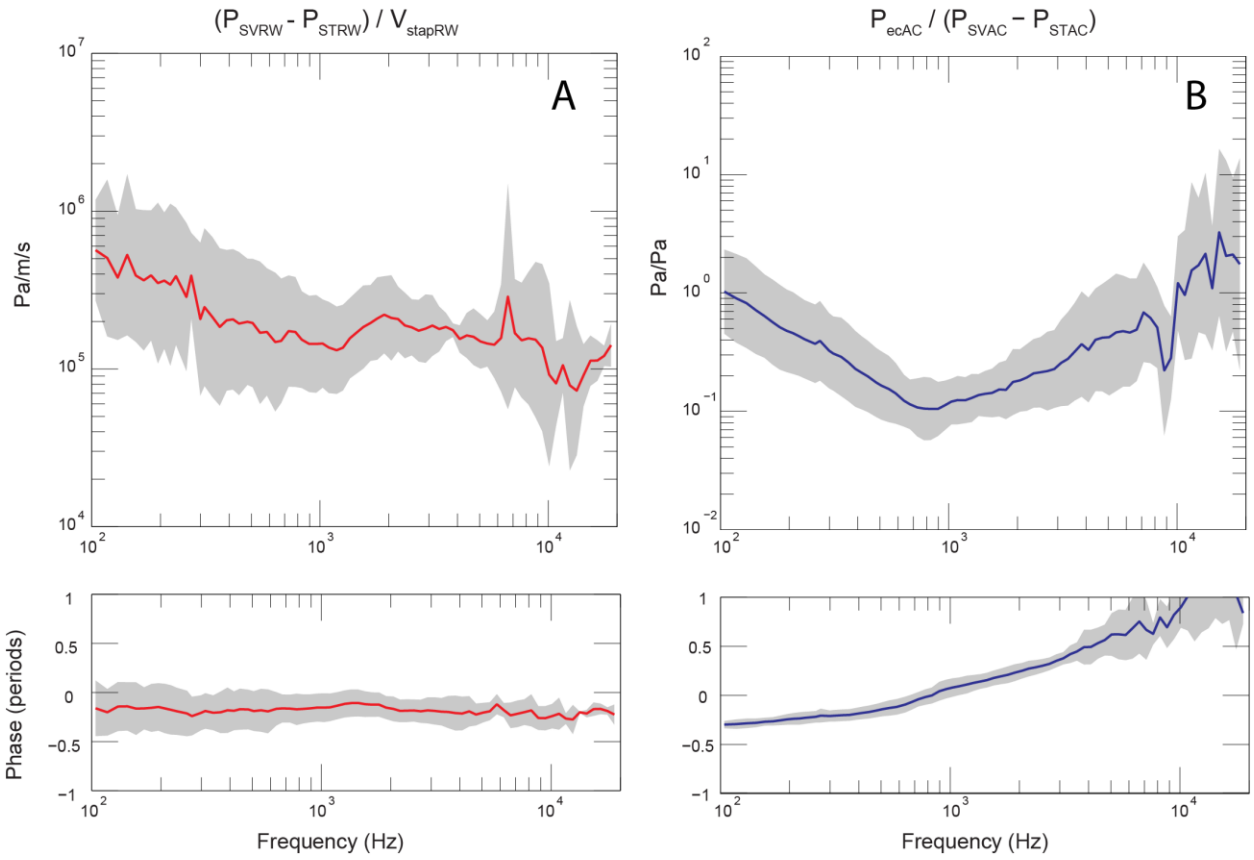

Figure 5.6: The mean and standard deviation (gray area) of two measured transfer functions obtained from experimental data from (Frear et al. 2019, Ch3). These transfer functions are used to determine the equivalent P_{ec}. A) Data from round window stimulation where the pressure differential is divided by the stapes velocity. B) Data from air conduction stimulation where the ear canal pressure is divided by the pressure differential.

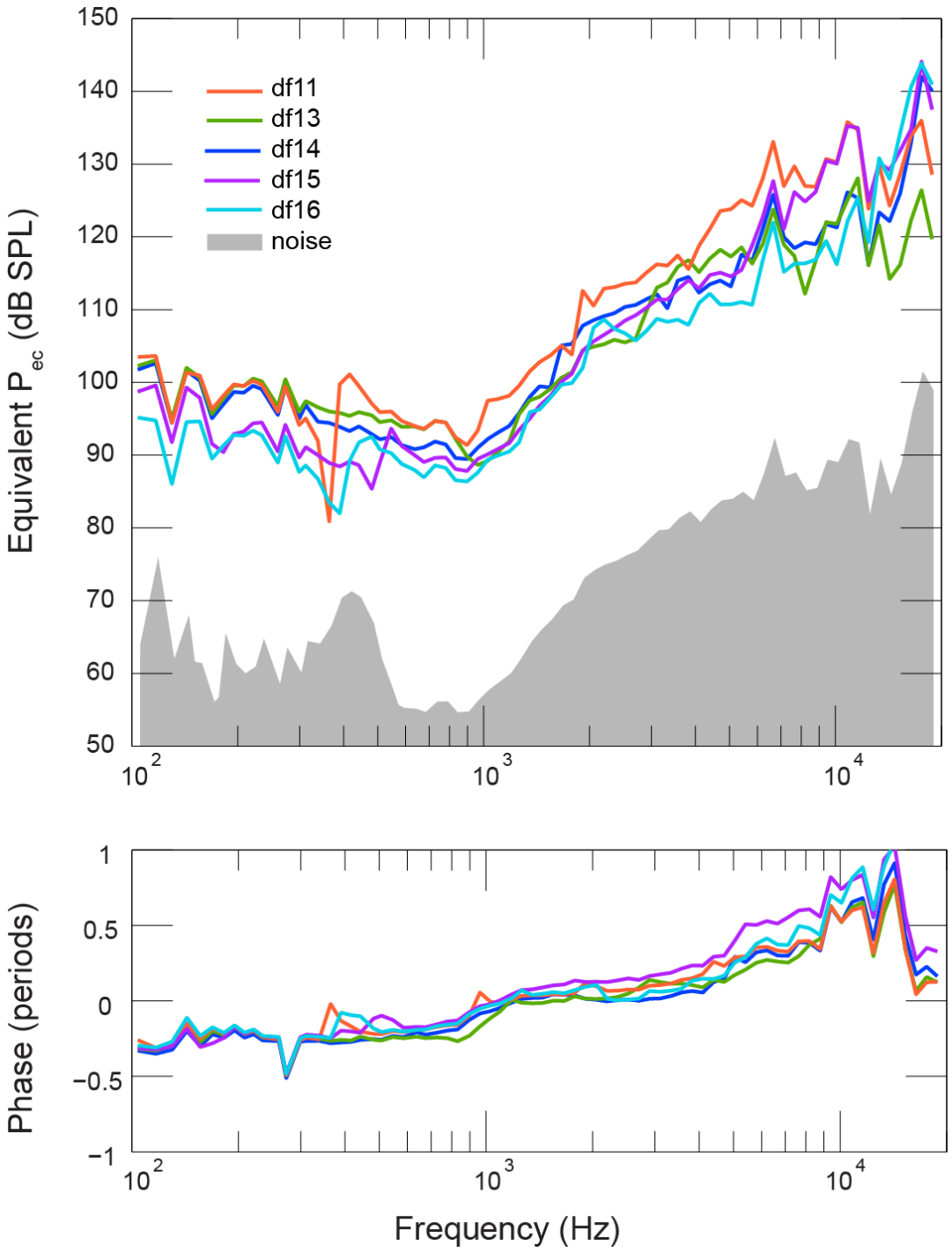

Figure 5.7: Equivalent ear canal pressure for the IC (ranging from 5.4 V_{peak} IC input for df11 and df13 to 6 V_{peak} IC input for df14-16). All the experiments provide similar ear canal pressure (80-100dB SPL) for low frequencies and increase in magnitude above 1kHz.

Discussion

In this study, we developed the IC system for RW stimulation to increase safety and consistency for a large variation in the anatomy of the RW membrane and surrounding bony architecture. The FMT device, most used for RW stimulation in patients, requires the bone surrounding the RW to be reduced by drilling, which risks introduction of air into the inner ear and trauma to the cochlear partition. The performance of the FMT is also variable across ears. Previously, we showed that an earlier prototype of the IC (without an internalized actuator) performed superiorly compared to the FMT. In this study, we demonstrate that the newly designed IC with an integral bellows actuator within the IC for RW stimulation performs remarkably similarly across ears despite the large variation in anatomy and without excessive drilling on the bone surrounding the RW niche. The bony anatomy around the RW vastly differs in shape and size, with niche depths ranging from 0 to 3 mm within our 5 specimens (Figure 5.2). Despite these anatomical differences, the new IC produces stapes velocities that generally varied by less than a factor of 3 (10 dB) for frequencies less than 4000 Hz, and no more than a factor of 10 (20 dB) at frequencies as high as 10 kHz. The variations at higher frequencies were likely due to the one-dimensional laser vibrometry measurements for stapes motion that is known to vibrate in complex 3-dimentional modes of motion above around 2 kHz (Chien et al. 2006; Hato, Stenfelt, and Goode 2003; Heiland et al. 1999; Sim et al. 2010). The new IC design is shown to perform quite consistently across large anatomical variation (without drilling or minimal drilling surrounding the RW niche) and with an interface to the RW membrane that is gentle (does not require force and tension to the RW membrane), thus should not risk

traumatizing the RW membrane or the inner ear behind the RW membrane, or allow for air to enter around the edge of the RW membrane.

RW stimulation with the FMT has poor linearity, limited dynamic range and bandwidth (Chapter 4; Rajan et al. 2011; Baumgartner et al. 2010; Martin et al. 2009; Beltrame et al. 2009). The newly designed IC stimulated the RW producing sound transmission linearly (thus low harmonic distortion), large dynamic range and bandwidth. Figure 5.4 shows that the output stapes velocity is generally linear across varying voltage inputs where all voltage-normalized stapes velocities (gain) are all within a factor of 2 (6 dB) of each other across frequencies. Figure 5.5 demonstrates that the generally linear behavior is observed over 30 dB or more of stimulus range. The results of Figures 5.4 and 5.5 suggest the device is most nearly linear with drive voltages of $1V_{peak}$ and above. Our assessment of linearity encompasses the whole system from voltage drive of the IC to the output velocity of the stapes. The slight non-linear behavior recorded at low voltages (low strokes of the actuator) is likely due to slightly poorer coupling between the IC membrane and RW membrane. As seen in Fig. 5.4, the gain improves monotonically with higher input voltage and increased stroke of the IC membrane up to 3 V_{peak} and then becomes stable above 3 V_{peak} input.

Because of data from previous experimental studies, we are able to estimate the sound transmission level (the level of hearing) produced by RW stimulation by the new IC. This estimate takes into consideration the effect of volume velocity leak through the scala vestibuli (likely via vestibular aqueduct) during RW stimulation, as was discovered by Stieger et al., 2013. Using data summarized by Frear et al 2018, we determine the frequency-dependent relationships between stapes velocity output and cochlear input drive (differential pressure

across the cochlear partition) during RW stimulation. We then calculate the cochlear input drive for the stapes velocity output measured during IC RW stimulation. We also have the relationship between ear canal pressure input and cochlear input drive during AC stimulation from Frear et al. 2018. With these experimentally derived relationships, we determine the equivalent input of ear canal sound pressure required for levels of cochlear input drive obtained during RW stimulation with the new IC (Figure 5.7). The results suggest that input stimulus of approximately $6V_{peak}$ to the new IC can give an equivalent level of hearing that is better than 80dB SPL input at the ear-canal during normal AC stimulation. The output greatly increases above 1 kHz for the same voltage input (30-40 dB per decade). However, the method used to calculate the equivalent ear canal pressure has limitations because it relied on transfer functions derived from the averages of data obtained from different temporal bones from this study. Thus accuracy of this estimate is limited by the frequency dependent variations seen across ears (standard deviation shown in Fig. 5.6).

Computational Modeling to Understand Sound Transmission

To better understand RW sound transmission with the IC, we used the impedance model of the inner ear from Frear et al. 2018 (Chapter 3) and incorporated the IC device coupled to the RW.

Modeling to estimate the device volume velocity

The volume velocity output of the IC device was estimated from velocity measurements at the center of the vibrating diaphragm of the bellows actuator made without load (before

attaching to the IC tubing). Such an estimate was necessary because the loaded IC vibrating membrane interfaced to the RW membrane was not accessible for measurement. The volume velocity of the bellows actuator given a 6 V_{peak} input with no load grows proportionally with stimulus level with a phase of 0.25 periods relative to the stimulus voltage, as plotted in Figure 5.8. This behavior is consistent with an ideal volume displacement source that can be described in the sinusoidal steady state by the following equation:

$$Model\ U_{device} = i * (f * 2\pi) * Area_{device} * Volt * C \qquad \text{Equation 5.2}$$

Where *i* is the imaginary number, $Area_{device}$ = $(0.0018/2)^2 * \pi$ m^2, *Volt* = the stimulus voltage, and *C* = constant = 1.3e-8 m/V for the bellows actuator. The constant was determined by fitting the model equation to the experimental data of the bellows actuator volume velocity (Figure 5.8). This ideal volume displacement source model (U_{device}) will be used as the estimated input to the RW in our inner and middle ear model.

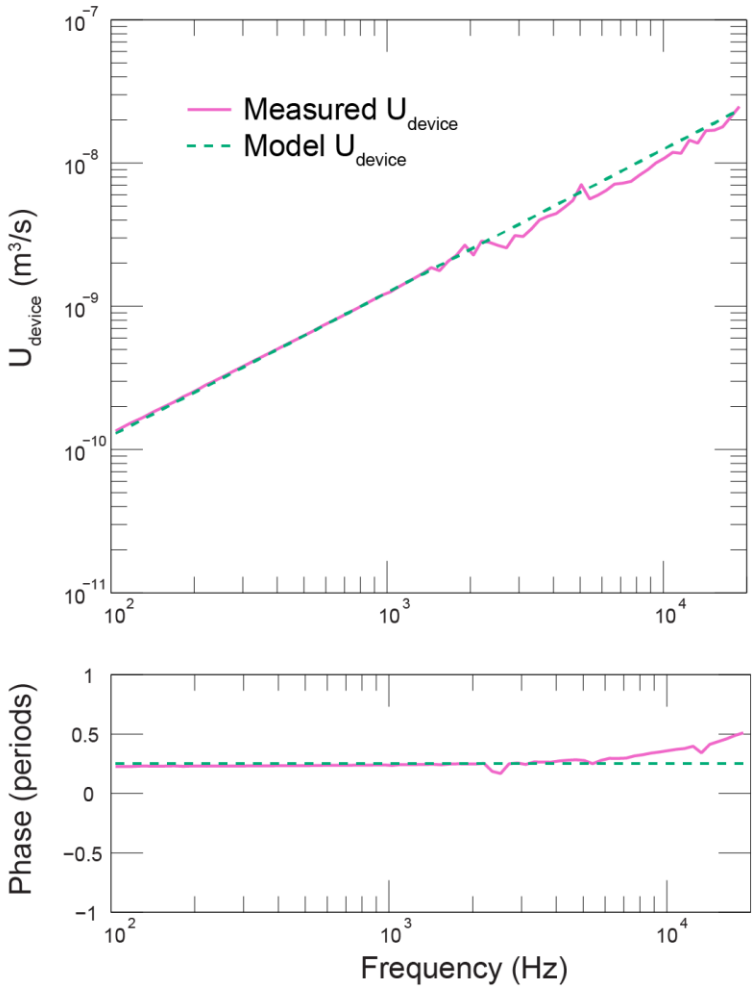

Figure 5.8: Modeling the bellows actuator of the IC as an ideal volume displacement source. The model (dashed line) fits well with the measured (solid line) device volume velocity especially below 3kHz. The measurement and model prediction were made with 6 V_{peak} stimulus drive without load.

Modeling the volume velocity of the stapes

The impedance model described in Frear et al. 2018 (Chapter 3) determined the impedances (Z) in Figure 5.9A: Z_{Diff}, $Z_{ME'}$, Z_{lkSV}, and Z_{lkSTRW} from experimental measurements of intracochlear pressures and velocities of the stapes and RW actuator during AC and RW stimulation. Z_{lkSTRW} is a combination of the physiological leakage impedance of the ST (possibly the cochlear aqueduct) and leakage at the RW-actuator interface, as these two leakages cannot

be separated given the stimulation method (described in Frear et al 2018). The leak due to Z_{lkSTRW} was likely dominated by the volume velocity leak at the RW membrane during stimulation with a rod smaller in diameter than the RW membrane (Frear et al 2018). By knowing the impedances from our earlier study and our estimated input (our modeled U_{device}), we can calculate the expected U_{stap}:

$$U_{stap} = \frac{Z_{lkSV} * U_{Diff}}{Z_{ME'} + Z_{lkSV}} \qquad \text{Equation 5.3}$$

$$U_{stap} = \frac{Z_{lkSV} * \frac{U_{device} * Z_{lkSTRW}}{Z_{c_{rev}} + Z_{lkSTRW}}}{Z_{ME'} + Z_{lkSV}} \qquad \text{Equation 5.4}$$

Where Z_{crev} is the combined impedance of Z_{Diff}, Z_{ME}, *and* Z_{lksv}; where the parallel Z_{ME} and Z_{lksv} are in series with Z_{Diff}:

$$Z_{c_{rev}} = Z_{Diff} + \frac{Z_{lkSV} * Z_{ME'}}{Z_{lkSV} + Z_{ME'}} \qquad \text{Equation 5.5}$$

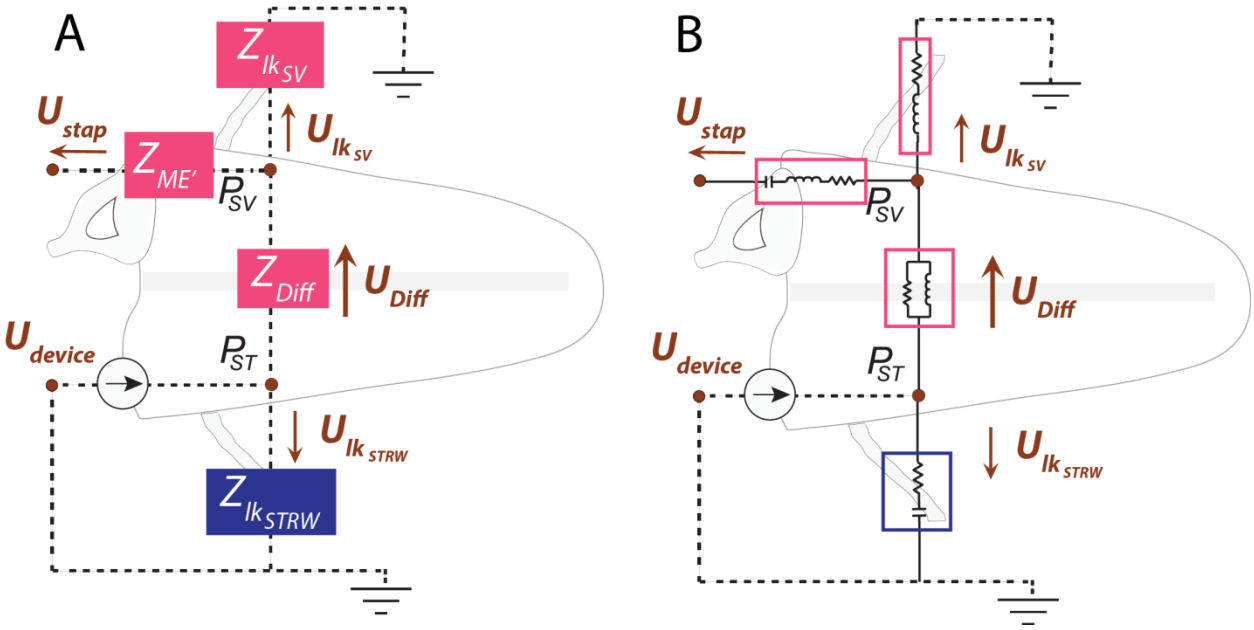

Figure 5.9: Impedance model. A) Impedance model during RW stimulation where impedances are represented by blocks. B) Diagram with circuit elements representing the impedances.

In Frear et al. 2018, Z_{lkSTRW} was low because the actuator rod tip only interfaced a portion of the RW membrane area. In this study, the coupling method of the IC with the RW membrane has less leakage of volume velocity as compared to the Frear et al. 2018 rod method. Therefore, we calculate a new Z_{lkSTRW} to determine the leak from the IC-RW coupling and physiological ST leak (likely the cochlear aqueduct).

To calculate U_{stap} (Equation 5.4), the circuit elements representing the impedance in Figure 5.9A are depicted in Figure 5.9B. The values for Z_{Diff}, $Z_{ME'}$, Z_{lksv}, and Z_{lkSTRW} were obtained from the average calculated model values in Frear et al 2018. In Figure 5.10, we plot the experimental U_{stap} / U_{device} when stimulating the RW with the IC (red); where U_{device} is the modeled (estimated) volume velocity described in Equation 5.2 and Fig. 5.8. The model data for the IC-driven case using the average values found in Frear et al 2018 is plotted with a purple line (Model with rod+actuator) in Fig. 5.10. Since the data using the rod and actuator results

(purple) do not adequately represent the experimental results (red), modification of the Z_{lkSTRW} impedance was necessary. Z_{lkSTRW} was found to be best modeled with a resistor and compliance in series and we did not alter this configuration, however new values for the elements were determined for the IC-RW coupling by fitting the predicted U_{stap} (Equation 5.4) to the experimental measurements (red) of Figure 5.10. Z_{lkSTRW} needed to increase as using the IC stimulator likely resulted in less leakage out of the RW than when using the rod+actuator. The increased leakage impedance resulted in our Model of the IC (blue) to better fit the experimental data (red) in Figure 5.10.

Component values are as below:

1. Z_{lkSTRW} for Model with rod-actuator driving the RW (from Frear et al. 2018):

   R = 4.10e9 and C = 7.49e-14 (purple) and

2. Z_{lkSTRW} for Model with IC driving the RW to best fit the experimental data:

   R = 1.07e10 and C = 7.43e-15 (blue).

The average Z_{lkSTRW} with rod+actuator results in a smaller U_{stap} than measured experimentally with IC stimulation, indicating more leakage with the rod+actuator stimulation used in Frear et al. 2018 as compared to the new IC-RW stimulation. The Z_{lkSTRW} with IC stimulation has a higher acoustic resistance and lower acoustic compliance to account for less leakage with the IC, demonstrating better sound transmission with the IC as compared to the rod-actuator method used in Frear et al 2018.

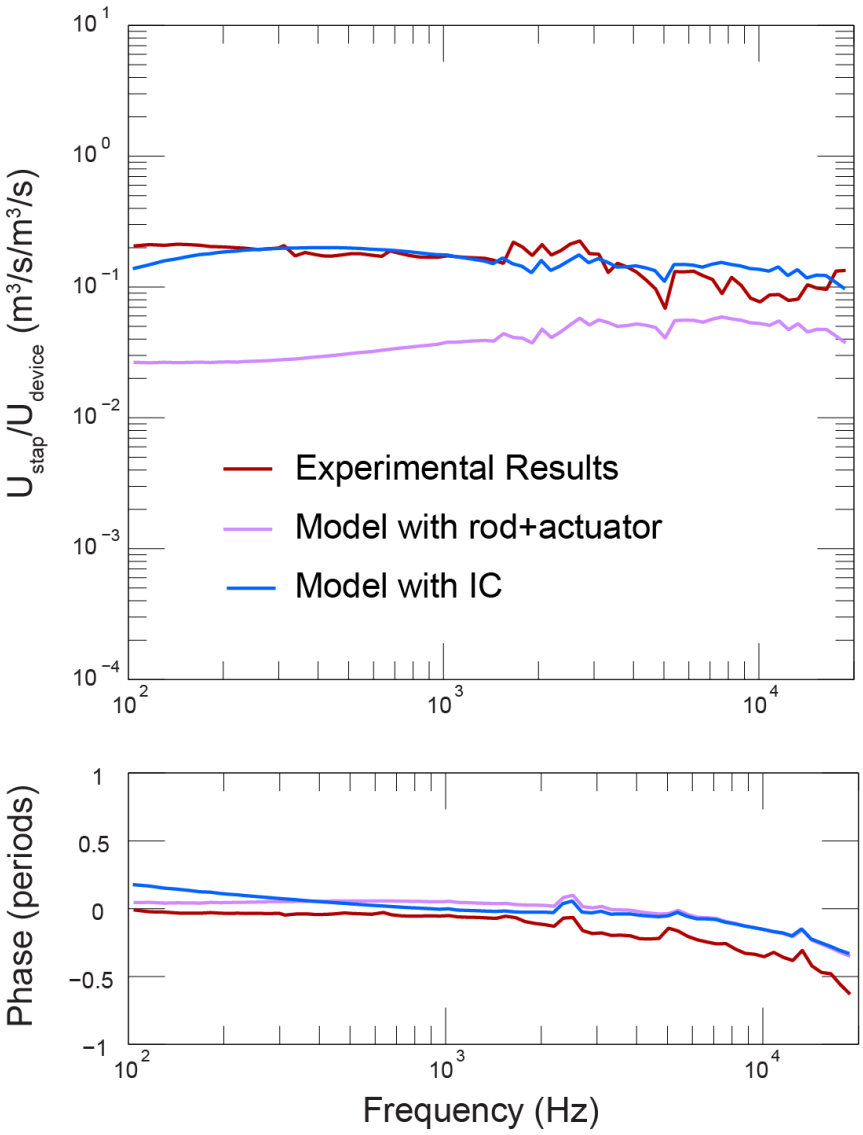

Figure 5.10: Modeling the volume velocity ratio. Measured U_{stap}/U_{device} with IC driven RW stimulation are plotted in red (experiment df14). The model data with rod-actuator are in purple (values from Frear et al 2018). The model data with IC are in blue. The model data with the IC values are similar to the experimental data.

The resistance and compliance in series work well to model the combined leakage at the ST and RW, Z_{lkSTRW}, during RW stimulation with the IC. The compliance could be representing 1) the compressibility of the water/fascia between the IC and the RW membrane or 2) a pocket of

air within the water/fascia. To better understand the compliance representation, we consider the two possibilities.

1) *Compressibility of the water/fascia:* The RW niche with a diameter of approximately 2.5mm and length of 2.7 mm, has a volume of approximately 1.33e-8 m^3 for a representative specimen df14. With the bulk modulus of water (2.15e9 N/m^2), the compliance can be calculated as C = volume / bulk modulus = 6.19e-18 m^5/N. This compliance, C, is about 3 orders of magnitude smaller than the C calculated for our new Z_{IkSTRW} with IC-RW stimulation. Thus, the compliance is unlikely representing the compressibility of the fluid between the IC and RW.

2) *Compressibility of air:* The bulk modulus of air is 1.42e5 N/m^2 in adiabatic conditions (assuming no heat transfer with its surroundings). The volume of the air is calculated by, volume of air = C*bulk modulus = (7.43e-15 m^5/N)*(1.42e5 N/m^2) = 1.05e-9 m^3.
The volume of the RW niche was estimated to be 1.33e-8 m^3, so the compliance could be representing air bubble(s) about a tenth of the size of the RW-niche volume between the IC and the RW membrane. Our calculations are consistent with the possibility that the compliance represents a small volume of air within the fluid/fascia in the RW niche between the IC and RW membrane.

The cochlear aqueduct is a physiologic leakage path from the ST, and is modeled as a resistor and mass (inductor) in series (i.e. modeled as a small tube) (Gopen, Rosowski, and Merchant 1997; Elliott, Ni, and Verschuur 2016; John J. Rosowski, Bowers, and Nakajima 2017). There are other cases where it is modeled with a compliance in series with a resistance which represents the compliance of the fluid-filled cranial space (Stenfelt 2015). Unfortunately, using the IC as a RW stimulator did not allow us to separate the RW leakage from the ST leakage

(cochlear aqueduct). The leakage at the RW dominates our Z_{lkSTRW} model (compliance) due to the air bubbles between the device and the RW membrane. Because removing all air bubbles is difficult and the leakage at the RW and ST is much more relevant during RW stimulation, our model is a good estimate of our experimental results and for future patients with a RW stimulation device. However, in the future we can change our model to incorporate the small tube model of the ST leakage with compliance and resistance model of the RW leakage.

Future Work

In addition to achieving our aims of improving the IC design for increased safety and sound transmission, the IC is an all-in-one device with internalized actuator, allowing for easy fit and surgical placement. The next step is to develop a simple robust method to stabilize the IC device at the RW niche. We had superior results when the IC was just touching the soft Jeltrate on the bony rim of the RW niche, stabilized with a rod slightly pushing the non-vibrating end of the IC to hold it in place. If the IC was pushed further towards the RW, the output stapes velocity showed fluctuations with change in frequency instead of the smooth frequency response obtained with less force from the stabilizing rod. The jagged frequency response obtained when the IC was pushed firmly towards the RW might be due to leakage of volume velocity (soft Jeltrate can no longer seal well) and/or bone conduction (metal rim of IC touching bone). There are various methods possible to secure the IC device in place. One possibility is by metal hardware (rod or plate) with a ball hinge to secure the IC to an adjacent wall of bone with screws (similar to ball and socket joints seen for middle-ear devices from Cochlear®). Another possibility is to use bone cement already used in otologic surgery. These methods will have to

be tested and made to work for anatomic variations across ears. Another important step is to have acceptable alternative materials that are biocompatible and stable for the IC's flexible membrane and the soft Jeltrate seal between bone surrounding the RW and IC rim. Also, available cements used for otologic surgery could be an alternative to dental cement to fill crevasses of the bony RW niche. We have designed the IC for safety, good sound transmission (linearity, dynamic range and bandwidth), consistency of performance across varied anatomy, and for the potential of mechanical stability. In the future, we can further modify the IC for ease of surgery and for biocompatibility.

CHAPTER 6.

Conclusion

This dissertation investigates how patients affected by surgically addressable conductive hearing loss may be helped by the implementation of a new round window (RW) stimulation device that is designed to fit across various RW niche anatomies. In investigating the need for such a device, in Chapter 2, we identified the fraction of hearing loss cases to which it might be applied. Of the almost 175,000 diagnosed patients visiting Massachusetts Eye and Ear hospitals for hearing loss over 3.5 years, 27% were sensorineural, 25% were earwax buildup/impaction, 19% were acute otitis media, 13% were unknown, and 16% were surgically treatable conductive hearing loss. This last group is the potential pool of patients that could be addressed by our RW stimulation device. The breakdown of patients diagnosed with hearing loss not only provides impact to the research surrounding the disease/problem but will also help target where to focus more resources and track types of hearing loss over time. In the future, this study will include more patient diagnosis data from different hospital networks to broaden the dataset.

In Chapter 3 we investigated the mechanical issues relevant to round-window stimulation by quantifying the mechanisms relevant to sound transmission to the inner ear, and constructing a computational impedance model that can predict the outcome of such stimulation. This study allowed a comparison of how conventional ossicular and RW stimulation produce a hearing response. For RW stimulation, unlike conventional air conduction stimulation, the leakage path from scala vestibuli is an important factor because the impedance of the reverse middle ear is much higher than the impedance of the scala vestibuli leakage path at low frequencies. This scala vestibuli leakage impedance plays an important role in producing a pressure differential across the cochlea partition (i.e. a vector difference in pressure between scala vestibuli compared to the scala tympani). Quantification of the volume velocity leak at the

RW/actuator interface helps us estimate the efficacy of RW stimulation. The computational model determined in Chapter 3 is also helpful in comparing past and future studies including the data obtained in Chapter 5. This model will also be useful in the future to understand the effect of pathologies and varied sound stimulation methods to transmit sound to the inner ear.

In Chapter 4, we designed and developed an early prototype device for RW stimulation, which was improved upon in Chapter 5. Chapter 4 focused on proof of concept of our design idea, as we used a human temporal bone experiment to compare the stimulus at the inner-ear provided by the prototype interface coupler (IC) to that produced by the currently used clinical device, the floating mass transducer (FMT). The design of the IC improved the coupling of the device to the RW membrane and enabled transmission of more volume velocity into the cochlea than the FMT. When comparing the results of the FMT and IC, the volume velocity of the stapes response was higher using the IC and linearity, dynamic range and bandwidth were greatly improved.

In Chapter 5 we focused our design improvements on: 1) consistency of RW coupling across widely varying anatomy, 2) increasing safety by minimizing the necessity of drilling the bone surrounding the RW to place the coupler, 3) integrating the actuator within the IC, 4) improving the architecture of the design for easy and reliable surgical implantation. These goals were achieved with a device that produced a linear output over a good dynamic range and wide bandwidth. The improved IC prototype further demonstrated a proof of concept. Future work needs to further improve the IC interface to the RW niche and determine biocompatibility. If improvements related to clinical applicability can be met, this device has the potential as a solution for those with conductive and mixed hearing loss that are not helped by conventional

means. It is also possible that surgeries such as certain tympanoplasties, ossicular reconstruction, stapedectomy, repair for aural atresia, and more could be replaced with the IC RW stimulation in certain circumstances.

Chapter 5 also utilized the computational impedance model of Chapter 3 to estimate the equivalent AC hearing produced by RW stimulation. The impedance model was also found to work well with the input used with the IC RW stimulator. By simulating the measurements with modeling, the leakage impedance at the IC-RW interface at the scala tympani was well characterized with a compliance and resistance in series. The compliance is likely from small pockets of air between the IC and the RW membrane. The compliance element likely represents the leakage at the RW, but another component in parallel would be needed to represent the leakage impedance of the scala tympani. This parallel component, the cochlear aqueduct, can be represented by a small tube, or a resistance and mass (inductor) in series. The resistor+inductor component of the cochlear aqueduct will be much higher in impedance than the resistor+capacitor of the inefficient RW coupling component. The cochlear aqueduct (leakage at scala tympani) and vestibular aqueduct (leakage at scala vestibuli which we characterized) likely have important frequency-dependent roles during various stimulation methods such as bone conduction. Our model is largely based on anatomical features of the ear, and addition of components such as leakage impedances will make it more accurate.

The goals of this thesis were to improve understanding of sound transmission through the ear by computational modeling where impedance values are obtained by detailed experimental measurements, to develop a high-performing RW stimulation device, and to determine the population impact of such studies and developments in the field of auditory

mechanics. Contributions from this thesis will enable further knowledge and developments to help the large number of patients who suffer conductive and mixed hearing loss.

Appendix A2

Sensorineural hearing loss
Acoustic Neuroma/Vestibular Schwannoma
(bacterial/viral) Labyrinthitis
Vestibular disequilibrium/hypofunction
Balance problem
Noise induced hearing loss
Inner ear dysfunction
Drug induced or ototoxic hearing loss
Presbycusis
Undefined SNHL
    SNHL
    Sudden idiopathic hearing loss
    Rubella, Deaf mutism

Conductive hearing loss
Ear Canal
    (Acquired) Stenosis of the external ear canal
    Atresia of auditory canal
    Cholesteatoma (of attic of ear)
Tympanic membrane
    Granuloma
    Cholesteatoma
    Perforation (attic/marginal/ multiple/total/healed)
    Atrophic (non)flaccid
    Retraction
    Irritation
    Disorder
    Abnormal
    Tympanosclerosis
    Retained myringotomy tube
    Acute OM with rupture of TM
Middle ear
    Adhesion
    Ossicular chain disarticulation
    Dislocation
    Ankylosis (malleus/ossicles)
    Necrosis/Erosion/loss
    Disorder
    Abnormality
    (Granulation) Polyp
    Granuloma
Mastoid
    Cholesteatoma
    Disorder
    Draining
    Infectious
    Other – classified elsewhere
Otosclerosis
    Involving oval window (nonobliterative/obliterative)
    Involving round window
    Other
Superior semicircular canal dehiscence
Undefined CHL
Chronic OM
    Chronic serous OM
    Chronic with rupture of TM
    Chronic myringitis
    Chronic tubotympanic OM
Mixed hearing loss

Acute OM
Acute Myringitis
Acute serous OM
Recurrent acute allergic OM
Acute effusion
Eardrum inflammation
Recurrent acute OM
OM undefined

Earwax
Excessive
Impacted cerumen

Unknown
Asymmetrical hearing loss
Decreased hearing
Generic hearing loss
Temporal bone fracture, Birth trauma, Old head trauma, enlarged vestibular aqueduct, congenital abnormality

Appendix A3

The error between the model and experimental data was calculated using a least squares technique as outlined below.

We define:
$x_{m,\nu}$ as the complex result of the model at the ν^{th} frequency,
$x_{e,\nu}$ as the complex result of the experiment (expt) at the ν^{th} frequency, and
T_ν as the complex ratio of these complex numbers:

$$T_\nu = \frac{x_{e,\nu}}{x_{m,\nu}}.$$

This ratio can be written as

$$T_\nu = Re\{T_\nu\} + jIm\{T_\nu\}$$

or

$$T_\nu = r_\nu e^{j\theta_\nu},$$

where $r_\nu = \frac{|\,expt\,|}{|\,model\,|}$ and θ_ν= phase of experiment – phase of model (in radians).

We want $T_\nu$to be as close to one as possible across frequency points *v* such that the model well fits the experimental data. In particular, we'd like both the log magnitude and phase of the model to match the experimental results. To accomplish this, we seek to minimize the root mean square of $\log_{10}(T_\nu)$ across points *v* as follows:

Taking the base 10 logarithm of the above equation:

$$\log_{10}(T_\nu) = \log_{10}(r_\nu) + \log_{10}(e^{j\theta_\nu})$$

$$= \log_{10}(r_\nu) + j\theta_\nu \log_{10}(e),$$

we find the model that minimizes the root mean square (RMS) of $\log_{10}(T_\nu)$ across frequencies *v,* where:

$$RMS(\log_{10}(T_\nu)) = \sqrt{\frac{1}{N}\sum_{\nu=1}^{N}((\log_{10}(r_\nu))^2 + (\log_{10}(e))^2 * (\theta_\nu)^2)}$$

$$= Total\ Error = \sqrt{\frac{1}{N}\sum_{\nu=1}^{N}\left(\left(Error_{mag}\right)^2 + (\log_{10}(e))^2 * \left(Error_{phase}\right)^2\right)}$$

where

$$Error_{mag}^2 = \frac{1}{N}\sum_{\nu=1}^{N}\left(\log_{10}\left(Model_{mag}\right) - \log_{10}\left(Expt_{mag}\right)\right)^2$$

and

$$Error_{phase}^{2} = \frac{1}{N}\sum_{\nu=1}^{N}\left(Model_{phase} - Expt_{phase}\right)^{2}.$$

Note that the error is based on ratios and is dimensionless. The model parameters were systematically adjusted to produce the lowest possible *Total Error* over the 100 to 2000 Hz frequency range. We also use the *Total Error* to compare the fits of all the models (Table 3.3).

References

Agrawal, Yuri, Bryan K. Ward, and Lloyd B. Minor. 2013. "Vestibular Dysfunction: Prevalence, Impact and Need for Targeted Treatment." *Journal of Vestibular Research : Equilibrium & Orientation* 23 (3): 113–17. https://doi.org/10.3233/VES-130498.

Aibara, R., J. T. Welsh, S. Puria, and R. L. Goode. 2001. "Human Middle-Ear Sound Transfer Function and Cochlear Input Impedance." *Hearing Research* 152 (1–2): 100–109.

Arnold, Andreas, Martin Kompis, Claudia Candreia, Flurin Pfiffner, Rudolf Häusler, and Christof Stieger. 2010. "The Floating Mass Transducer at the Round Window: Direct Transmission or Bone Conduction?" *Hearing Research* 263 (1–2): 120–27. https://doi.org/10.1016/j.heares.2009.12.019.

Arnold, Andreas, Christof Stieger, Claudia Candreia, Flurin Pfiffner, and Martin Kompis. 2010. "Factors Improving the Vibration Transfer of the Floating Mass Transducer at the Round Window:" *Otology & Neurotology* 31 (1): 122–28. https://doi.org/10.1097/MAO.0b013e3181c34ee0.

Ballenger, John Jacob, and James Byron Snow. 2003. *Ballenger's Otorhinolaryngology: Head and Neck Surgery*. PMPH-USA.

Baumgartner, W.-D., K. Böheim, R. Hagen, J. Müller, T. Lenarz, S. Reiss, M. Schlögel, et al. 2010. "The Vibrant Soundbridge for Conductive and Mixed Hearing Losses: European Multicenter Study Results" 69: 38–50. https://doi.org/10.1159/000318521.

Beltrame, Achille M., Alessandro Martini, Silvano Prosser, Nadia Giarbini, and Christian Streitberger. 2009. "Coupling the Vibrant Soundbridge to Cochlea Round Window: Auditory Results in Patients with Mixed Hearing Loss." *Otology & Neurotology: Official Publication of the American Otological Society, American Neurotology Society [and] European Academy of Otology and Neurotology* 30 (2): 194–201.

Bernardeschi, Daniele, Caroline Hoffman, Tarek Benchaa, Samia Labassi, Michel Beliaeff, Olivier Sterkers, and Alexis Bozorg Grayeli. 2011. "Functional Results of Vibrant Soundbridge Middle Ear Implants in Conductive and Mixed Hearing Losses." *Audiology and Neurotology* 16 (6): 381–387.

Brackmann, D. E., J. L. Sheehy, and W. M. Luxford. 1984. "TORPs and PORPs in Tympanoplasty: A Review of 1042 Operations." *Otolaryngology--Head and Neck Surgery: Official Journal of American Academy of Otolaryngology-Head and Neck Surgery* 92 (1): 32–37.

Browning, George GG. 2008. "Ear Wax." *BMJ Clinical Evidence* 2008 (January). https://www.ncbi.nlm.nih.gov/pmc/articles/PMC2907972/.

Chien, Wade, Michael E. Ravicz, Saumil N. Merchant, and John J. Rosowski. 2006. “The Effect of Methodological Differences in the Measurement of Stapes Motion in Live and Cadaver Ears.” *Audiology & Neuro-Otology* 11 (3): 183–97. https://doi.org/10.1159/000091815.

Chien, Wade, John J. Rosowski, Michael E. Ravicz, Steven D. Rauch, Jennifer Smullen, and Saumil N. Merchant. 2009. “Measurements of Stapes Velocity in Live Human Ears.” *Hearing Research* 249 (1–2): 54–61. https://doi.org/10.1016/j.heares.2008.11.011.

Colletti, Liliana, Marco Carner, Marco Mandalà, Sheila Veronese, and Vittorio Colletti. 2011. “The Floating Mass Transducer for External Auditory Canal and Middle Ear Malformations:” *Otology & Neurotology* 32 (1): 108–15. https://doi.org/10.1097/MAO.0b013e3181ff752a.

Colletti, V., M. Carner, L. Colletti, and others. 2005. “Round Window Stimulation with the Floating Mass Transducer: A New Approach for Surgical Failures of Mixed Hearing Losses.” *IFOS, Rome*.

Colletti, Vittorio, Sigfrid D. Soli, Marco Carner, and L. Colletti. 2006. “Treatment of Mixed Hearing Losses via Implantation of a Vibratory Transducer on the Round Window.” *International Journal of Audiology* 45 (10): 600–608. https://doi.org/10.1080/14992020600840903.

Crane, Benjamin T., Frank R. Lin, Lloyd B. Minor, and John P. Carey. 2010. “Improvement in Autophony Symptoms after Superior Canal Dehiscence Repair.” *Otology & Neurotology: Official Publication of the American Otological Society, American Neurotology Society [and] European Academy of Otology and Neurotology* 31 (1): 140–46.

Crane, Benjamin T., Lloyd B. Minor, and John P. Carey. 2008. “Superior Canal Dehiscence Plugging Reduces Dizziness Handicap.” *The Laryngoscope* 118 (10): 1809–13. https://doi.org/10.1097/MLG.0b013e31817f18fa.

Cuda, Domenico, Alessandra Murri, and Nicoletta Tinelli. 2009. “Piezoelectric Round Window Osteoplasty for Vibrant Soundbridge Implant.” *Otology & Neurotology* 30 (6): 782. https://doi.org/10.1097/MAO.0b013e3181b04d4d.

Dallos, Peter. 1970. “Low?Frequency Auditory Characteristics: Species Dependence.” *The Journal of the Acoustical Society of America* 48 (2B): 489–99. https://doi.org/10.1121/1.1912163.

Dancer, A., and R. Franke. 1980. “Intracochlear Sound Pressure Measurements in Guinea Pigs.” *Hearing Research* 2 (3–4): 191–205. https://doi.org/10.1016/0378-5955(80)90057-X.

Elliott, Stephen J., Guangjian Ni, and Carl A. Verschuur. 2016. “Modelling the Effect of Round Window Stiffness on Residual Hearing after Cochlear Implantation.” *Hearing Research* 341 (November): 155–67. https://doi.org/10.1016/j.heares.2016.08.006.

Frear, Darcy L., Xiying Guan, Christof Stieger, John J. Rosowski, and Hideko Heidi Nakajima. 2018. “Impedances of the Inner and Middle Ear Estimated from Intracochlear Sound Pressures in Normal Human Temporal Bones.” *Hearing Research* 367 (September): 17–31. https://doi.org/10.1016/j.heares.2018.06.019.

Georg von Békésy, and Ernest Glen Wever. 1960. *Experiments in Hearing*. Vol. 8. New York: MCGraw-Hill. https://scholar.google.com/scholar_lookup?title=Experiments%20in%20hearing&author=B%C3%A9k%C3%A9sy&publication_year=1960.

Goode, R. L., G. Ball, and S. Nishihara. 1993. “Measurement of Umbo Vibration in Human Subjects--Method and Possible Clinical Applications.” *The American Journal of Otology* 14 (3): 247–51.

Gopen, Quinton, John J Rosowski, and Saumil N Merchant. 1997. “Anatomy of the Normal Human Cochlear Aqueduct with Functional Implications.” *Hearing Research* 107 (1–2): 9–22. https://doi.org/10.1016/S0378-5955(97)00017-8.

Goycoolea, Marcos V., and Lars Lundman. 1997. “Round Window Membrane. Structure Function and Permeability: A Review.” *Microscopy Research and Technique* 36 (3): 201–11. https://doi.org/10.1002/(SICI)1097-0029(19970201)36:3<201::AID-JEMT8>3.0.CO;2-R.

Hato, Naohito, Stefan Stenfelt, and Richard L. Goode. 2003. “Three-Dimensional Stapes Footplate Motion in Human Temporal Bones.” *Audiology and Neurotology* 8 (3): 140–52. https://doi.org/10.1159/000069475.

Heiland, K. E., R. L. Goode, M. Asai, and A. M. Huber. 1999. “A Human Temporal Bone Study of Stapes Footplate Movement.” *The American Journal of Otology* 20 (1): 81–86.

Henning Frenzel, Frauke Hanke, Millo Beltrame, Armin Steffen, Rainer Schönweiler, and Barbara Wollenberg. 2008. “Application of the Vibrant Soundbridge® to Unilateral Osseous Atresia Cases.” *The Laryngoscope* 119 (1): 67–74.

Hoffman, Howard J., Robert A. Dobie, Katalin G. Losonczy, Christa L. Themann, and Gregory A. Flamme. 2017. “Declining Prevalence of Hearing Loss in US Adults Aged 20 to 69 Years.” *JAMA Otolaryngology–Head & Neck Surgery* 143 (3): 274–85. https://doi.org/10.1001/jamaoto.2016.3527.

Holmquist, J., R. Oleander, and O. Hallén. 1979. “Peroperative Drill-Generated Noise Levels in Ear Surgery.” *Acta Oto-Laryngologica* 87 (5–6): 458–60.

Iwasaki, Satoshi, Hiroaki Suzuki, Hideaki Moteki, Maiko Miyagawa, Yutaka Takumi, and Shin-ichi Usami. 2012. “Experience with the Vibrant Soundbridge RW-Coupler for Round Window Vibroplasty with Tympanosclerosis.” *Acta Oto-Laryngologica* 132 (6): 676–82. https://doi.org/10.3109/00016489.2011.649492.

Kiefer, Jan, Wolfgang Arnold, and Rainer Staudenmaier. 2006. “Round Window Stimulation with an Implantable Hearing Aid (Soundbridge®) Combined with Autogenous Reconstruction of the Auricle – A New Approach.” *ORL* 68 (6): 378–85. https://doi.org/10.1159/000095282.

Kringlebotn, Magne. 1995. “The Equality of Volume Displacements in the Inner Ear Windows.” *The Journal of the Acoustical Society of America* 98 (1): 192–96. https://doi.org/10.1121/1.413746.

Kylén, P., and S. Arlinger. 1976. “Drill-Generated Noise Levels in Ear Surgery.” *Acta Oto-Laryngologica* 82 (1–6): 402–9. https://doi.org/10.3109/00016487609120925.

Lee, K., and H. F. Schuknecht. 1971. “Results of Tympanoplasty and Mastoidectomy at the Massachusetts Eye and Ear Infirmary.” *The Laryngoscope* 81 (4): 529–43. https://doi.org/10.1288/00005537-197104000-00004.

Li, Peter M. M. C., Haobing Wang, Clarinda Northrop, Saumil N. Merchant, and Joseph B. Nadol. 2007. “Anatomy of the Round Window and Hook Region of the Cochlea With Implications for Cochlear Implantation and Other Endocochlear Surgical Procedures:” *Otology & Neurotology* 28 (5): 641–48. https://doi.org/10.1097/mao.0b013e3180577949.

Lin, Frank R., John K. Niparko, and Luigi Ferrucci. 2011. “Hearing Loss Prevalence in the United States.” *Archives of Internal Medicine* 171 (20): 1851–52. https://doi.org/10.1001/archinternmed.2011.506.

Lupo, J. Eric, Kanthaiah Koka, N. Julian Holland, Herman A. Jenkins, and Daniel J. Tollin. 2009. “Prospective Electrophysiologic Findings of Round Window Stimulation in a Model of Experimentally Induced Stapes Fixation.” *Otology & Neurotology* 30 (8): 1215–1224.

Lynch, T. J., V. Nedzelnitsky, and W. T. Peake. 1982. “Input Impedance of the Cochlea in Cat.” *The Journal of the Acoustical Society of America* 72 (1): 108–30.

Maier, Hannes, Rolf Salcher, Burkard Schwab, and Thomas Lenarz. 2013. “The Effect of Static Force on Round Window Stimulation with the Direct Acoustic Cochlea Stimulator.” *Hearing Research* 301 (July): 115–24. https://doi.org/10.1016/j.heares.2012.12.010.

Marco Mandalà, Liliana Colletti, and Vittorio Colletti. 2011. “Treatment of the Atretic Ear With Round Window Vibrant... : Otology & Neurotology.” 2011. https://doi.org/10.1097/MAO.0b013e31822e9513.

Marino, Roberta, Nicola Linton, Robert H. Eikelboom, Elle Statham, and Gunesh P. Rajan. 2013. “A Comparative Study of Hearing Aids and Round Window Application of the Vibrant Sound Bridge (VSB) for Patients with Mixed or Conductive Hearing Loss.” *International Journal of Audiology* 52 (4): 209–18. https://doi.org/10.3109/14992027.2012.750431.

Martin, Christian, Arnaud Deveze, Céline Richard, Philippe P. Lefebvre, Monique Decat, Luis Garcia Ibañez, Eric Truy, et al. 2009. “European Results with Totally Implantable Carina Placed on the Round Window: 2-Year Follow-Up.” *Otology & Neurotology* 30 (8): 1196–1203.

Merchant, Saumil N., Michael J. McKenna, Ritvik P. Mehta, Michael E. Ravicz, and John J. Rosowski. 2003. “Middle Ear Mechanics of Type III Tympanoplasty (Stapes Columella): II. Clinical Studies.” *Otology & Neurotology: Official Publication of the American Otological Society, American Neurotology Society [and] European Academy of Otology and Neurotology* 24 (2): 186–94.

Minor, L. B., D. Solomon, J. S. Zinreich, and D. S. Zee. 1998. “Sound- and/or Pressure-Induced Vertigo Due to Bone Dehiscence of the Superior Semicircular Canal.” *Archives of Otolaryngology--Head & Neck Surgery* 124 (3): 249–58.

Minor, Lloyd B., Phillip D. Cremer, John P. Carey, Charles C. Della Santina, Sven-Olrik Streubel, and Noah Weg. 2001. “Symptoms and Signs in Superior Canal Dehiscence Syndrome.” *Annals of the New York Academy of Sciences* 942 (1): 259–73. https://doi.org/10.1111/j.1749-6632.2001.tb03751.x.

Monasta, Lorenzo, Luca Ronfani, Federico Marchetti, Marcella Montico, Liza Vecchi Brumatti, Alessandro Bavcar, Domenico Grasso, Chiara Barbiero, and Giorgio Tamburlini. 2012. “Burden of Disease Caused by Otitis Media: Systematic Review and Global Estimates.” *PloS One* 7 (4): e36226. https://doi.org/10.1371/journal.pone.0036226.

Nadol, Joseph B., and Michael J. McKenna. 2005. *Surgery of the Ear and Temporal Bone*. Lippincott Williams & Wilkins.

Nakajima, Hideko Heidi, Wei Dong, Elizabeth S. Olson, Saumil N. Merchant, Michael E. Ravicz, and John J. Rosowski. 2009. “Differential Intracochlear Sound Pressure Measurements in Normal Human Temporal Bones.” *Journal of the Association for Research in Otolaryngology* 10 (1): 23–36. https://doi.org/10.1007/s10162-008-0150-y.

Nakajima, Hideko Heidi, Wei Dong, Elizabeth S. Olson, John J. Rosowski, Michael E. Ravicz, and Saumil N. Merchant. 2010. “Evaluation of Round Window Stimulation Using the Floating Mass Transducer by Intracochlear Sound Pressure Measurements in Human Temporal Bones.” *Otology & Neurotology: Official Publication of the American Otological Society, American Neurotology Society [and] European Academy of Otology and Neurotology* 31 (3): 506–11. https://doi.org/10.1097/MAO.0b013e3181c0ea9f.

Nakajima, Hideko Heidi, Saumil N. Merchant, and John J. Rosowski. 2010. “Performance Considerations of Prosthetic Actuators for Round-Window Stimulation.” *Hearing Research* 263 (1–2): 114–19. https://doi.org/10.1016/j.heares.2009.11.009.

Nakajima, Hideko Heidi, Michael E. Ravicz, Saumil N. Merchant, William T. Peake, and John J. Rosowski. 2005. “Experimental Ossicular Fixations and the Middle Ear’s Response to Sound: Evidence for a Flexible Ossicular Chain.” *Hearing Research* 204 (1–2): 60–77. https://doi.org/10.1016/j.heares.2005.01.002.

Nakajima, Hideko Heidi, Michael E. Ravicz, John J. Rosowski, William T. Peake, and Saumil N. Merchant. 2005. “Experimental and Clinical Studies of Malleus Fixation.” *The Laryngoscope* 115 (1): 147–54. https://doi.org/10.1097/01.mlg.0000150692.23506.b7.

Nedzelnitsky, V. 1980. “Sound Pressures in the Basal Turn of the Cat Cochlea.” *The Journal of the Acoustical Society of America* 68 (6): 1676–89. https://doi.org/10.1121/1.385200.

Niesten, Marlien E.F., Christof Stieger, Daniel J. Lee, Julie P. Merchant, Wilko Grolman, John J. Rosowski, and Hideko Heidi Nakajima. 2015. “Assessment of the Effects of Superior Canal Dehiscence Location and Size on Intracochlear Sound Pressures.” *Audiology and Neurotology* 20 (1): 62–71. https://doi.org/10.1159/000366512.

Olson, E. S. 1998. “Observing Middle and Inner Ear Mechanics with Novel Intracochlear Pressure Sensors.” *The Journal of the Acoustical Society of America* 103 (6): 3445–63.

Otto F. Ranke. 1953. “Physiologie Des Gehörs.” In *Gehör-Stimme-Sprache*, 3–110. Berlin: Springer. http://www.springer.com/us/book/9783642926006.

Pau, Hans Wilhelm, Tino Just, Matthias Bornitz, Nikoloz Lasurashvilli, and Thomas Zahnert. 2007. “Noise Exposure of the Inner Ear during Drilling a Cochleostomy for Cochlear Implantation.” *The Laryngoscope* 117 (3): 535–40. https://doi.org/10.1097/MLG.0b013e31802f4169.

Pennings, Ronald J. E., Allan Ho, Jeremy Brown, René G. van Wijhe, and Manohar Bance. 2010. “Analysis of Vibrant Soundbridge Placement against the Round Window Membrane in a Human Cadaveric Temporal Bone Model.” *Otology & Neurotology: Official Publication of the American Otological Society, American Neurotology Society [and] European Academy of Otology and Neurotology* 31 (6): 998–1003. https://doi.org/10.1097/MAO.0b013e3181e8fc21.

Perez, Ronen, Cahtia Adelman, and Haim Sohmer. 2016. “Fluid Stimulation Elicits Hearing in the Absence of Air and Bone Conduction--An Animal Study.” *Acta Oto-Laryngologica* 136 (4): 351–53. https://doi.org/10.3109/00016489.2015.1113560.

Pisano, Dominic V., Marlien E.F. Niesten, Saumil N. Merchant, and Hideko Heidi Nakajima. 2012. “The Effect of Superior Semicircular Canal Dehiscence on Intracochlear Sound Pressures.” *Audiology and Neurotology* 17 (5): 338–48. https://doi.org/10.1159/000339653.

Pleis, John R., and Margaret Lethbridge-Cejku. 2007. “Summary Health Statistics for U.S. Adults: National Health Interview Survey, 2006: (403882008-001).” American Psychological Association. https://doi.org/10.1037/e403882008-001.

Puria, Sunil. 2003. “Measurements of Human Middle Ear Forward and Reverse Acoustics: Implications for Otoacoustic Emissions.” *The Journal of the Acoustical Society of America* 113 (5): 2773–89.

Rajan, Gunesh P., Peter Lampacher, Ranjeeta Ambett, Gregor Dittrich, Jafri Kuthubutheen, Bradley Wood, Anne McArthur, and Roberta Marino. 2011. “Impact of Floating Mass Transducer Coupling and Positioning in Round Window Vibroplasty.” *Otology & Neurotology* 32 (2): 271–277.

Ravicz, Michael E, Saumil N Merchant, and John J Rosowski. 2000. “Effect of Freezing and Thawing on Stapes-Cochlear Input Impedance in Human Temporal Bones.” *Hearing Research* 150 (1): 215–24. https://doi.org/10.1016/S0378-5955(00)00200-8.

Rosowski, J.J., W. Chien, M.E. Ravicz, and S.N. Merchant. 2007. “Testing a Method for Quantifying the Output of Implantable Middle Ear Hearing Devices.” *Audiology & Neuro-Otology* 12 (4): 265–76. https://doi.org/10.1159/000101474.

Rosowski, John J., Peter Bowers, and Hideko H. Nakajima. 2017. “Limits on Normal Cochlear ‘Third’ Windows Provided by Previous Investigations of Additional Sound Paths into and out of the Cat Inner Ear.” *Hearing Research*, November. https://doi.org/10.1016/j.heares.2017.11.003.

Saliba, Issam, Marie-Eve Gingras-Charland, Karine St-Cyr, and Jean-Claude Décarie. 2012. “Coronal CT Scan Measurements and Hearing Evolution in Enlarged Vestibular Aqueduct Syndrome.” *International Journal of Pediatric Otorhinolaryngology* 76 (4): 492–99. https://doi.org/10.1016/j.ijporl.2012.01.004.

Schraven, Sebastian P., Bernhard Hirt, Erich Goll, Andreas Heyd, Anthony W. Gummer, Hans-Peter Zenner, and Ernst Dalhoff. 2012. “Conditions for Highly Efficient and Reproducible Round-Window Stimulation in Humans.” *Audiology and Neurotology* 17 (2): 133–38. https://doi.org/10.1159/000333807.

Schraven, Sebastian P., Bernhard Hirt, Anthony W. Gummer, Hans-Peter Zenner, and Ernst Dalhoff. 2011. “Controlled Round-Window Stimulation in Human Temporal Bones Yielding Reproducible and Functionally Relevant Stapedial Responses.” *Hearing Research* 282 (1–2): 272–82. https://doi.org/10.1016/j.heares.2011.07.001.

Shin, Dong Ho, Ki Woong Seong, Sunil Puria, Kyu-Yup Lee, and Jin-Ho Cho. 2016. “A Tri-Coil Bellows-Type Round Window Transducer with Improved Frequency Characteristics for Middle-Ear Implants.” *Hearing Research* 341 (November): 144–54. https://doi.org/10.1016/j.heares.2016.08.013.

Sim, Jae Hoon, Michail Chatzimichalis, Michael Lauxmann, Christof Röösli, Albrecht Eiber, and Alexander M. Huber. 2010. “Complex Stapes Motions in Human Ears.” *Journal of the Association for Research in Otolaryngology* 11 (3): 329–41. https://doi.org/10.1007/s10162-010-0207-6.

Sim, Jae Hoon, Michail Chatzimichalis, Christof Röösli, Roman D. Laske, and Alexander M. Huber. 2012. “Objective Assessment of Stapedotomy Surgery From Round Window Motion Measurement:” *Ear and Hearing* 33 (5): e24–31. https://doi.org/10.1097/AUD.0b013e318258c7a6.

Skarzynski, Henryk, Lukasz Olszewski, Piotr H. Skarzynski, Artur Lorens, Anna Piotrowska, Marek Porowski, Maciej Mrowka, and Adam Pilka. 2014. “Direct Round Window Stimulation with the Med-El Vibrant Soundbridge: 5 Years of Experience Using a Technique without Interposed Fascia.” *European Archives of Oto-Rhino-Laryngology* 271 (3): 477–82. https://doi.org/10.1007/s00405-013-2432-1.

Spindel, J. H., P. R. Lambert, and R. A. Ruth. 1995. “The Round Window Electromagnetic Implantable Hearing Aid Approach.” *Otolaryngologic Clinics of North America* 28 (1): 189–205.

Stenfelt, Stefan. 2015. “Inner Ear Contribution to Bone Conduction Hearing in the Human.” *Hearing Research* 329: 41–51.

———. 2016. “Model Predictions for Bone Conduction Perception in the Human.” *Hearing Research* 340 (October): 135–43. https://doi.org/10.1016/j.heares.2015.10.014.

Stenfelt, Stefan, and Richard L. Goode. 2005. “Bone-Conducted Sound: Physiological and Clinical Aspects.” *Otology & Neurotology: Official Publication of the American Otological Society, American Neurotology Society [and] European Academy of Otology and Neurotology* 26 (6): 1245–61.

Stenfelt, Stefan, Naohito Hato, and Richard L. Goode. 2004a. “Fluid Volume Displacement at the Oval and Round Windows with Air and Bone Conduction Stimulation.” *The Journal of the Acoustical Society of America* 115 (2): 797–812. https://doi.org/10.1121/1.1639903.

———. 2004b. “Round Window Membrane Motion with Air Conduction and Bone Conduction Stimulation.” *Hearing Research* 198 (1–2): 10–24. https://doi.org/10.1016/j.heares.2004.07.008.

Stieger, Christof, John J. Rosowski, and Hideko Heidi Nakajima. 2013. “Comparison of Forward (Ear-Canal) and Reverse (Round-Window) Sound Stimulation of the Cochlea.” *Hearing Research* 301 (July): 105–14. https://doi.org/10.1016/j.heares.2012.11.005.

Su, Wen-Yang, Mitchell S. Marion, Raul Hinojosa, and Gregory J. Matz. 1982. “Anatomical Measurements of the Cochlear Aqueduct, Round Window Membrane, Round Window

Niche, and Facial Recess." *The Laryngoscope* 92 (5): 483–86. https://doi.org/10.1288/00005537-198205000-00003.

Tonndorf, J. 1972. "Bone Conduction." In *Foundations of Modern Auditory Theory*, II:197–237. New York: Academic Press.

Tringali, Stéphane, Kanthaiah Koka, Arnaud Deveze, N. Julian Holland, Herman A. Jenkins, and Daniel J. Tollin. 2010. "Round Window Membrane Implantation with an Active Middle Ear Implant: A Study of the Effects on the Performance of Round Window Exposure and Transducer Tip Diameter in Human Cadaveric Temporal Bones." *Audiology and Neurotology* 15 (5): 291–302. https://doi.org/10.1159/000283006.

Voss, Susan E., John J. Rosowski, and William T. Peake. 1996. "Is the Pressure Difference between the Oval and Round Windows the Effective Acoustic Stimulus for the Cochlea?" *The Journal of the Acoustical Society of America* 100 (3): 1602–16. https://doi.org/10.1121/1.416062.

Wever, Ernest Glen, and Merle Lawrence. 1950. "The Acoustic Pathways to the Cochlea." *The Journal of the Acoustical Society of America* 22 (4): 460–67. https://doi.org/10.1121/1.1906628.

Zou, Jing, Ilmari Pyykkö, Päivi Sutinen, and Esko Toppila. 2005. "Vibration Induced Hearing Loss in Guinea Pig Cochlea: Expression of TNF-α and VEGF." *Hearing Research* 202 (1): 13–20. https://doi.org/10.1016/j.heares.2004.10.008.

Zwislocki, Jozef J. 1963. "Analysis of Some Auditory Characteristics: Technical Report." In *Handbook of Mathematical Psychology*, 3–97. Laboratory of Sensory Communication, Syracuse University.